# Consistent forest leaf area index retrieval using ground and airborne data

Ronghai Hu

# UNIVERSITÉ DE STRASBOURG

*ÉCOLE DOCTORALE MSII (ED n°269)*

**LABORATOIRE ICUBE (UMR 7357)**

# THÈSE présentée par :

**Ronghai HU**

soutenue le : **27 août 2018**

pour obtenir le grade de : **Docteur de l'université de Strasbourg**

Discipline/ Spécialité : Télédétection

# Estimation cohérente de l'indice de surface foliaire en utilisant des données terrestres et aéroportées

**THÈSE dirigée par :**

| | |
|---|---|
| **Mme NERRY Françoise** | Directeur de Recherches, CNRS |

**RAPPORTEURS :**

| | |
|---|---|
| **M. SOBRINO José** | Professor, University of Valencia |
| **M. ROUJEAN Jean Louis** | Directeur de Recherches, CNRS |

**EXAMINATEUR :**

| | |
|---|---|
| **Mme LANDES Tania** | Maître de Conférences, INSA Strasbourg |

# Acknowledgements

The PhD stage in France is a very important experience and precious memory for me. As a Chinese student, it is my first time to do research with international colleagues and live independently abroad for a long time. This experience largely broadened my horizons, helped me establish collaboration with international researchers, trained me to live independently and enjoy life, and provided me a good opportunity to learn French. I would like to express my gratitude to all those who helped me during my PhD period in France.

First, I would like to thank three professors without whom I would not complete my PhD successfully. I would like to thank Dr. Françoise NERRY, my French supervisor who always encourages me and offers me this PhD opportunity. Many thanks for inviting me to your laboratory in France, helping me contact and set up my fieldwork in the historical garden of university of Strasbourg, and patiently helping me revise all the documents. I enjoy the time in France and I'm missing the life there already. I would like to thank Dr. Zhao-Liang LI, who recommended me and helped me apply for the PhD in France. Many thanks for helping me adapt to life in France and is always concerned about my future development. I would like to thank Prof. Guangjian YAN, my Chinese promoter who always cares about my growth and recommended me to France for further study. Many thanks for guiding me through my entire study and research career. I am lucky to become a student of you.

I would like to express my sincere gratitude to all my colleague in France. Elena BOURNEZ and Tania LANDES support me with the laser scanner data and helped advance my

research in France. I'm particularly grateful to my main collaborator Elena BOURNEZ without whom I cannot work smoothly on my research about terrestrial laser scanner. You are always nice and support me with my research wholeheartedly. I really enjoyed the cooperation with you. Jihad ZALLAT helped me practice French and helped me lay the foundation for further French learning. Jerome COLIN introduced me the coffee time and helped me integrate into TRIO group. Laure ROUPIOZ, who kindly shared a office with me, always patiently explained to me the French chat that I didn't understand or didn't keep up with. Raphaël LUHAHE always cheered me up and treated me as a family member. Hervé YÉSOU often brought me into French chat and brought a lot of French special gifts to my family. I have already missed our daily coffee time.

I am grateful to the chinese students and visiting scholars of the TRIO team, Zhuoya NI, Enyu ZHAO, Yuanyuan CHEN, Xiaojing HAN, Xiaopo ZHENG, Xinyu LAN, Yanlong WANG, Chao REN, Wei WANG, and Wenping YU, who help me adapt to the environment and accompany me in daily life and work. Wenhui YU took me to start European self drive tours. Yang Xiucheng accompanied me to play badminton and exercise. Yuan YE brought me know a lot of Chinese friends in Strasbourg. Dr. Wei Ruicheng took me to set up a hiking group, as well as Peng JING, Jianmin YANG. Baihui Li, Wenjin YAO, Peng ZHAO, Guixian LIU, Shangzhi CHEN, Lihong LIU, Xiaoguang SUN, Fujiao TANG, Shuangqi TANG, Jian WANG, Jinyang FAN, Chen LI, Li JIANG, and many friends in the hiking group. Accompanied by them, I traveled through more than ten countries in Europe, climbed more than ten mountains with kilometers height and experienced extraodinary scenery. I never felt lonely in Europe.

Finally, I would like to thank my family. Without their understanding and support I cannot wholeheartedly devoted to research work. I am lucky to growing up in such a family.

I am fortunate enough to know a lot of people who accompanied me, helped me, and concerned about me. There are too many people helped me. Thank you for all that I mentioned or I didn't mention here. I hope our friendship will last forever. I sincerely thank you and wish you all a happy life!

# Contents

**Acknowledgements** ..... **i**

**Contents** ..... **iii**

**List of Figures** ..... **v**

**List of Tables** ..... **ix**

**List of Acronyms** ..... **xi**

**Résumé** ..... **I**

**Chapter 1 Introduction** ..... **1**

**Chapter 2 Review of Indirect Methods for Leaf Area Index Measurement** ..... **5**

2.1 Introduction ..... 5

2.2 Basic Concepts and Theoretical Background ..... 11

2.3 Methods to Retrieve True LAI from Indirect Gap Fraction Measurements ..... 19

2.4 Instruments for Indirect LAI Measurement ..... 30

2.5 Recent Advances and Future Perspectives ..... 43

2.6 Gaps of Current Methods and Possible Solutions ..... 52

**Chapter 3 Modelling Leaf Area Index Based on Path Length Distribution** ..... **55**

3.1 Beer-Lambert law ..... 56

3.2 Essential Reason for LAI Underestimation: Inconstant Path Length ..... 57

3.3 New LAI Retrieval Method Based on Path Length Distribution ..... 59

3.4 Calculation of Path Length Distribution ..... 62

3.5 Materials ..... 66
3.6 Results and Discussion ..... 75
3.7 Conclusion ..... 84

**Chapter 4 Estimating Leaf Area of An Individual Tree in Urban Areas Using Terrestrial Laser Scanner and Path Length Distribution Model ..... 85**

4.1 Introduction ..... 86
4.2 Modeling Leaf Area of a Single Tree ..... 88
4.3 Materials ..... 90
4.4 Methods ..... 95
4.5 Results ..... 101
4.6 Discussion ..... 107
4.7 Conclusions ..... 113

**Chapter 5 Quantifying Clumping Effect and Estimating Leaf Area Index Using Airborne Laser Scanner and Path Length Distribution Model ..... 115**

5.1 Introduction ..... 116
5.2 Materials ..... 119
5.3 Methods ..... 123
5.4 Results ..... 131
5.5 Discussion ..... 137
5.6 Conclusion ..... 143

**Chapter 6 Summary and Perspective ..... 145**

6.1 Major Findings and Discussions ..... 146
6.2 Perspectives ..... 148

**References ..... 151**

**List of Publications ..... 167**

# List of Figures

Fig. 2.1 Yearly published items and citations related to indirect LAI measurement. ..... 8
Fig. 2.2 Citation network on indirect LAI measurement since the 1990s..... 10
Fig. 2.3 Overview of a 25×25 m² homogeneous canopy composed of 79577 randomly distributed disc-shaped green leaves with a radius of 0.05 m (LAI=1) ..... 13
Fig. 2.4 Typical LAD (g) and projection functions (G) ..... 17
Fig. 2.5 Gap-size distributions in the zenith direction of a homogeneous canopy with planophile LAD..... 23
Fig. 2.6 Illustration of path length distribution ..... 25
Fig. 2.7 Comparison of various clumping correction methods in discrete broadleaf forest scenes ..... 29
Fig. 2.8 Illustration of various clumping correction methods..... 47
Fig. 3.1 Path length within the homogenous scene. ..... 57
Fig. 3.2 Path length within a cylindrical canopy. ..... 58
Fig. 3.3 Path length of the ellipse and circle. ..... 64
Fig. 3.4 Flow of obtaining path length distribution from measured gap data. ..... 66
Fig. 3.5 Overview of the cylindrical row canopy scene. ..... 67
Fig. 3.6 Overview of discrete cylindrical (a) and spherical (b) tree canopy scenes..... 68

Fig. 3.7 Pear orchard located in Huailai, Hebei province, China. ..... 70
Fig. 3.8 Visible (a) and near-infrared (b) image pair and classified canopy (c) and woody (d) component in site 1 ..... 73
Fig. 3.9 Validation of the retrieved LAI in cylindrical row canopy scenes ..... 75
Fig. 3.10 Validation of the retrieved LAI in different zenith angles in discrete broadleaf forest scenes ..... 77
Fig. 3.11 Validation of the retrieved LAI in discrete broadleaf forest scenes ..... 79
Fig. 3.12 Comparison of indirect leaf area index measurement in 2014 ..... 81
Fig. 3.13 Effect of woody components on the indirect leaf area index measurement ..... 83
Fig. 4.1 Illustration of Beer-Lambert law-based method for a forest stand (a) and for a single tree (b). ..... 88
Fig. 4.2 Overview of the studied tree in the historical garden of the University of Strasbourg, France. ..... 91
Fig. 4.3 Overview of the studied tree (red circle) and the seven TLS stations in June 27, 2016 ..... 92
Fig. 4.4 Allometric relationship between leaf area and shoot length ..... 93
Fig. 4.5 Terrestrial laser scanning data acquisition, pre-processing, and reconstruction of the studied tree (Source : E. Bournez). ..... 94
Fig. 4.6 Leaf projection functions (G) computed from the point cloud of each station and the merged point cloud of four stations in July 3, 2013 ..... 95
Fig. 4.7 The merged point cloud (a), convex envelope (b), and concave envelope (c) of the studied tree crown ..... 97
Fig. 4.8 Illustration of laser pulses, gap probability and path length calculation for the studied tree using its envelope ..... 98
Fig. 4.9 Path length distributions from seven TLS stations using a concave tree crown envelope in June 27, 2016 ..... 102
Fig. 4.10 Plant area or woody area of the studied tree retrieved using TLS data and path length distribution model at different dates and seasons ..... 103

Fig. 4.11 Validation of the retrieved leaf area using TLS data and path length distribution model. Both refined concave envelope and convex envelope were tested ..... 104
Fig. 4.12 Comparison of woody area retrieved using refined concave envelope and convex envelope ..... 105
Fig. 4.13 TLS-derived leaf area and gap probability of the studied tree crown at different resolutions ..... 107
Fig. 5.1 Workflow diagram for estimating the clumping index and LAI by using the path length distribution model and airborne laser scanner data ..... 119
Fig. 5.2 Airborne laser scanner data area and 18 field sites in the Genhe forestry reserve ..... 121
Fig. 5.3 Workflow diagram for processing the normalized point cloud data and calculating the LAI for each grid cell ..... 125
Fig. 5.4 Vertical crown cover from first-returns proportion. ..... 128
Fig. 5.5 Validation of the laser penetration metrics using field photography ..... 133
Fig. 5.6 The 0.5 m-resolution pit-free CHM generated using the ALS data ..... 134
Fig. 5.7 The 5 m-resolution LAI generated using the ALS data using the path length distribution model ..... 135
Fig. 5.8 Field validation of the LAI from the ALS data using the path length distribution model ..... 136
Fig. 5.9 Comparison of the LAIs with different resolutions ..... 137
Fig. 5.10 Clumping index maps at different scales ..... 138
Fig. 5.11 Comparison of LAI using two field-based methods ..... 142

# List of Tables

Table 2.1 Relevant journals that published more than four papers related to indirect LAI measurement ..... 8
Table 2.2 Accuracy of Beer-Lambert law in homogeneous canopies for indirect LAI measurement ..... 13
Table 2.3 Typical LADs (g) ..... 16
Table 2.4 Accuracy of leaf projection function (G) in homogeneous canopies for indirect LAI measurement ..... 17
Table 2.5 Representative methods for indirect LAI measurement ..... 27
Table 2.6 Representative instruments for indirect LAI measurement ..... 31
Table 3.1 Scene characteristics of broadleaf cylindrical canopies ..... 68
Table 3.2 Scene characteristics of broadleaf spherical canopies ..... 69
Table 3.3 Scene characteristics of the pear orchard in Huailai, Hebei province, China .. 70
Table 3.4 Description of Study Sites and Results of The Indirect Measurement ..... 72
Table 3.5 Description of MCI Measurement ..... 72
Table 3.6 Description of the Direct Measurement Site (White Birch) in Chengde, Hebei Province, China ..... 73
Table 3.7 Validation of the retrieved LAI weighted in seven zenith angles ..... 78

Table 3.8 In situ validation of LAI retrieval in the pear orchard..... 80

Table 4.1 Technical parameters of the two TLS systems ..... 92

Table 4.2 Foliage Area Volume Density retrieved from seven TLS stations using path length distribution model and concave envelope in June 27, 2016..... 102

Table 4.3 Plant Area of ten trees retrieved from seven TLS stations in June 27, 2016.. 106

Table 5.1 Representative Laser Penetration Metrics (LPM) ..... 129

Table 5.2 Clumping Index of Airborne Laser Scanner (ALS), field photography and TRAC in 18 field sites. TRAC measurements were made on 13 sites ..... 139

# List of Acronyms

| | |
|---|---|
| **LAI** | Leaf Area Index |
| **PAI** | Plant Area Index |
| **WAI** | Woody Area Index |
| **LAD** | Leaf Angle Distribution |
| **FAVD** | Foliage Area Volume Density |
| **LAIe** | Effective Leaf Area Index |
| **PAIe** | Effective Plant Area Index |
| **GLAI** | Green Leaf Area Index |
| **GAI** | Green Area Index |
| **TRAC** | Tracing Radiation and Architecture of Canopies |
| **DHP** | Digital Hemispherical Photography |
| **DCP** | Digital Cover Photography |
| **MVI** | Multiband Vegetation Imager |
| **MCI** | Multiband Canopy Imager |
| **LiDAR** | Light Detection and Ranging |
| **TLS** | Terrestrial Laser Scanner |
| **ALS** | Airborne Laser Scanner |
| **SLS** | Spaceborne Laser Scanner |
| **UAV** | Unmanned Aerial Vehicle |

| | |
|---|---|
| **VIS** | Visible |
| **NIR** | Near-infrared |
| **PPFD** | Photosynthetic Photon Flux Density |
| **DBH** | Diameter at Breast Height |
| **CHM** | Canopy Height Models |
| **AGL** | Above Ground Level |
| **VCC** | Vertical Crown Cover |
| **LPM** | Laser Penetration Metrics |
| **LPI** | Laser Penetration Index |
| **3D** | Three Dimensional |
| **CC** | Gap-size distribution method |
| **LX** | Finite-length averaging method |
| **CLX** | Combination of CC and LX Methods |
| **PATH** | Path length distribution method |
| **PATH_MES** | Path length distribution method based on measured gap data |
| **PATH_ELL** | Path length distribution method based on ellipse section assumption |

# Résumé

La végétation est l'élément le plus important de la biosphère. C'est un facteur clé pour relier les différentes couches du système terrestre et réguler le cycle biogéochimique global qui a un impact profond sur l'avenir de l'humanité et de la Terre. La photosynthèse végétale est la réaction chimique la plus importante sur Terre. Le processus d'utilisation de l'énergie lumineuse pour assimiler le dioxyde de carbone et l'eau pour produire de la matière organique et libérer de l'oxygène est le principal moyen pour l'écosystème terrestre d'obtenir de l'énergie externe et de maintenir l'équilibre du carbone et de l'oxygène. La végétation a donc un impact sur l'équilibre radiatif du système gaz terrestre, sur le cycle de l'eau et du carbone et la régulation du sol, l'environnement écologique et le climat global.

La surface foliaire est l'un des facteurs majeurs de la production d'un écosystème. L'indice de surface foliaire (Leaf Area Index, LAI), défini comme la moitié de la surface foliaire par unité de surface de sol, est un paramètre clé de la structure de la végétation pour la modélisation des échanges de masse (eau et carbone) et d'énergie (rayonnement et chaleur) dans le système Terre-atmosphère. Une mesure précise du LAI est particulièrement importante pour le calcul quantitatif du cycle global des matériaux et de l'énergie. Au cours des dernières décennies, les exigences de précision de l'inversion du LAI ont également été continuellement renforcées du fait du développement rapide du changement global, l'évaluation écologique, de l'agriculture de précision et d'autres domaines. Le Système mondial d'observation du climat (Global Climate

Observing System, GCOS) exige que l'erreur relative du produit indice de surface foliaire ne dépasse pas 20% et que l'erreur absolue ne dépasse pas 0,5.

La méthode indirecte par inversion de la loi d'extinction du rayonnement de Beer-Lambert est actuellement la principale méthode de mesure terrestres et aéroportées du LAI en raison de sa grande efficacité et de son mécanisme concis. L'effet d'agrégation du feuillage est le facteur le plus critique qui influence la précision de l'estimation du LAI. Dans la mesure indirecte au sol, les algorithmes précédents corrigent dans une large mesure l'effet d'agrégation en considérant les espaces entre les couronnes. Cependant, l'effet d'agrégation causé par des longueurs incohérentes de trajets dans la couronne n'est pas pris en compte.

La recherche cohérente de LAI avec des données de télédétection à plusieurs échelles, en particulier à l'échelle au sol et à l'échelle aéroportée ou satellitaire, est une tâche permanente importante. Traditionnellement, la mesure indirecte utilisant la loi de Beer-Lambert et les instruments optiques étaient utilisés pour la mesure de LAI au sol, tandis que le modèle de transfert de rayonnement et l'image de télédétection multispectrale étaient utilisés pour la détermination aéroportée et spatiale de LAI.

Le scanner laser offre une opportunité pour une détermination LAI cohérente à plusieurs échelles, car le scanner laser terrestre et le scanner laser aéroporté ont le même mécanisme physique. Le balayage laser est une technologie de télédétection active qui capture les nuages de points tridimensionnels de l'objet scanné. Il a été largement utilisé pour obtenir les paramètres des auvents et des couronnes, tels que la hauteur des arbres, le diamètre à hauteur de poitrine, la densité de la canopée et la biomasse, etc.

À l'échelle du terrain, les méthodes d'estimation du LAI peuvent être classées en méthodes directes et indirectes. Les méthodes directes, y compris la récolte, l'allométrie et la collecte des déchets, peuvent être utilisées pour mesurer un arbre individuel et sont considérées comme plus précises que les méthodes indirectes mais présentent l'inconvénient d'être longues, laborieuses et destructrices pour la végétation. Les méthodes indirectes, dans lesquelles la surface foliaire est déduite des mesures d'autres variables, telles que la fraction de trou ou la transmission de la lumière à travers les auvents, sont efficaces, non destructives et modifiables en automatisation ; ainsi, ces méthodes sont largement utilisées. Cependant, les travaux antérieurs sur la mesure

indirecte du LAI se sont principalement concentrés au niveau du peuplement, c'est-à-dire sur une communauté contiguë d'arbres. La mesure de la surface foliaire d'un arbre individuel est rarement explorée bien que les arbres isolés soient plus communs que les forêts dans les zones urbaines. La plupart des instruments et des théories ne sont pas directement applicables à la mesure du LAI d'arbres individuels urbains, en raison de l'influence des bâtiments environnants ou d'autres objets. Le scanner laser terrestre peut séparer l'arbre étudié de l'environnement urbain en utilisant ses informations de distance uniques, tandis que la théorie traditionnelle de la végétation continue devrait être adaptée pour les arbres isolés en milieu urbain.

À l'échelle aéroportée, l'estimation du LAI repose principalement sur l'imagerie optique passive précoce ou sur la technologie émergente du scanner laser actif. La récupération de LAI en utilisant l'imagerie optique passive est facilement affectée par de multiples facteurs tels que l'atmosphère, la structure de la canopée, l'hétérogénéité du sol et l'effet d'échelle, et est facilement saturé. En tant que moyen d'observation émergent développé au cours des 20 dernières années, le scanner laser aéroporté est devenue le principal moyen de cartographie régionale de l'indice foliaire du fait de sa meilleure pénétrabilité et de son accès direct à l'information tridimensionnelle de la canopée forestière. À l'heure actuelle, la détermination du LAI utilisant le scanner laser aéroporté est principalement obtenue via un modèle semi-empirique, réalisé par l'équation de régression semi-empirique avec l'indice de pénétration laser, le rapport de nuages de points ou d'autres paramètres intermédiaires. Des recherches antérieures montrent que le modèle semi-empirique et semi-physique basé sur l'indice de pénétration du laser et la loi de Beer-Lambert donne les meilleurs résultats. Cette méthode est devenue le principal moyen de récupération du LAI utilisant le scanner laser aéroporté car elle a une certaine signification physique et réduit le problème de saturation dans l'inversion d'image optique. Le scanner laser aéroporté partage le même principe La loi de Beer avec mesure indirecte, permettant à l'inversion LiDAR aéroportée de tenir compte des progrès de la recherche et de l'expérience de mesure indirecte de l'indice de surface foliaire depuis plus d'un demi-siècle, mais il fait également face à des problèmes similaires avec la mesure indirecte au sol. L'effet d’agrégation est le facteur clé. La grande empreinte et la faible densité ponctuelle du scanner laser aéroporté sont deux contraintes majeures pour appliquer la méthode au sol traditionnelle afin de corriger l'effet d’agrégation, car les empreintes LiDAR aéroportées (dizaines de centimètres ou plus) sont trop grandes pour capturer les petits espaces et la taille

détaillée la distribution, qui est un intrant nécessaire pour la méthode au sol traditionnelle. De plus, les informations tridimensionnelles ne sont pas non plus utilisées efficacement. Par conséquent, la correction de l'effet d'agrégation est toujours un problème non résolu pour la détermination du LAI utilisant le scanner laser aéroporté.

En résumé, le LAI est un paramètre clé du cycle écologique de la Terre, et sa précision d'acquisition a toujours la nécessité et la possibilité d'amélioration. La technologie du scanner laser actif offre une possibilité de récupération cohérente du LAI à plusieurs échelles, alors que les théories traditionnelles ont besoin d'adaptation. Il est nécessaire de démarrer de la mesure au sol la plus basique et de l'inversion du scanner laser aéroporté de pointe pour améliorer la précision et la fiabilité du produit du LAI de la source. Dans cette thèse, le modèle de distribution de longueur de trajet est introduit pour corriger l'effet d'agrégation, et il est appliqué aux données du scanner laser terrestre et du scanner laser aéroporté. La méthode d'obtention de la distribution de longueur de trajet de différentes plates-formes est étudiée et le modèle de récupération cohérent est établi. Le modèle devrait faciliter la récupération cohérente de l'indice de surface foliaire des forêts à l'aide de données au sol et aéroportées.

Le chapitre 1 présente en introduction les motivations de ce travail de thèse après une brève discussion sur l'état de l'art et la nécessité d'étudier l'estimation du LAI. La base théorique, les progrès et les problèmes de l'estimation de l'indice foliaire sont tout d'abord résumés. Les méthodes indirectes ont connu des progrès considérables au cours des dernières années, les rendant ainsi opérationnelles dans la mesure LAI au sol et même dans le cas de l'estimation aéroportée. L'amélioration de la précision de ces méthodes a toujours été une tâche permanente étant donné l'exigence croissante de relier la précision aux mesures réelles. La dernière décennie a été témoin de progrès associés au balayage laser, à la photographie de couverture, à l'estimation de l'agrégation à l'intérieur de la cime, aux effets de pente, à la composante ligneuse et à la mesure de la distribution de l'angle foliaire.

Le chapitre 2 passe en revue de manière exhaustive le cadre théorique et les méthodologies de mesure indirecte des LAI, suivis des descriptions des instruments et des plates-formes actuels. Les développements futurs et les perspectives d'amélioration de l'applicabilité et de la précision

de la mesure indirecte du LAI sont ensuite discutés.

Pour faire face à l'effet d'agrégation dans l'estimation de l'indice foliaire des forêts, ce travail effectue des recherches pertinentes basées sur la distribution de la longueur de la trajectoire sous trois aspects : modélisation théorique, mesure terrestre et estimation aéroportée.

Dans le chapitre 3, prenant les longueurs incohérentes de trajets dans la couronne comme point de rupture, ce travail analyse le mécanisme de sous-estimation du LAI de la loi de Beer-Lambert, puis propose le modèle de l'estimation du LAI en introduisant la distribution de la longueur de trajet pour modéliser l'effet d'agrégation au sein d'une couronne causé par la forme de la couronne. Contrairement au modèle précédent, le modèle de distribution de longueur de trajet a l'avantage d'utiliser la distribution de longueur de trajet pour décrire la distribution spatiale tridimensionnelle des feuilles et de considérer la forme de la couronne tridimensionnelle et la distribution en hauteur de l'arbre. De plus, il peut traiter la distribution non aléatoire de la fraction de trou dans les couronnes. Grâce à différentes formes d'intrants, le modèle peut être appliqué aux instruments et plates-formes terrestres et aéroportés existants pour améliorer efficacement la précision de la mesure de l'indice de surface foliaire.

Le chapitre 4 présente une méthode pour estimer la surface foliaire des arbres isolés en milieu urbain en utilisant le modèle de distribution de la longueur de trajet. La méthode d'obtention de la distribution de la longueur du trajet proposée est basée sur l'enveloppe de la couronne d'arbre reconstruite à partir du nuage de points 3D mesuré par le scanner laser terrestre. L'objectif est d'appliquer et vérifier le modèle de distribution de la longueur de trajet sur les données du scanner laser terrestre pour les arbres isolés en milieu urbain. Ainsi, l'effet d'agrégation pourra être corrigé pour améliorer la précision de l'estimation de la surface foliaire. La mesure de la surface foliaire urbaine est importante pour bien évaluer l'impact des arbres urbains sur la régulation du microclimat, l'effet d'îlot de chaleur, le refroidissement du bâtiment, l'amélioration de la qualité de l'air et la formation d'ozone. Les travaux antérieurs sur la mesure de la surface foliaire portaient principalement sur le niveau du peuplement, bien que la présence d'arbres individuels soit plus fréquente que celle des forêts dans les zones urbaines. Les seules méthodes réalisables pour la mesure non destructive de la surface foliaire, à savoir les méthodes indirectes optiques, sont largement limitées dans les zones urbaines parce que le trajet de la

lumière est toujours intercepté par les bâtiments environnants ou d'autres objets.

Le scanner laser terrestre, qui permet d'extraire l'arbre individuel en utilisant ses informations de distance uniques, offre une possibilité de mesurer indirectement l'indice de surface foliaire dans les zones urbaines. Cependant, la théorie de mesure indirecte du LAI, qui utilise le cosinus de l'angle zénithal d'observation pour la correction de longueur de trajectoire, est incompatible pour un arbre individuel car la zone projetée de LAI change à mesure que l'angle zénithal change, rendant les résultats incomparables et ambigus.

Par conséquent, le modèle de distribution de la longueur de trajet a été modifiée pour la mesure de la surface foliaire pour les arbres isolés en remplaçant la correction de la longueur du trajet cosinus traditionnel par la canopée continue avec la distribution de la longueur du trajet réel. Puisque les données du scanner laser terrestre sont plus détaillées (meilleure résolution spatiale) que les données du scanner laser aéroporté, la distribution de longueur de trajet pourra être calculée de façon plus précise. De façon spécifique, chaque enveloppe de l'arbre est composée d'une multitude de triangles. Pour chaque rayon, les intersections avec tous les triangles sont calculées. Généralement, on détecte deux intersections. La longueur du trajet de ce rayon est calculée par la distance entre ces deux points. Puis la longueur du trajet de tous les rayons sont calculées. Dans un deuxième temps, la fraction de trouée est calculée par les proportions des rayons passant à travers l'arbre. Les rayons qui n'ont pas de retours ou qui ont des rendements au-delà de l'enveloppe sont considérés comme passant à travers l'arbre. Enfin, la fraction de trouée et la distribution de longueur de trajet sont utilisées comme entrées du modèle de distribution de longueur de trajet. La densité de la surface foliaire de chaque arbre est ainsi obtenue. Pour chaque arbre, les résultats des différentes observations sont cohérents, démontrant la stabilité et la validité de la méthode.

Le chapitre 5 présente une méthode de cellule de grille basée sur le modèle de distribution de longueur de trajet pour calculer le LAI corrigé par agrégation en utilisant les données du scanner laser aéroporté sans exigence de mesures de terrain supplémentaires. Nous avons séparé les zones à l'intérieur et entre les couronnes afin de prendre en compte l'agrégation entre les couronnes, et migré le modèle de distribution de la longueur du trajet pour prendre en compte le profil du feuillage 3D et l'agrégation à l'intérieur de la couronne.

La méthode d'obtention de la distribution de la longueur du trajet proposée est basée sur un modèle de hauteur de la canopée reconstruite à partir du nuage de points 3D mesuré par le scanner laser aéroporté. Dans un premier temps, les données du scanner laser aéroporté sont lues et prétraitées. Pour chaque ligne de vol, les points relatifs au bruit ont été enlevés et l'élévation du sol a été soustraite. Puis les 20 lignes de vol ont été fusionnées. Les résultats de ce processus conduisent à des données normalisées, dans lesquelles la valeur de z représente la hauteur de chaque point au-dessus du sol. Deuxièmement, les données normalisées sont utilisées pour calculer la LPM (Laser Penetration Metrics). Une méthode multi-niveaux a été appliquée pour générer un modèle de hauteur de la canopée (Canopy Height Models, CHM) sans trou. Troisièmement, la LPM a été utilisée comme une approximation de la fraction de trouée, et la CHM comme celle de la distribution de longueur de trajet. Ces deux données ont été utilisées comme entrées du modèle de distribution de longueur de trajet. Ainsi, la carte de LAI a pu être obtenue. Finalement, les LPM et LAI ont été validées avec des mesures sur le terrain.

La précision sur la fraction de l'écart et sur le LAI efficace est la même que pour les recherches précédentes. Notre nouvelle méthode est capable de calculer le LAI réel. Avec les données du scanner laser aéroporté de 0,4 m-empreinte, les résultats sont généralement prometteurs et une analyse d'agglutination à plusieurs niveaux est compatible avec le paysage parcouru. Les LAI de différentes résolutions sont cohérents, avec une différence de moins de 5% entre 5 et 250 m de résolution. En raison de sa constance et de sa configuration simple, la méthode fournit une occasion de cartographier le LAI corrigé par agglutination et renforce la capacité du LiDAR aéroporté à surveiller le changement de végétation et à valider le produit satellite. Cette méthode de cellule de grille basée sur la distribution de longueur de trajet mérite d'être testée et appliquée en utilisant une technologie laser plus récente.

Le chapitre 6 présente et discute les principales conclusions de cette thèse ainsi que les perspectives et les limites rencontrées. Le modèle de distribution de la longueur de la trajectoire et les conclusions proposées dans ce document peuvent faciliter l'amélioration de la précision de la récupération de l'indice LAI forestier et de l'inversion cohérente aéroportée et terrestre.

À l'échelle du sol, le modèle de distribution de longueur de trajet est mis en œuvre pour la

mesure du LAI des arbres isolés en milieu urbain en utilisant des données du scanner laser terrestre en remplaçant la correction de longueur de trajet cosinus traditionnelle par une distribution en longueur réelle. À l'échelle aéroportée, un modèle de distribution de la longueur du trajet est mis en œuvre pour corriger l'effet d'agrégation en utilisant le modèle de hauteur de la canopée acquis à partir des données du scanner laser aéroporté. Ils fournissent également l'occasion de cartographier le LAI corrigé par agrégation et renforcent la capacité du scanner laser aéroporté à surveiller la dynamique de la végétation. La récupération cohérente du LAI forestières à l'aide de données au sol et aéroportées est réalisée en utilisant la distribution de la longueur du trajet.

Par rapport à la recherche existante, les caractéristiques de recherche et les innovations de cette thèse sont les suivantes :

(1) Un modèle de distribution de la longueur du trajet a été proposé pour tenir compte de l'indice d'agrégation à l'intérieur de la couronne et de l'estimation du LAI. Le concept de fonction de distribution de longueur de trajet est introduit, et le modèle d'inversion du LAI basé sur la distribution de longueur de trajet est établi. L'un des avantages de la théorie de la distribution de la longueur de trajet est qu'elle permet de caractériser et de traiter le caractère non aléatoire induit par la forme de la couronne au sein des auvents qui peut entraîner une sous-estimation allant jusqu'à 25%. Cet aspect n'a jusqu'à présent pas été traité de manière appropriée par les algorithmes existants et on s'attend à ce que la théorie de longueur de trajet améliore la précision de mesure indirecte de LAI avec l'utilisation des instruments optiques courants.

(2) Une méthode d'estimation précise de la surface foliaire des arbres isolés a été proposée en remplaçant la correction de la longueur du trajet en cosinus traditionnel pour la canopée continue avec la distribution de la longueur du trajet réel. La distribution de la longueur du trajet réel a été calculée au moyen d'intersections d'enveloppes d'impulsions laser basées sur l'enveloppe de couronne d'arbre reconstruite à partir du nuage de points du scanner laser terrestre. En conséquence, la densité volumique de la surface du feuillage a été séparée du modèle de distribution de la longueur du trajet pour le calcul de la surface foliaire. Les résultats de différentes stations sont globalement cohérents et l'utilisation de la moyenne pondérée des

différentes stations par les nombres d'échantillons améliore encore l'universalité et l'efficacité de la méthode proposée.

(3) Une correction indépendante de l'effet d'agrégation à l'aide des données du scanner laser aéroporté a été obtenue avec l'utilisation de la distribution de longueur de trajet. L'algorithme de correction de l'effet agrégation traditionnel est difficile à appliquer pour les données du scanner laser aéroporté. La principale limitation est que le scanner laser aéroporté a une grande empreinte et une faible densité de nuages, ce qui rend difficile l'obtention de l'information précise de distribution de brèche requise par l'algorithme d'index d'agrégation au sol traditionnel. Dans cette thèse, le modèle de distribution de longueur de trajet est introduit dans l'inversion du scanner laser aéroportée et la distribution de longueur de trajet est directement obtenue en utilisant le nuage de points 3D pour corriger l'effet d'agrégation et estimer le LAI. Il permet de se soustraire à la limitation du scanner laser aéroporté de ne pas obtenir la distribution précise des tailles de trous en utilisant le processus de la correction indépendante de l'effet d'agrégation avec les données du scanner laser aéroporté ce qui améliore grandement la précision et la praticabilité de la cartographie rapide du LAI.

Les applications de l'acquisition de la distribution de la longueur du trajet ne se limitent pas à la méthode proposée dans ce document. Les perspectives sont nombreuses aussi bien pour l'extension de la méthode que pour son amélioration.

(1) Acquisition de la distribution de la longueur du trajet avec reconstruction précise de l'enveloppe à l'aide d'une matrice de voxels

Dans cette étude, les feuilles sont généralement uniformément réparties dans l'enveloppe et l'écart de distribution des feuilles pour les arbres plus complexes n'est pas pris en compte, ce qui pourrait entraîner une sous-estimation des arbres ayant des structures complexes. Une reconstruction d'enveloppe précise utilisant une matrice de voxels sera utile pour décrire des structures arborescentes complexes.

(2) Correction de l'effet d'agrégation et estimation du LAI basé sur un scanner laser aéroporté à onde complète

Le scanner laser à pleine longueur d'onde fournit plus d'informations que le scanner laser à retour discret traditionnel, en particulier les informations de largeur d'impulsion obtenues lorsque l'impulsion laser traverse la canopée. Ce type d'information a un grand potentiel d'application pour l'acquisition d'une longueur de trajet. Les données à retour discret ont certaines limites pour obtenir le profil inférieur de la canopée. Bien que l'inversion de l'indice de surface foliaire puisse toujours être obtenue par la longueur de trajet relative, une distribution de longueur de trajet absolue plus précise peut être obtenue si l'information de forme d'onde complète peut être obtenue. Cela contribuera à l'inversion de la densité de la surface foliaire et améliorera encore la précision de l'estimation de l'indice de surface foliaire par le scanner laser aéroporté.

(3) Utilisation du scanner laser satellitaire pour corriger les effets d'agrégation et estimer le LAI

Le scanner laser satellitaire peut également acquérir des informations 3D. Bien que sa résolution soit beaucoup plus faible que celle du scanner laser aéroporté, ses mécanismes sont similaires. Il est également possible d'obtenir des informations de distribution de longueur de trajet pour corriger l'effet d'agrégation. Si la correction de l'effet d'agrégation des données du scanner laser satellitaire peut être réalisée, la précision de l'inversion du LAI du scanner laser satellitaire sera grandement améliorée, et une nouvelle source de données du LAI globale pourra être fournie. L'application du modèle de distribution de trajet avec des données acquises par le scanner laser satellitaire pose encore de grands défis. Différent d'un scanner laser à petite empreinte avec une impulsion laser correspondant à une longueur de trajet, la taille d’une empreinte est de plusieurs dizaines de mètres, couvrant une grande surface incluant la canopée et le sol, et l'unique écho contient différentes composantes. Pour des informations de hauteurs différentes, il est nécessaire d'explorer toutes les informations de forme d'onde et d'étudier la méthode d'extraction de la distribution de longueur de trajet à partir des informations de forme d'onde complète.

# Chapter 1 Introduction

Vegetation is the most important component of the biosphere. It is a key factor in connecting the various layers of the earth system and regulating the global biogeochemical cycle, which has profoundly impact on the future of mankind and the earth. Plant photosynthesis is the most important chemical reaction on the earth. The process of using light energy to assimilate carbon dioxide and water to produce organic matter and release oxygen is the main means for the earth ecosystem to obtain external energy and maintain the balance of carbon and oxygen. Vegetation has a profound impact on the radiation balance of the Earth's gas system, water cycle, carbon cycle, and soil regulation, ecological environment and global climate.

Leaf area index (LAI), defined as one half of the total leaf area per unit ground surface area (Chen and Black 1992a), is a key parameter of canopy structure. It controls a variety of biophysical and physiological processes and is widely used in ecology, forestry, botany and agronomy (Jonckheere et al. 2004; Myneni et al. 1989; Ross 1981). Most ecosystem models require an accurate estimate of LAI, as leaf area directly regulates productivity for all ecosystems (Asner et al. 2003; Clark et al. 2008; Stark et al. 2012). From the perspective of material, LAI has a direct impact on photosynthesis and respiration, further affecting the global material cycle, especially carbon cycle. From the perspective of energy, it characterizes the canopy-atmosphere interface, where most of the energy fluxes exchanges (Breda 2003). Accurate measurement of LAI is particularly important for the quantitative calculation of global material and energy cycle. In recent decades, the accuracy requirements of leaf area index inversion have also been continuously improved with the rapid development of global change,

ecological assessment, precision agriculture and other fields. The Global Climate Observing System (GCOS) requires that the relative error of the leaf area index product does not exceed 20% and the absolute error does not exceed 0.5.

Consistent LAI retrieval with multi-scale remotely sensed data, especially between ground scale and airborne or satellite scale, is an important on-going task. Traditionally, indirect measurement using Beer-Lambert law and optical instruments were employed for ground LAI measurement while radiation transfer model and multispectral remote sensing image were employed for airborne and spaceborne LAI retrieval. Ground measurement is the basis, not only for fine modeling at small regional scale, but also for reference value of airborne and spaceborne inversion, which determines the overall accuracy of leaf area index inversion. Airborne and spaceborne retrieval has an obvious advantage in coverage, and is an irreplaceable means of obtaining regional and global data.

Laser scanning provides an opportunity for consistent LAI retrieval at multiple scales because terrestrial laser scanning (TLS) and airborne laser scanning (ALS) have the same physical mechanism. Laser scanning is an active remote sensing technology which captures three-dimensional (3D) point clouds of the scanned object. It has been widely used in obtaining parameters of canopies and crowns, such as tree height, diameter at breast height (DBH), canopy density, and biomass, etc. (Bouvier et al. 2015; Koch et al. 2006; Wang et al. 2009).

At ground scale, the LAI estimation methods can be classified as direct and indirect methods. Direct methods, including harvesting, allometry, and litter collection, can be used for measuring an individual tree and are regarded as more accurate than indirect methods but have a disadvantage of time-consuming, labor-intensive, and destructive to vegetation (Colaizzi et al. 2017; Daughtry 1990; Peper and McPherson 2003; Simioni et al. 2004). Indirect methods, in which leaf area is inferred from measurements of other variables, such as the gap probability or light transmission through canopies, are efficient, nondestructive and amendable to automation; thus, these methods are widely used (Macfarlane et al. 2014; Mu et al. 2017; Ryu et al. 2010b; Yao et al. 2011). However, previous work on indirect LAI measurement mainly focused on the stand level, i.e. a contiguous community of trees (Leblanc and Fournier 2014; Nowak et al. 2008; Strahler et al. 2008; Weiss et al. 2004). Leaf area measurement for an individual tree is rarely explored although isolated trees are more common than forests in urban areas. Most instruments and theories are not directly applicable to urban individual tree LAI measurement, because of the influence of the surrounding buildings or other objects. TLS can

separate the studied tree from the urban environment using its unique distance information, while the traditional theory for continuous vegetation should be adapted for isolated trees in urban environment.

At airborne scale, the LAI estimation is mainly based on early passive optical imaging or emerging active laser scanner technology. The LAI retrieval using passive optical imaging is easily affected by multiple factors such as atmosphere, canopy structure, soil heterogeneity and scale effect, and is easy to be saturated. As an emerging means of observation developed in the past 20 years, ALS has become the main means of regional leaf area index mapping because its better penetrability and direct access to the three-dimensional information of forest canopy. At present, the LAI retrieval using ALS is mainly realized by semi-empirical model, which is realized by the semi-empirical regression equations with laser penetration index, point cloud ratio or other intermediate parameters. Previous researches show that the semi-empirical and semi-physical model based on laser penetration index and Beer-Lambert law performs best. This method has become the main means for ALS LAI retrieval because it has certain physical meaning and reduces the saturation problem in optical image inversion. Airborne LiDAR shares the same principle Beer-Lambert law with indirect measurement, making it possible for airborne LiDAR inversion to learn from the research progress and experience of indirect measurement of the ground leaf area index for more than half a century, but it also faces similar problems with ground indirect measurement. The clumping effect is the key factor. The large footprint and low point density of airborne LiDAR are two major constraints for applying the traditional ground method to correct the clumping effect, as airborne LiDAR footprints (tens of centimeters or larger) are too large to capture the small gaps and the detailed gap size distribution, which is necessary input for traditional ground method. In addition, the three-dimensional (3D) information is also not utilized efficiently. Therefore, correcting clumping effect is still an unsolved problem for ALS LAI retrieval.

In summary, the LAI is a key parameter of the Earth's ecological cycle, and its acquisition accuracy still has the necessity and possibility of improvement. Active laser scanning technology provides an opportunity for consistent LAI retrieval at multiple scales while traditional theories need adaptation. It is necessary to start from the most basic leaf area index ground measurement and the cutting-edge airborne laser scanner inversion to improve the accuracy and reliability of the leaf area index product from the source. In this thesis, the path length distribution model is introduced to correct the clumping effect, and it is applied to the

TLS and ALS data. The method of obtaining the path length distribution of different platforms is studied, and the consistent retrieval model is established. The model is expected to facilitate the consistent retrieval of the forest leaf area index using ground and airborne data.

Chapter 1 introduces in the introduction the motivation of this thesis work after a brief discussion on the state of the art and the need to study the estimation of LAI. The theoretical basis, progress and problems of foliar index estimation are first summarized.

Chapter 2 provides a comprehensive review of the theoretical framework and methodologies for indirect measurement of LAI, followed by descriptions of current instruments and platforms. Future developments and prospects for improving the applicability and accuracy of indirect LAI measurement are then discussed. To deal with the clumping effect in estimating the leaf area index of forests, this work carries out relevant research based on the path length distribution under three aspects: theoretical modeling, terrestrial measurement and airborne retrieval.

Chapter 3 analyzes the mechanism of LAI underestimation of the Beer-Lambert law, then proposes LAI estimation model in introducing the path length distribution to model the clumping effect caused by the crown shape.

Chapter 4 presents a method to estimate the leaf area of isolated trees based on the path length distribution and TLS data. The method for obtaining the path length distribution is proposed based on the envelope of the reconstructed tree crown from the 3D point cloud measured by the TLS.

Chapter 5 presents a method to correct the clumping effect based on the path length distribution and ALS data. The method of obtaining the proposed path length distribution is based on a canopy height model reconstructed from the 3D point cloud measured by the airborne laser scanner.

Chapter 6 summarizes and discusses the main conclusions of this thesis as well as the perspectives and limitations encountered.

# Chapter 2 Review of Indirect Methods for Leaf Area Index Measurement

Optical indirect methods based on the Beer-Lambert law are widely adopted in numerous fields given their high efficiency and feasibility for LAI estimation. These methods have undergone considerable progress in the past decades, thereby making them operational in ground-based LAI measurement and even in airborne estimation. Improving the accuracy of these methods has always been an ongoing task given the increasing requirement for relating accuracy to actual measurements. The last decade witnessed progress associated to laser scanning, cover photography, within-crown clumping, slope effect, woody component, and leaf angle distribution measurement. This chapter comprehensively reviews the theoretical framework and methodologies of indirect LAI measurement, followed by current instruments and platforms. Future development and perspectives to improve the applicability and accuracy of indirect LAI measurement are then discussed.

## 2.1 Introduction

Leaf area index (LAI), which describes the amount of leaf area per unit horizontal ground surface area, is a key vegetation parameter for modeling mass (water and carbon) and energy (radiation and heat) exchange between the biosphere and the atmosphere (Asner et al. 2003; GCOS 2011; Ren et al. 2014; Stark et al. 2012; Tian et al. 2015b).

LAI ground measurement plays an important role in vegetation monitoring and serves as the true value for remote sensing validation (Breda 2003; Gower et al. 1999; Yan et al. 2016d; Yin et al. 2017). Methods for LAI ground measurement can be classified as direct or indirect. Direct methods generally consist in sampling manually leaves in a destructive way and measuring their area by means of instruments such as LI-3000C Portable Leaf Area Meter (LI-COR, Lincoln, NE, USA), LI-3100C Area Meter (LI-COR, Lincoln, NE, USA), and CI-202 Portable Laser Leaf Area Meter (CID Bio-Science, Camas, WA, USA) before calculating LAI by definition. A complete manual measurement is thus only feasible for small samples of low vegetation. However, manual sampling is also employed for forests or large samples of low vegetation by selecting small amounts of representative leaves and establishing allometric relationships. The allometric relationships are empirical functions that relate leaf area or leaf weight (gravimetric method) to any dimension of the woody element that carries leaves, including sapwood area, stem diameter, and crown base height (Colaizzi et al. 2017; Jonckheere et al. 2004). These relationships, dependent on the site, species, and even years (Breda 2003), are then used for upscaling (Daughtry 1990; Gower et al. 1999). We classify the allometric method as a direct method in the present study because the sampled leaves and the branch structures for determining the allometric relations are measured manually. When the samples are representative enough, direct methods are regarded as more accurate than indirect methods and, thus, are often used to validate indirect methods. However, direct methods are generally time consuming, labor intensive, and often destructive to vegetation, which limits their applications and render them unfeasible for high temporal and spatial frequency measurements (Jonckheere et al. 2004; Weiss et al. 2004). Indirect methods, including optical and inclined point quadrat methods, infer LAI by measuring other variables, such as gap fraction, light transmission, and contact number. It could be noticed that the allometric method could also be viewed as an indirect-contact LAI measurement method because it infers LAI based on the relationship with other vegetation characteristics. Indirect methods consist of Beer-Lambert law-based optical methods and inclined point quadrat methods. Optical methods infer LAI from measurements of radiation transmission through canopies with the use of optical instruments (e.g., LAI-2000, Tracing Radiation and Architecture of Canopies [TRAC], and Digital Hemispherical Photographs), which are efficient and nondestructive; thus, these methods are widely used for ground measurement and remote sensing validation (Chen and Cihlar 1996; Dou et al. 2016; Qu et al. 2014; Zeng et al. 2015). The inclined point quadrat method consists in using thin needles (point quadrats) to pass through the canopy and count the number of

contacts of touches between point quadrats and leaves. It therefore requires a large number of insertions, which leads to huge fieldworks (Jonckheere et al. 2004). Optical point-quadrat method, which consists in measuring heights to the lowest leaves above a set of sample points established on the ground beneath the canopy, is a modification of the point-intercept method (Radtke and Bolstad 2001). This method is less labor-intensive with the use of laser scanning but underestimates total LAI when the foliage is clustered and foliage density is high (Coops et al. 2007; Radtke and Bolstad 2001). Thus, Beer-Lambert law-based optical methods have become the mainstream approach for LAI measurement.

Indirect methods have been rapidly developed and widely used since the 1990s. Literature searches were conducted in Web of Science using the keyword combination TOPIC: ("leaf area index" OR "plant area index") AND TOPIC: (measur* OR estimat* OR method) AND TOPIC: (indirect OR "optical instrument*") (Fig. 2.1, Table 2.1). Results indicate that the number of published items generally increased and approximately 25 papers are being published annually (Fig. 2.1a) in journals on agriculture, forestry, remote sensing, and global change (Table 2.1). The number of citations is one to two orders of magnitude larger than that of published items. The citations are nearly 1200 times in 2016, which is approximately 42 times the number of published items that year (Fig. 2.1b). Several reviews were cited more than 500 times, many of which come from other fields. This finding indicates that LAI indirect measurement methods are widely recognized in the scientific community and have been applied in large fields and industries.

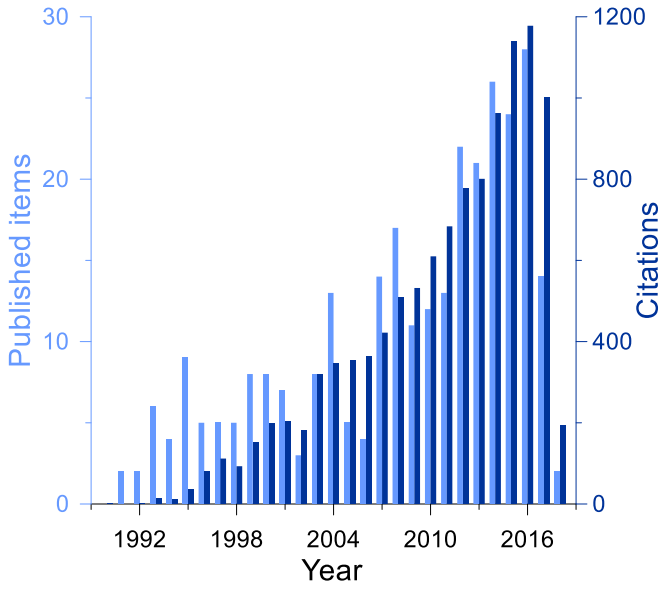


Fig. 2.1 Yearly published items and citations related to indirect LAI measurement. (The search was conducted on March 18, 2018, using Web of Science with the keyword combination TOPIC: ["leaf area index" OR "plant area index"] AND TOPIC: (measur* OR estimat* OR method) AND TOPIC: [indirect OR "optical instrument*"].)

Table 2.1 Relevant journals that published more than four papers related to indirect LAI measurement. (The search was conducted on March 18, 2018, using Web of Science with the keyword combination TOPIC: ["leaf area index" OR "plant area index"] AND TOPIC: [measur* OR estimat* OR method] AND TOPIC: [indirect OR "optical instrument*"].)

| Journal | No. of published items |
|---|---|
| *Agricultural and Forest Meteorology* | 40 |
| *Journal of Applied Remote Sensing* | 36 |
| *Forest Ecology and Management* | 11 |
| *Remote Sensing of Environment* | 9 |
| *Remote Sensing* | 9 |
| *Canadian Journal of Forest Research* | 7 |
| *Tree Physiology* | 6 |
| *Field Crops Research* | 6 |
| *International Journal of Remote Sensing* | 5 |
| *IEEE Transactions on Geoscience and Remote Sensing* | 4 |
| *Global Change Biology* | 4 |
| *Agronomy Journal* | 4 |
| *Sensors* | 4 |

We analyzed the citation network on indirect LAI measurement using CiteSpace (Chen 2006) (Fig. 2.2) starting in the 1990s to consider only complete records of the Web of Science. Four main periods can be considered. In the first period, indirect instruments based on light transmission were widely and successfully used in low crops (Welles 1990). Indirect measurement techniques started to be operational and commercialized during this period. However, these indirect instruments underestimate LAI when applied to forests where leaves are not randomly distributed (Chason et al. 1991; Deblonde et al. 1994; Fassnacht et al. 1994; Smith 1993). Thus, the focus in the second period was dedicated to a better understanding of non-random or clumped forest canopy. The physical definition of LAI was first discussed (Chen and Black 1992a), and the gap-size distribution model was developed for the measurement of forest LAI (Chen 1996; Chen and Cihlar 1995a). The physical mechanism and sampling scheme for measuring forest LAI, which includes clumping index, woody-to-total area ratio, and needle-to-shoot area ratio, were proposed. Several comprehensive reviews and comparisons were made in the third period to summarize theories, sensors, errors, and sampling in indirect LAI measurement (Breda 2003; Garrigues et al. 2008; Jonckheere et al. 2004; Leblanc et al. 2005b; Weiss et al. 2004). The combination of gap-size distribution and finite-length averaging method was also proposed (Leblanc et al. 2005b). In the fourth period, namely, the current one, indirect LAI measurement continues to move forward with wide applications. Considerable efforts were exerted in the past decades to quantify and correct clumping effect, woody components, and leaf angle distribution (LAD) (Hu et al. 2014; Ryu et al. 2010b; Zou et al. 2009); considerable progress was achieved in improving the accuracy and applicability of indirect measurement on slopes (Baret et al. 2010; Gonsamo and Pellikka 2009). A number of new platforms, instruments, and methods, such as laser scanning (Hu et al. 2018; Jupp et al. 2009; Tang et al. 2014a), cover photography (Macfarlane et al. 2007b), and within-crown clumping modeling (Hu et al. 2014; Hu et al. 2018), were recently employed or developed. The cost with hemispherical or cover photography became much less expensive than commercial instruments such as LAI-2000 and also made the success of indirect measurements (Chianucci and Cutini 2013; Garrigues et al. 2008; Ryu et al. 2010b).Two book chapters mainly introduce satellite remote sensing of LAI and clumping index (Chen 2013; Chen 2018), but a comprehensive review of indirect LAI measurement was not conducted since the reviews of Breda (2003), Jonckheere et al. (2004), and Weiss et al. (2004).

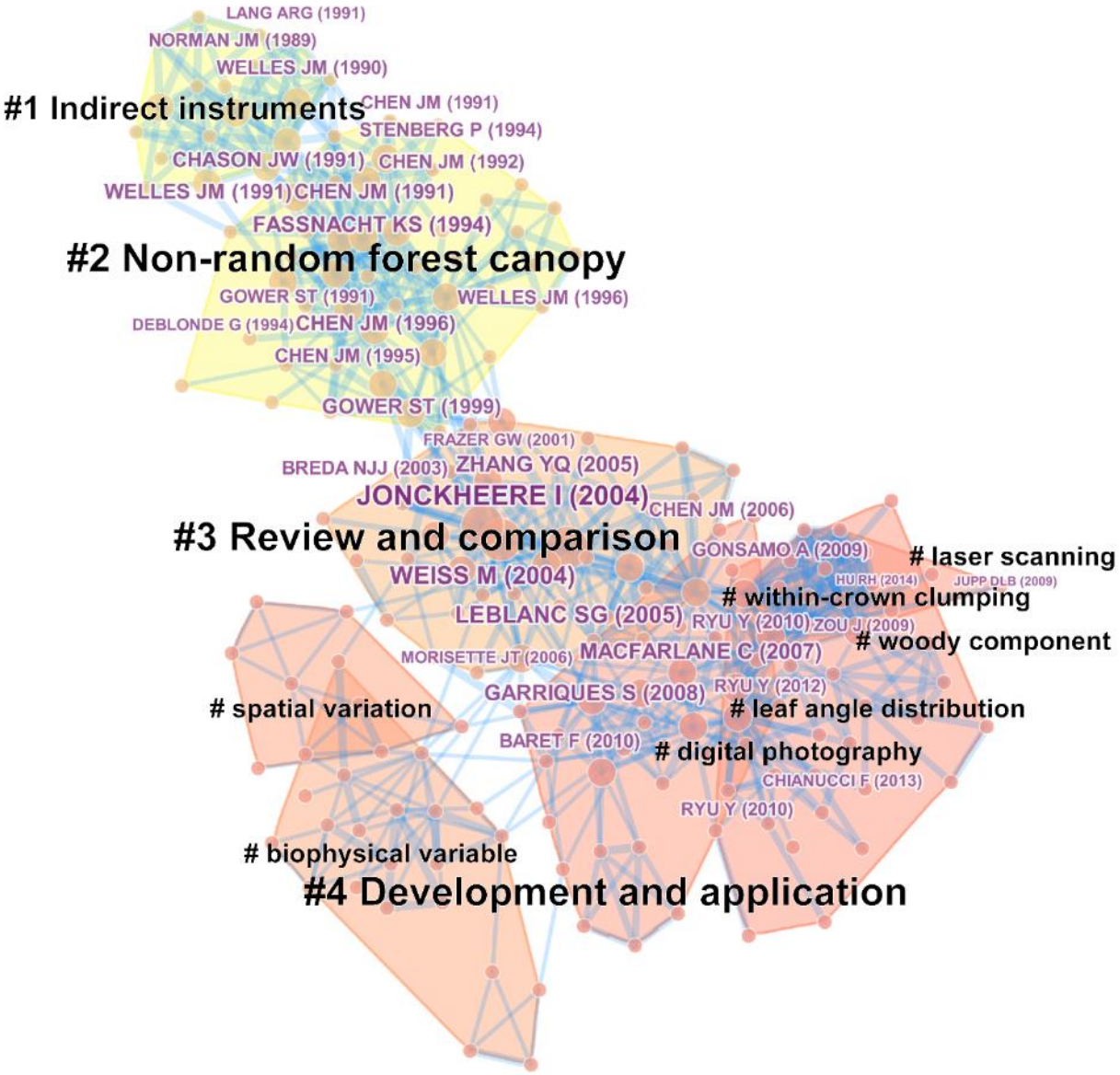


Fig. 2.2 Citation network on indirect LAI measurement since the 1990s

This study comprehensively reviews the development and status of indirect LAI measurement and related theories, algorithms, instruments, and influencing factors. The latest progresses and prospects are summarized and discussed by considering four challenges, namely, clumping/scale effect, LAD, woody component, and slope effect.

## 2.2 Basic Concepts and Theoretical Background

### 2.2.1 LAI definition

LAI is a dimensionless variable originally defined as leaf area (one side) per unit area of land (Watson 1947). This definition is suitable for flat leaves, but unclear for curly or needle-shaped leaves. Therefore, to clarify the notion of leaf area index, detailed definitions were proposed in relation to different applications and contexts. Representative definitions include "half the total leaf area" (Chen and Black 1991; Fassnacht et al. 1994), "half the total intercepting area" (Chen and Black 1992a), and "projected leaf area" (Myneni et al. 1997). The definition "half the total leaf area" pertains to biological processes, such as gas exchange, whereas "total intercepting area" concerns physical processes, such as radiation interception. The definition "projected leaf area" was disregarded because projection of a given area in one direction may differ in another direction when leaves are not flat, thick, or 3D-shaped. Meanwhile, the definitions "half the total leaf area" and "total intercepting area" make no difference for flat leaves, but may introduce large differences for leaves with concave shapes, such as curved or wrinkled broadleaves. Currently, "half the total leaf area per unit ground surface area" is the widely used definition of LAI (Chen and Black 1991; Chen et al. 1991; Jonckheere et al. 2004). Moreover, "ground surface area" is specifically defined as "horizontal ground surface area" to clarify LAI on sloping surface (Gonsamo and Pellikka 2008; Leblanc et al. 2005b). The definition "half the total leaf area per unit horizontal ground surface area" is suitable for all flat and needle-shaped leaves and flat and sloping surface and is friendly for applications.

Given the limitation of instruments and algorithms, indirect LAI measurements are influenced by the architecture of the canopy (e.g. clumping) and by the nature of the vegetation elements that are present, including woods, organs, stems, green or senescent elements. Thus, the measured quantity does not exactly correspond to the actual definition of LAI and additional denominations were proposed in the literature. First, the inversion of the Beer-Lambert law to retrieve LAI assumes a random spatial distribution of the foliage, which leads to the estimation of an effective quantity (effective leaf area index, LAIe) in clumped canopies like forests or row crops (Chen et al. 1991). Second, most of the optical instruments have only one visible band and cannot distinguish leaf and woody components; thus, the results obtained are plant

area index (PAI), which is the sum of the leaf and Woody Area Index (WAI) (Neumann et al. 1989). In addition, some distinctions can also be achieved between green leaves (GLAI – Green Leaf Area Index) and other photosynthetic organs that contain chloroplasts. The Green Area Index (GAI) considers photosynthetically active (e.g. green) plant areas without making differences between leaves, stems, and reproductive organs (Baret et al. 2010). Most users are interested in photosynthesis and carbon and energy exchanges; hence, the definition of LAI (GLAI and GAI) is preferred and widely used for remote sensing products, such as MODIS, GEOLAND, and GLOBCARBON (Baret et al. 2013; Myneni et al. 2002; Plummer et al. 2006).

In most studies, LAI is almost the same as GLAI and GAI, especially when only green leaves are involved. However, PAIe and LAIe are generally different from LAI because leaves are generally clumped in most vegetations, and PAI is also relatively different from LAI in forests because of the presence of woody components.

### 2.2.2 Beer-Lambert Law and Gap Probability Model

The theoretical basis of indirect LAI measurement is the Beer-Lambert law, also known as Beer-Lambert law. It was originally used to describe the attenuation of light in uniform mediums and further extended to light interception of homogenous canopies (De Wit 1965; Monsi and Saeki 2005; Monteith 1965; Ross 1981). The classic relationship between LAI and gap probability was established as follows:

$$P(\theta) = e^{-G(\theta)\cdot LAI/\cos(\theta)}, \qquad (1.1)$$

where $P(\theta)$ denotes the gap probability in viewing zenith angle $\theta$. Gap probability can also be written as gap fraction, where gap probability is close to theory and gap fraction is close to measurement. $G(\theta)$ represents the leaf projection function in the $\theta$ direction that can be calculated from the leaf inclination distribution, and $\cos(\theta)$ is used for considering the optical path length through the homogeneous vegetation layer with random foliage distribution.

Leaves are considerably larger than the molecules in gas or liquid media, but this difference does not limit Beer-Lambert law for indirect LAI measurement because Eq. (1.1) can also be derived from contact frequency theory and binomial models that assume finite leaf size (Monsi and Saeki 2005; Nilson 1971; Wilson 1960). Here, Eq. (1.1) was validated in an accurately simulated homogeneous canopy with random foliage distribution (Fig. 2.3) to show

the accuracy of the theoretical derivation. In the fully controlled environment, the LAI of the canopy is known as 1 by definition and gap fraction could be measured accurately by ray intersection (Widlowski et al. 2013). For simplicity, leaf arrangement is totally horizontal, which provides $G(\theta)=\cos(\theta)$. Theoretical gap probability is consistent with the measured values (Table 2.2) with a difference of less than 5% for 200 m transects and less than 3% for 400 m transects.

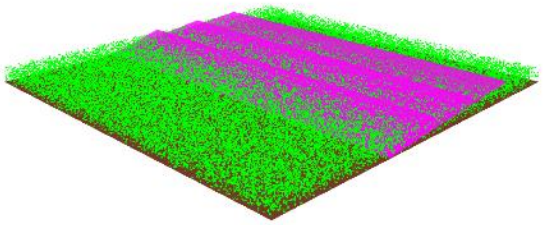

Fig. 2.3 Overview of a 25×25 m² homogeneous canopy composed of 79577 randomly distributed disc-shaped green leaves with a radius of 0.05 m (LAI=1). The pink planes represent the measurement transects.

Table 2.2 Accuracy of Beer-Lambert law in homogeneous canopies for indirect LAI measurement

| Zenith angle (°) | Gap fraction | | |
|---|---|---|---|
| | Theoretical value | Measured value (200 m transect) | Measured value (400 m transect) |
| 0 | 0.3679 | 0.3617 (-1.7%) | 0.3654 (-0.7%) |
| 10 | 0.3679 | 0.3728 (+1.3%) | 0.3650 (-0.8%) |
| 20 | 0.3679 | 0.3742 (+1.7%) | 0.3683 (+0.1%) |
| 30 | 0.3679 | 0.3514 (-4.5%) | 0.3646 (-0.9%) |
| 40 | 0.3679 | 0.3526 (-4.2%) | 0.3637 (-1.1%) |
| 50 | 0.3679 | 0.3758 (+2.1%) | 0.3774 (+2.6%) |
| 60 | 0.3679 | 0.3709 (+0.8%) | 0.3725 (+1.3%) |
| 70 | 0.3679 | 0.3704 (+0.7%) | 0.3680 (+0.0%) |
| 80 | 0.3679 | 0.3594 (-2.3%) | 0.3672 (-0.2%) |

Eq. (1.1) is the classic formula used to calculate LAI in a specific zenith angle. When measurements are conducted at several zenith angles, the final LAI becomes the integration of all zenith angles (Chen and Black 1991; Miller 1967):

$$LAI = 2\int_0^{\pi/2} -\ln\left[P(\theta)\right]\cdot\cos(\theta)\cdot\sin(\theta)d\theta \quad . \tag{1.2}$$

If only the measurements at several discrete zenith angles are available, the final LAI can be weighted as follows:

$$LAI = \sum_{i=1}^{n} LAI(\theta_i)\cdot W_i \quad , \tag{1.3}$$

where $n$ is the number of discrete zenith angles, $LAI(\theta_i)$ denotes the LAI calculated at the zenith angle $\theta_i$, and $W_i$ represents the weighting factor that is proportional to $\sin(\theta_i)\mathrm{d}\theta_i$ and normalized to sum to 1.0.

Several instruments were developed based on this theory for indirect LAI measurement; promising results were achieved in low crops, such as wheat and corn (Ross 1981; Welles and Cohen 1996; Welles and Norman 1991). These instruments underestimate LAI for 30% to 70% in field measurements when applied to a highly complex forest (Chen and Cihlar 1995b; Weiss et al. 2004). The underestimation caused by the clumping effect exists not only in forests, but also in row crops with an underestimation of 11% (Baret et al. 2010). Underestimation is critical, with an underestimation of approximately 20% to 60% when vegetation is small and row structure is significant (Demarez et al. 2008). The main error is caused by homogenous assumption, but the leaves are generally highly clumped in forests.

### 2.2.3 LAD and Leaf Projection Function

The community recognized the impact of LAD as early as the 1950s and 1960s, and a leaf projection function G was introduced to represent its impact on transmission and thus, on indirect LAI measurement (Monsi and Saeki 1953, 2005; Monteith 1965; Wang et al. 2007; Watson 1958)

#### 2.2.3.1 LAD

LAD refers to the mathematical description of the angular orientation of leaves in the vegetation. It is defined as the probability of leaf normal falling within a unit interval of inclination angle. This function meets the condition as follows under the assumption of random distribution of the azimuth angles:

$$\int_0^{\pi/2} g(\theta_l)\,d\theta_l = 1 \quad , \tag{1.4}$$

where $\theta_l$ is the leaf inclination angle.

Several functions with one or two parameters were developed to characterize LAD. Representative forms include trigonometric (De Wit 1965), two-parameter beta distribution (Goel and Strebel 1984), ellipsoidal distribution (Campbell 1990), and rotated ellipsoidal distribution functions (Kuusk 1995; Thomas and Winner 2000). Evaluation with field measurement shows that two-parameter functions, especially beta function, generally perform better than one-parameter functions (Wang et al. 2007).

Ross (1981) summarized various LADs, including spherical, uniform, planophile, erectophile, plagiophile, and extremophile distributions. Various distribution patterns are based on deviation from the spherical LAD, which provides a constant projection coefficient of 0.5 (Table 2.3; Fig. 2.4a):

(1) Spherical distribution, where leaf normals are oriented in all directions with equal probability, is the basic LAD.

(2) Uniform distribution means that leaf normals are oriented in zenith directions with equal probability.

Notably, spherical distribution differs from uniform distribution. Spherical distribution consists of leaves with normals uniformly distributed in hemispherical directions, whereas uniform distribution consists of leaves with normals uniformly distributed in zenith directions.

Other typical patterns, such as planophile, erectophile, plagiophile, and extremophile distributions proposed by De Wit (1965), are defined based on deviation from the spherical distribution:

(3) Planophile distribution refers to leaf arrangement that is predominantly horizontal or has more horizontal leaves than the spherical distribution.

(4) Erectophile distribution denotes leaf arrangement that is predominantly vertical or has more vertical leaves than the spherical distribution.

(5) Plagiophile distribution concerns inclined leaf arrangement with a predominantly inclination angle.

(6) Extremophile distribution consists of double peak curves of the distribution of inclination angles with maxima near 0° and 90°.

Table 2.3 Typical LADs (g)

| | LAD function g($\theta_l$) | Average leaf inclination angle ($\theta$) |
|---|---|---|
| Spherical | $g(\theta_l) = \sin\theta_l$ | 57.30 |
| Uniform | $g(\theta_l) = 2/\pi$ | 45.00 |
| Planophile | $g(\theta_l) = 2\cdot(1+\cos 2\theta_l)/\pi$ | 26.76 |
| Erectophile | $g(\theta_l) = 2\cdot(1-\cos 2\theta_l)/\pi$ | 63.24 |
| Plagiophile | $g(\theta_l) = 2\cdot(1-\cos 4\theta_l)/\pi$ | 45.00 |
| Extremophile | $g(\theta_l) = 2\cdot(1+\cos 4\theta_l)/\pi$ | 45.00 |

#### 2.2.3.2 Leaf projection function

The leaf projection function (G) is the projection coefficient function of unit foliage area on a plane perpendicular to the viewing direction. G has a direct effect on gap fraction at specific viewing angles. G can be represented through LAD (Nilson 1971; Ross 1981):

$$G(\theta,\varphi) = \frac{1}{2\pi}\int_0^{2\pi}\int_0^{\pi/2} g(\theta_l,\varphi_l)\cdot\left|\vec{r}_l\cdot\vec{r}\right| d\theta_l d\varphi_l \tag{1.5}$$

$$\vec{r}_l\cdot\vec{r} = \cos(\theta)\cdot\cos(\theta_l)+\sin(\theta)\cdot\sin(\theta_l)\cdot\cos(\varphi_l-\varphi)\ , \tag{1.6}$$

where $\vec{r}$ is the viewing direction normal; $\vec{r}_l$ denotes the leaf normal; $\theta$ and $\varphi$ represent the zenith and azimuth angles of the viewing direction, respectively; and $\theta_l$ and $\varphi_l$ refers to the zenith and azimuth angles of the leaf, respectively.

In the absence of preferred azimuth orientation (random azimuthal distribution), $G$ can be simplified as follows (Wang et al. 2007; Wilson 1960):

$$G(\theta) = \int_0^{\pi/2} A(\theta,\theta_l)\cdot g_l(\theta_l)\, d(\theta_l) \tag{1.7}$$

$$A(\theta,\theta_L) = \begin{cases} \cos\theta\cdot\cos\theta_l, & \left|\cot\theta\cdot\cot\theta_l\right| > 1 \\ \cos\theta\cdot\cos\theta_l\cdot\left[1+(2/\pi)\cdot(\tan\psi-\psi)\right], & \left|\cot\theta\cdot\cot\theta_l\right| \le 1 \end{cases}, \tag{1.8}$$

where $\psi$=$\cos^{-1}(\cot\theta\cdot\cot\theta_l)$.

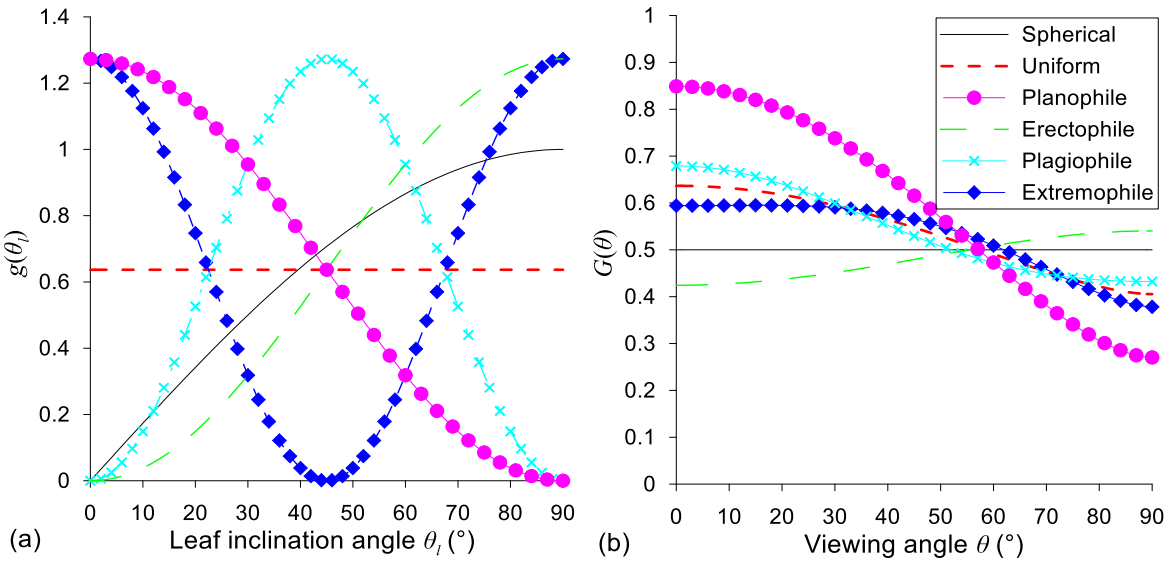


Fig. 2.4 Typical LAD (g) and projection functions (G)

The theoretical derivations of LAD and leaf projection functions are rigorous. The accuracy of G functions was validated by changing the LAD of the homogeneous canopy (Fig. 2.3) to six typical LADs. Gap probabilities vary considerably in different zenith angles and types of LADs, but the LAIs retrieved using Beer-Lambert law are consistent and close to the true value of 1 (Table 2.4) after applying the value of $G(\theta)$ in Eq. (1.1).

Table 2.4 Accuracy of leaf projection function (G) in homogeneous canopies for indirect LAI measurement

| Zenith angle (°) | | LAD | | | | | |
|---|---|---|---|---|---|---|---|
| | | Spherical | Uniform | Planophile | Erectophile | Plagiophile | Extremophile |
| 0 | P | 0.613 | 0.533 | 0.432 | 0.660 | 0.518 | 0.554 |
| | LAI | 0.98 | 0.99 | 0.99 | 0.98 | 0.97 | 0.99 |
| 10 | P | 0.611 | 0.530 | 0.431 | 0.653 | 0.517 | 0.550 |
| | LAI | 0.97 | 0.99 | 0.99 | 0.98 | 0.97 | 0.99 |
| 20 | P | 0.593 | 0.520 | 0.432 | 0.635 | 0.516 | 0.534 |
| | LAI | 0.98 | 1.00 | 0.99 | 0.98 | 0.97 | 0.99 |
| 30 | P | 0.566 | 0.507 | 0.433 | 0.601 | 0.510 | 0.510 |
| | LAI | 0.99 | 0.99 | 0.98 | 0.98 | 0.97 | 0.99 |
| 40 | P | 0.525 | 0.484 | 0.427 | 0.552 | 0.493 | 0.475 |
| | LAI | 0.99 | 0.99 | 0.99 | 0.97 | 0.98 | 0.99 |
| 50 | P | 0.466 | 0.443 | 0.416 | 0.473 | 0.459 | 0.430 |
| | LAI | 0.98 | 0.99 | 0.99 | 0.98 | 0.98 | 0.99 |
| 60 | P | 0.373 | 0.380 | 0.392 | 0.370 | 0.395 | 0.366 |
| | LAI | 0.99 | 0.99 | 0.99 | 0.98 | 0.98 | 0.99 |

P refers to the measured gap fraction; LAI is the result of Beer-Lambert law [Eq. (1.1)]

### 2.2.4 Clumping Index

The underestimation of Beer-Lambert law in non-random distributed canopies is widely recognized. The clumping index is defined to quantify underestimation and correct LAI estimation. Nilson (1971) synthesized the gap probability in canopies with random, regular or clumped distribution of leaves based on Markov model and proposed a common formula by introducing parameter $\lambda_0$ to Eq. (1.1):

$$P(\theta) = e^{-\lambda_0 \cdot G(\theta) \cdot LAI / \cos\theta} \quad , \tag{1.9}$$

where $\lambda_0$=1 represents random distribution, $\lambda_0$>1 denotes the regular distribution, and $\lambda_0$<1 is the clumping distribution; $\lambda_0$ was also called clumping index Ω by Black et al. (1991):

$$\Omega = LAI_e / LAI \quad , \tag{1.10}$$

where LAIe is the effective LAI defined as the product of clumping index Ω and LAI (Black et al. 1991; Chen et al. 1991), i.e., the result of Beer-Lambert law including clumping. In coniferous forests, the clumping index could be calculated from two components:

$$\Omega = \Omega_E / \gamma_E \quad , \tag{1.11}$$

where $\Omega_E$ is the clumping index at scales larger than the shoot and can be measured by optical instruments. $\gamma_E$ is the needle-to-shoot ratio that describes the clumping at scales smaller than the shoot; this variable is introduced to convert the shoot area to the needle area and should be measured by destructive sampling (Chen and Cihlar 1995b). In broadleaf forests, $\gamma_E$=1 and $\Omega=\Omega_E$; thus, clumping index can be measured by optical instruments alone.

### 2.2.5 Woody-to-total Area Ratio

The results of indirect methods in forests are PAI and include the contribution of woody components and leaves because traditional optical instruments cannot distinguish leaves from branches (Chen 1996; Neumann et al. 1989; Whitford et al. 1995). The impact of woody components varies for different species; direct measurements show that the ratio of woody components to leaves is approximately 8% to 12% in red pine and approximately 10% to 33% in jack pine (Deblonde et al. 1994). Gower et al. (1999) summarized the ratios of WAI to PAI for some species; however, the ratio varies with the viewing zenith angle and azimuth angle (Zou et al. 2009). The ratio of woody components also varies with seasons. Thus, using

empirical values does not cause errors to the optical indirect measurement.

To remove the impact of woody components, a woody-to-total area ratio $\alpha$ is introduced to represent the ratio of woody component to PAI (Chen 1996):

$$LAI = (1-\alpha) \cdot PAI \quad , \tag{1.12}$$

where PAI can be calculated using Eq. (1.13):

$$PAI = \frac{-\ln\left[P(\theta)\right] \cdot \cos\theta}{G(\theta) \cdot \Omega} \quad . \tag{1.13}$$

The measurements of woody components could be classified into three main categories. The first is direct measurement of woody components by destructive sampling and regression, which is time consuming and labor intensive (Deblonde et al. 1994; Lang et al. 1991). The second is indirect measurement in the leafless period. The LAI and woody-to-total area ratio are obtained from two measurements in the leafless and leafy periods (Barclay et al. 2000; Cutini et al. 1998). This method is more convenient than the direct method, but is not suitable for evergreen forests and does not consider mutual occlusion between leaf and woody components (Zou et al. 2009). The third method is indirect measurement with near-infrared photography, which distinguishes woody components using its low reflectance characteristics in near-infrared band (Kucharik et al. 1998a; Yan et al. 2008; Zou et al. 2009). Near-infrared photography quantifies woody-to-total area ratio in one observation; thus, it has great advantages in efficiency but its results are partly influenced by the mutual occlusion between leaf and woody components. Considering the mutual occlusion between leaf and woody components is not a major error source, this method is still practical for operational measurements of woody-to-total area ratio. However, the woody components were not measured in most ground experiments because current commercial instruments do not have near-infrared band and are incapable of directly distinguishing woody and leaf components. In additions to woody components in trees, other non-photosynthetic components, such as stems of corns and ears of wheats, may also significantly contribute to PAI for crops.

## 2.3 Methods to Retrieve True LAI from Indirect Gap Fraction Measurements

Several methods were developed to quantify the clumping index and calculate the true

LAI. Representative methods include the finite-length averaging method (Lang and Xiang 1986), gap-size distribution method (Chen and Cihlar 1995b; Leblanc 2002), combination of the gap-size distribution and the finite-length averaging methods (Leblanc et al. 2005a), and path length distribution method (Hu et al. 2014).

### 2.3.1 Finite-Length Averaging Method

The finite-length averaging method (LX) is an early attempt to address clumping effect. Stating that if the LAI is a logarithmic function of the gap fraction, then, the average LAI should be a logarithmic function of the average gap fraction, Lang and Xiang (1986) proposed averaging the logarithms of gap probabilities over segments of finite length.

In accordance with the finite-length averaging method, LAI can be calculated using gap fraction at viewing direction $\theta$:

$$LAI_{LX}(\theta) = -\frac{\overline{\ln\left[P(\theta)\right]}\cdot\cos\theta}{G(\theta)} \quad , \tag{1.14}$$

where $\overline{\ln\left[P(\theta)\right]}$ is the mean value of logarithmic gap fractions of all segments.

This method is based on the assumptions that (1) the leaves within the finite length segments are randomly distributed, and (2) each segment contains gaps. The finite-length averaging method is widely used, especially in crop and grass measurements, because this method easy to use and can correct clumping to some degree (Lang 1991; Liu et al. 2013; Ryu et al. 2012). However, while it corrects from non-randomness among segments, it cannot correct from non-randomness within each segment. Furthermore, it is necessary to define the segment length: if the segment is too short, then the sampling does not meet the Beer law requirements (infinite turbid medium); if the segment is too long, then the clumping effect within segments becomes more significant. The choice of 10 times the characteristic width of a leaf for segment length appears as a good compromise because, theoretically, the error introduced by applying Beer-Lambert law on such a short segment is about 5% (Lang and Xiang 1986).

When a segment does not contain any gap, the method fails since logarithm of zero (no gaps) is undefined (Leblanc et al. 2005b). The segment can then be removed or assigned a value. For photography method, a gap of one pixel is added in the segment. The LAI of segments with no gaps is given by:

$$LAI_{\max}(\theta) = -\ln\left(\frac{1}{N_{pixel}}\right)\cdot\cos\theta / G(\theta) \ , \qquad (1.15)$$

where $N_{pixel}$ denotes the number of pixels in a segment for photography, and high LAI values are forced to the upper limit of 10 (Leblanc et al. 2005a; Pisek et al. 2011a). Another method is to directly assign a maximum LAI to the segment in agreement with the observed canopy and to assign the corresponding gap fraction value (Weiss and Baret 2016).

Segments without gap appear frequently in dense forests. The methods employed to deal these segments are generally empirical without prior reasons. Removing these segments underestimates LAI, whereas adding a gap of one pixel is dependent on the pixel resolution of the photograph (Leblanc et al. 2005b). Thus, this method is a mathematical fix of the problem in the right direction, but not a solution.

### 2.3.2 Gap-Size Distribution Method

The gap-size distribution method (CC) was proposed by Chen and Cihlar (1995a) to quantify the clumping effect in vegetation covers with distinct structure and was later corrected by Leblanc (2002). The method removes non-random gaps based on gap-size distribution theory and can efficiently eliminate large gaps between crowns (Chen and Cihlar 1995a; Leblanc 2002).

LAI in the total transect can be expressed as follows:

$$LAI_{CC} = -\frac{\ln\left[F_{mr}(0,\theta)\right]\cdot\cos\theta}{G(\theta)}\cdot\frac{1-F_{m}(0,\theta)}{1-F_{mr}(0,\theta)} \ . \qquad (1.16)$$

The measured gap-size accumulation function $F_m(\lambda,\theta)$, which is defined as the fraction of gaps larger than λ, can be obtained through an optical instrument, such as TRAC or digital photography.

$F_m(0,\theta)$ is the accumulated canopy gap fraction, and $F_{mr}(0,\theta)$ is the reduced gap-size accumulation fraction after removal of the large, non-random gaps based on the gap-size accumulation function of random canopy $F_r(\lambda,\theta)$:

$$F_r(\lambda,\theta) = \left(1+L_p(\theta)\cdot\frac{\lambda}{W_p(\theta)}\right)\exp\left[-L_p(\theta)\cdot\left(1+\frac{\lambda}{W_p(\theta)}\right)\right] \ , \qquad (1.17)$$

where $L_p$ is the projected LAI and first taken as $-\ln[F_m(0,\theta)]$, and $W_p$ represents the mean projected width of foliage element.

The presence of large gaps is the main cause for the underestimation of LAI. Thus, the measured gaps appearing at probabilities $F_m(\lambda,\theta)$ in excess of $F_r(\lambda,\theta)$ are then removed. A new gap-size accumulation function $F_{mr}(\lambda,\theta)$ is computed, and $L_p$ is assigned a new value of $-\ln[F_{mr}(\lambda,\theta)]$. The final $F_{mr}(\lambda,\theta)$ and $F_{mr}(0,\theta)$ are found after several iterations until the new distribution closely overlaps $F_r(\lambda,\theta)$ (Chen and Cihlar 1995a).

The gap-size distribution method is widely used in vegetation covers with a distinct structure because this method effectively eliminates large gaps between tree crowns and branches (Chen et al. 1997; Gonsamo and Pellikka 2009; Leblanc and Chen 2001).

This method is derived based on physical principles. The measured gap-size distribution $F_m(\lambda,\theta)$ in a homogeneous canopy with random foliage distribution is consistent with the theoretical value of $F_r(\lambda,\theta)$ (Fig. 2.5), which was calculated from Eq. (1.17). However, several potential problems still exist in the gap-removal process. First, the start condition of gap-removal process is that $F_m(\lambda,\theta)$ exceeds $F_r(\lambda,\theta)$, and the stop conditions include a portion of $F_{mr}(\lambda,\theta)$, which falls below $F_r(\lambda,\theta)$. $F_r(\lambda,\theta)$ is an ideal smooth curve, whereas $F_m(\lambda,\theta)$ is a measured jagged curve. Thus, these two curves may not fully overlap, even in an ideal homogeneous canopy. These two curves have the same starting point because $F_r(0,\theta)$ is equal to $F_m(0,\theta)$ by definition. $F_m(\lambda,\theta)$ often partly falls below and partly exceeds $F_r(\lambda,\theta)$, especially at small λ value. Therefore, the start and stop conditions are often met at the same time. The $F_r(\lambda,\theta)$ represents the homogeneous canopies accurately, but the gap-removal process cannot guarantee that the $F_{mr}(\lambda,\theta)$ also agrees with $F_r(\lambda,\theta)$ well. Second, this method separates the data into two parts, wherein one part is composed of large gaps and the second part is composed of the remaining data after removing large gaps. Beer-Lambert law is applied in part two, and the result is extended to the complete area using the proportion of part one. In addition, a homogeneous canopy with leaves randomly distributed results in a theoretical $F_r(\lambda,\theta)$, whereas a theoretical $F_r(\lambda,\theta)$ does not necessarily result from a homogeneous canopy. If the spatial position of the gaps can be arranged according to gap size, then $F_r(\lambda,\theta)$ will not change but the canopy will not remain homogeneous. However, gap-size distribution is a groundbreaking method that should be further explored.

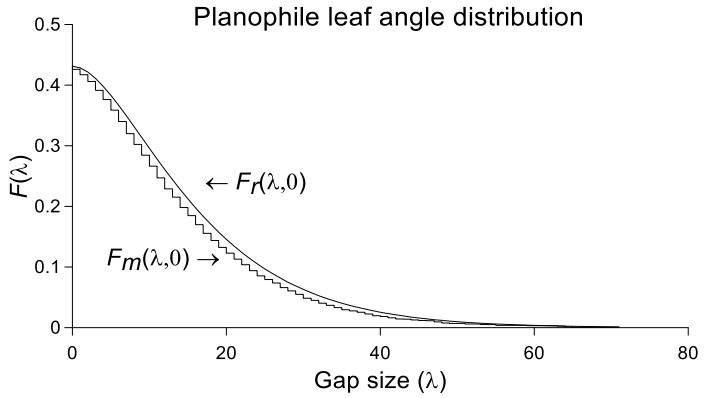


Fig. 2.5 Gap-size distributions in the zenith direction of a homogeneous canopy with planophile LAD

### 2.3.3 Combination of Gap-Size Distribution and Finite-Length Averaging Methods

To address the two problems of segment length in the finite-length averaging method, Leblanc et al. (2005b) developed a new method (CLX method) by combining CC and LX methods.

Given that the large segments might not be homogeneous, the CC method is used within every segment to address heterogeneity within segments. The final LAI is then calculated over $n$ segments as follows:

$$LAI_{CLX}(\theta) = -\frac{\sum_{k=1}^{n} \ln\left[P_k(\theta)\right] / \Omega_{CCk}(\theta) \cdot \cos\theta}{n \cdot G(\theta)} \quad , \qquad (1.18)$$

where $\Omega_{CCk}(\theta)$ is the clumping index within segment $k$ using the CC method and $P_k(\theta)$ is the gap fraction of segment $k$.

Combining mathematical fixes and physical methods is an interesting idea, which theoretically considers non-randomness within and between segments. However, if the CLX method was found less affected by the choice of the segment length than the LX method (Leblanc and Fournier 2014), some authors also demonstrated that this latter has still an impact on the LAI estimation (Pisek et al. 2011a). However, considering that the CLX method showed better retrieval statistics than the CC method which underestimates LAI (Hu et al. 2014; Leblanc et al. 2005b), further investigation is required to determine a proper segment length for the CLX method. Validation using hemispherical photography and 3D forest simulation showed that CLX method with 45° segments is more robust than that with 15° segments over a wide

range of conditions (Leblanc and Fournier 2014). The result is reasonable because the CC method requires sufficient gap-size distribution data to be stable (Yan et al. 2016b).

### 2.3.4 Path Length Distribution Method

To address the crown-shape-induced clumping effect within crowns, Hu et al. (2014) proposed the path length distribution method (PATH) by introducing path length distribution to the theoretical prototype of Beer-Lambert law. Path length distribution theory can address not only the clumping effect between crowns, but also crown-shape-induced non-randomness within crowns, which may lead to a LAI underestimation of up to 25%.

As a relatively new method, its main difference from other better-known methods is the consideration of path length, which is defined in the theoretical prototype of Beer-Lambert law, but is not explicitly considered in other methods. Path length distribution has the advantages of considering tree crown shapes and tree height distributions, which are essential for modeling the 3D spatial distribution of leaves and within-crown clumping.

The input of the path length distribution model is the average gap probability and the corresponding path length distribution. Path length distribution, which is used to consider the clumping effect, can be obtained by traditional gap transect measurement, 3D construction, or elliptical cross section assumption. Thus, PATH is applicable for TRAC, photography, terrestrial or airborne laser scanner, and LAI-2000.

Path length is defined as the length of a ray passing through a tree crown or several tree crowns (Fig. 2.6a). The distance between two tree crowns or between the sensor and a tree crown is not regarded as path length, which only concerns media with leaves.

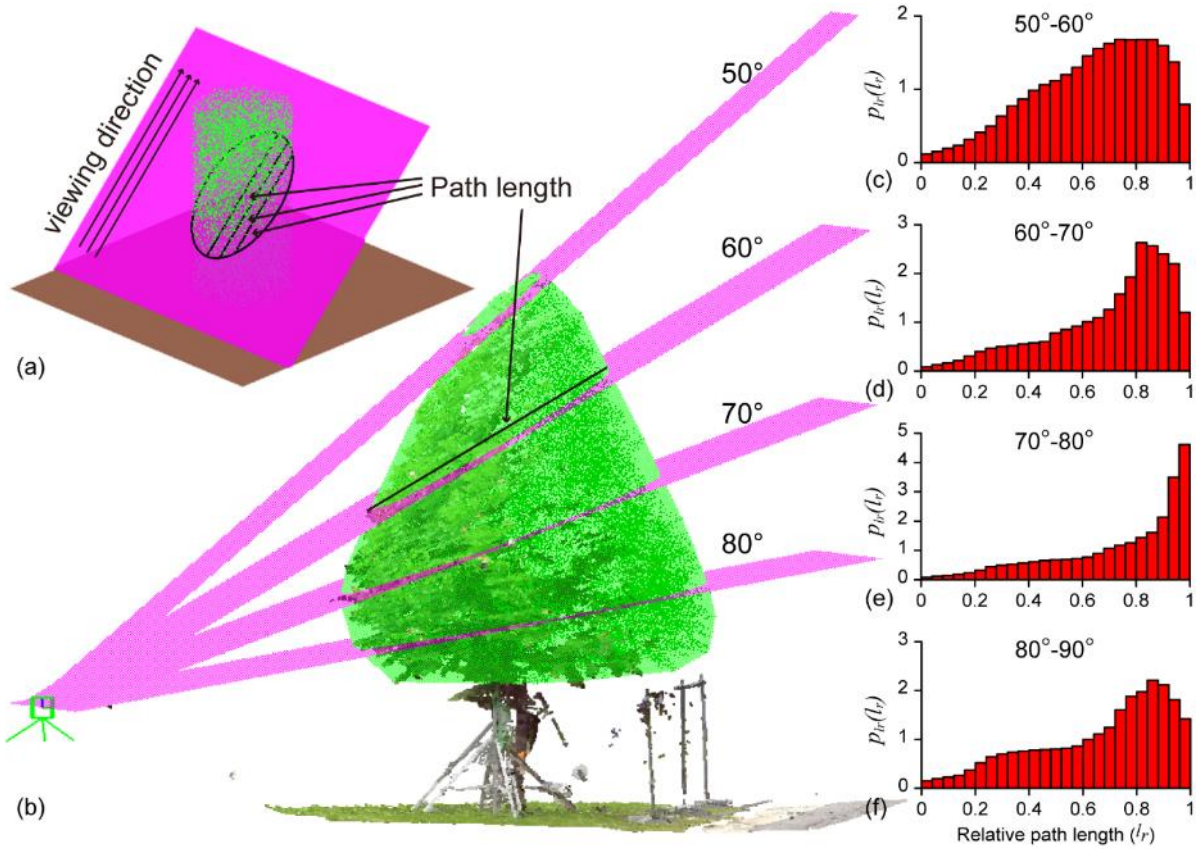


Fig. 2.6 Illustration of path length distribution: (a) path length within a tree crown observed by parallel projected instruments, (b) path length within a silver linden observed by a terrestrial laser scanner in different zenith angle ranges, (c)–(f) path length distribution ($p_{lr}(lr)$) in 50°–60°, 60°–70°, 70°–80°, and 80°–90° zenith angle, respectively. The path lengths are normalized to 1 as relative path lengths ($lr$) with regards to the maximum value

Path length distribution is defined as the probability density function of path lengths that correspond to the gap probability measurement. The integral of the distribution function is normalized to 1 for convenience of further calculation. Fig. 2.6a illustrates path lengths within a tree crown observed by parallel projected instruments, such as TRAC. For instruments with perspective projection, such as terrestrial laser scanner, hemispherical instruments, and LAI-2000, the path lengths are also measured in perspective projection that correspond to gap probability observation (Fig. 2.6b).

The final LAI can be expressed as follows:

$$LAI_{PATH}(\theta) = \int_0^1 (\rho \cdot l_{\max}) \cdot \cos\theta \cdot lr \cdot p_{lr}(lr)\, d(lr) \quad , \qquad (1.19)$$

where $\rho$ is the foliage area volume density and $l_{\max}$ denotes the maximum path length along the transect. Intermediate variables $\rho \cdot l_{\max}$ can be retrieved by Eq. (1.20) with root-finding

algorithms. Relative path length $lr = l / l_{\max}$ and the path length distribution function $p_{lr}(l_r)$, where $\int_0^1 p_{lr}(lr)\,d(lr) = 1$, can be obtained from the measured gap transect or an elliptical cross-section assumption (Hu et al., 2014):

$$\overline{P} = \int_0^1 e^{-G\cdot(\rho\cdot l_{\max})\cdot lr} \cdot p_{lr}(lr)\,d(lr) \quad , \tag{1.20}$$

where $\overline{P}$ is the total gap probability along the transect. All other quantities are known in Eq. (1.20); hence, $\rho \cdot l_{\max}$ can be retrieved. The final LAI is obtained from Eq. (1.19).

Field measurements and realistic simulations show that the path length distribution method characterizes the non-randomness caused by inconsistent path length within crowns. This method improves the accuracy of indirect LAI measurement with a deviation of less than 10% (Hu et al. 2016a; Hu et al. 2014; Yan et al. 2016b; Zeng et al. 2015).

As a new method, path length distribution requires further studies and improvements, such as the study of heterogeneous leaf area density within crowns and the removal of large gaps between crowns. First, several methods have been used to obtain path length distribution for different instruments, including ellipse assumption, traditional gap transect measurement (Hu et al. 2014), and 3D construction. The ellipse assumption corrects the crown-shape-induced clumping but is not tailored. Thus, this assumption is only recommended when no additional information is available for applying any other method. This assumption is useful for legacy instruments, such as LAI-2000, which only measures total gap fraction. The other two methods, namely, inversion from traditional gap transect measurement and 3D construction, have their own advantages and disadvantages. The 3D construction that uses laser scanner provides an accurate crown envelope, but it cannot consider heterogeneous leaf area density within crowns. The inversion from traditional gap transect measurement is based on a sliding window, which will smoothen the change of path lengths. However, this inversion considers heterogeneous leaf area density because its path length distribution is inversed from the measured gap probability distribution, which reflects the information of both variable path length and variable leaf area density. Second, the removal of large gaps between crowns is based on a simple threshold of 10 times the characteristic width of a leaf in the current version, which works well for most situations but needs to be further investigated. The simple threshold fails in some simulated canopies with extremely large leaves and sometimes requires adjustment. Given that the CC method performs very well in removing large gaps, it might be a potential alternative to integrating the CC method and PATH.

Table 2.5 Representative methods for indirect LAI measurement

| Algorithm | Main formula |
|---|---|
| Beer-Lambert law | $LAI_e = -\frac{\ln\left[\overline{P(\theta)}\right]\cdot\cos\theta}{G(\theta)}$ |
| Finite-length averaging method (Lang and Xiang 1986) | $LAI_{LX}(\theta) = -\frac{\overline{\ln\left[P(\theta)\right]}\cdot\cos\theta}{G(\theta)}$ |
| Gap-size distribution method (Chen and Cihlar 1995a; Leblanc 2002) | $LAI_{CC}(\theta) = -\frac{\ln\left[F_{mr}(0,\theta)\right]\cdot\cos\theta}{G(\theta)}\cdot\frac{1-F_m(0,\theta)}{1-F_{mr}(0,\theta)}$ |
| Combination of gap-size distribution and finite-length averaging methods (Leblanc et al. 2005b) | $LAI_{CLX}(\theta) = -\frac{\sum_{k=1}^{n}\ln\left[P_k(\theta)\right]/\Omega_{CCk}(\theta)\cdot\cos\theta}{n\cdot G(\theta)}$ |
| Path length distribution method (Hu et al. 2014) | $LAI_{PATH}(\theta) = \int_0^1(\rho\cdot l_{\max})\cdot\cos\theta\cdot lr\cdot p_{lr}(lr)\,d(lr)$<br>$\overline{P} = \int_0^1 e^{-G\cdot(\rho\cdot l_{\max})\cdot lr}\cdot p_{lr}(lr)\,d(lr)$ |

$F_m(0,\theta)$ and $F_{mr}(0,\theta)$ are the total gap fraction before and after removing large gaps, respectively; $P_k(\theta)$ and $\Omega_{CCk}(\theta)$ represent the gap fraction and clumping index within segment k using the gap-size distribution method, respectively; and $p_{lr}(lr)$ denotes path length distribution.

### 2.3.5 Comparison of Various Clumping Correction Methods

Several comparisons were made to analyze strengths and weaknesses of multiple methods (Gonsamo and Pellikka 2009; Hu et al. 2014; Leblanc et al. 2005b; Pisek et al. 2011a; Woodgate et al. 2017). The LX, CC, and CLX methods are the most validated methods and the relative magnitude of their results is generally consistent among all comparisons. Among these three methods, the CC method generally provides the lowest LAI, the LX methods provides larger results than the CC method, the CLX method provides the largest results. The CC method does not need spatial pattern assumptions but underestimates LAI in several comparisons (Hu et al. 2014; Leblanc et al. 2005b; Pisek et al. 2011a; Yan et al. 2016b). The CLX was reported to give results closest to reference values in several comparisons (Leblanc et al. 2005b; Leblanc and Fournier 2014; Woodgate et al. 2017) but its performance is affected by the choice of segment size (Pisek et al. 2011a). Leblanc and Fournier (2014) shows that the CLX method with 45° segments performs better than that with 15° segments over a wide range of conditions but

Woodgate et al. (2017) provides the opposite results. The validations in the scenes with different LAI values also show considerable differences (Leblanc et al. 2005b). Moreover, the validation is also limited by the accuracy of reference values because allometric methods used in some validations also have uncertainties.

In this thesis, we validate the clumping correction methods (Table 2.5) in several realistic discrete broadleaf forest scenes (Hu et al. 2014); LAI ranged from 1.19 to 9.92, each of which consists of 614 cylindrical or spherical plant crowns in a 270 m × 270 m plot. Each plant crown is composed of circular leaves with known leaf areas and leaf angles. All methods correct the clumping effect and improved the results compared with LAIe, but some differences were found among different methods (Fig. 2.7).

The LX method is sensitive to the choice of amending method for segments in dense forests without gap. Adding a gap of one pixel is a common way to deal with segments without gap, but its results (LAI_LX_1) theoretically underestimate LAI because a segment without gap generally has larger LAI than a segment with gap of one pixel. The underestimation of LAI_LX_1 is more serious when LAI is larger than 6 because there are more segments without gap in dense forests. Assigning twice the result of a segment with a gap of one pixel is an alternative to avoid underestimation, but the results (LAI_LX_2) overestimate LAI. Removing segments without gap will provide smaller result than LAI_LX_1 because the average result of all segments is smaller than that of a segment with a gap of one pixel. Therefore, there is no good solution to deal with segments without gap in dense forests. Adding one pixel to the LX method is favorable in sparse forests where the LAI is approximately less than 4.

The CC method underestimates LAI in these scenes, where leaf density is uniform in tree crowns but the path lengths within crowns vary. The CC method tends to underestimate LAI because small gaps are not accurately determined when the solar beam is used as probe because of the penumbra effect, while the variation of path length through the canopy due to tree crown shape may distort gap-size distribution in a way that prevents the reconstruction of a random canopy through large gap-size removal. The stop condition of the gap-removal process was met after large gaps between crowns were removed. However, the non-random spatial distribution of leaves caused by crown shape was not corrected completely.

The LAI_CLX_45, whose segment length is 45 times the characteristic width of a leaf, is consistent with the true value and underestimates LAI when it is very large. However, the LAI_CLX_10, whose segment length is 10 times the characteristic width of a leaf, is not good

enough. The CLX method is less affected by segment length, but additional studies are needed to determine a proper and consistent segment length for ground measurements.

The path length distribution method performs best here because the between-crowns and within-crowns clumping in the scenes are considered in path length distribution model. The results (LAI_PATH) present and prove its advantages of considering tree crown shape and the variable path lengths over other methods. However, the real forests are more complex. In addition to the variable path lengths caused by the tree crown shape, leaf density also varies within crowns. Inverting path length distribution from traditional gap transect measurement can theoretically conserve the information of variable leaf density and path length, but the sliding window smoothens the change of path length distribution and requires further study.

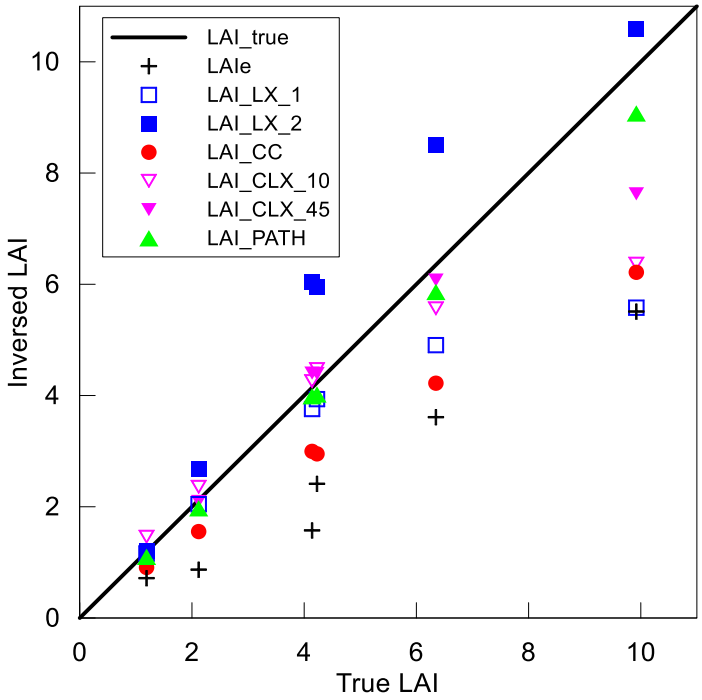


Fig. 2.7 Comparison of various clumping correction methods in discrete broadleaf forest scenes, using the finite-length averaging method by adding a gap of one pixel (LAI_LX_1) and by assigning twice the result of a segment with a gap of one pixel (LAI_LX_2) for a segment with no gap, the gap-size distribution method (LAI_CC), the combination of the gap-size distribution and the finite-length averaging method with a segment length of 10 times (LAI_CLX_10) and 45 times (LAI_CLX_45) the characteristic width of a leaf, the path length distribution method (LAI_PATH).

## 2.4 Instruments for Indirect LAI Measurement

Several instruments in different forms were developed for indirect LAI measurement (Table 2.6). These instruments retrieve LAI indirectly based on Beer-Lambert law by measuring gap fraction or transmission. However, they have differences in theory, usage, processing, and application.

Table 2.6 Representative instruments for indirect LAI measurement

| Instrument | Spectral domain | Source data | Sensor | Sampling strategy | Gap distribution | Reference measurement | Real-time results | Zenithal coverage | Azimuthal coverage |
|---|---|---|---|---|---|---|---|---|---|
| LAI-2000 | 320–490 nm | Diffuse | Fisheye optical sensor | Point | No | Yes | Yes | 0°–75° | 0°–360° |
| TRAC | PAR (400–700 nm) | Direct | 3 PAR sensors | Transect | Yes | Yes | No | Direction of the sun | Direction of the sun |
| DEMON | 430 nm | Direct | Narrow-FOV sensor | Transect | No | Yes | Yes | Direction of the sun | Direction of the sun |
| AccuPAR | PAR (400–700 nm) | Diffuse and direct | 80 PAR sensors | Point | Yes | Yes | Yes | - | - |
| SunScan | PAR (400–700 nm) | Diffuse and direct | 64 PAR sensors | Point | Yes | Yes | Yes | - | - |
| DHP | Depending on the camera | Hemispheric images | Digital camera | Point | Yes | No | No | 0°–90° | 0°–360° |
| DCP | Depending on the camera | Cover images | Digital camera | Point | Yes | No | No | ~0° | - |
| MVI | VIS (400–620 nm) and NIR (720–950 nm) | Cover images | Multispectral digital camera | Point | Yes | No | No | ~0° | - |
| MCI | VIS (390–690 nm) and NIR (760–900 nm and 850–900 nm) | Cover images | Multispectral digital camera | Point | Yes | No | No | 0°–90° | 0°–360° |
| Terrestrial LiDAR | Depending on the hardware | Distance, intensity | Laser scanner | Point | Yes | No | No | 0°–90° | 0°–360° |
| Airborne LiDAR | Depending on the hardware | Distance, intensity | Laser scanner | - | - | No | No | Typically 0°–30° | - |
| Spaceborne LiDAR | 1064 nm (GLAS) | Distance, intensity | Laser scanner | - | No | No | No | Nadir | - |

### 2.4.1 LAI-2000

The LAI-2000 Plant Canopy Analyzer (LI-COR, Lincoln, NE, USA) and its improved successors LAI-2200 and LAI-2200C are commonly used as portable instruments for indirect LAI measurement by diffuse transmission (Welles and Cohen 1996). They use a fish-eye optical sensor with a field of view of 148°, which includes five rings with central zenith angles of 7°, 23°, 38°, 53°, and 68°.

Measurements made above and below the canopy are used to calculate canopy light interception at five zenith angles. The retrieval of LAI-2000 is based on four assumptions: (1) the foliage is an optically black body that does not reflect or transmit light from 320 nm to 490 nm; (2) the foliage is randomly distributed within the canopy; (3) foliage elements are small relative to the area of view of each ring; and (4) the foliage has random azimuthal orientations.

LAI-2000 can be used for all measurements, logging, and processing in the control unit. The successors of LAI-2000 use the same theory while making some improvements. LAI-2200 mainly upgrades the hardware and provides a powerful post-processing software that enables detailed data analysis (Li-COR 2011). LAI-2200C provides a mechanism for correcting light scattering with a diffuser cap (Kobayashi et al. 2013), thereby allowing users to perform measurements under almost any sky condition (Pearse et al. 2016).

LAI-2000 was successfully used to estimate LAI in homogeneous canopies, such as soybean, wheat, and grass (Jonckheere et al. 2004; Welles and Norman 1991). However, in heterogeneous canopies such as forests, LAI-2000 provide underestimations of LAI by approximately 35% to 40% because of foliage clumping (Chen and Black 1992b; Gower and Norman 1991). Ryu et al. (2010a) suggested calculating LAIe by taking the logarithm of the mean gap fraction of LAI-2000 and calculating LAI by taking the mean of the logarithms of multiple gap fraction measurements (Lang and Xiang 1986). Their ratio is the apparent clumping factor (Ryu et al. 2010a), which accounts for clumping on spatial scales larger than the field of view of the sensor (Li-COR 2011). However, clumping still exists on spatial scales smaller than the field of view of the sensor because detailed information within the field of view of each LAI-2000 ring is unavailable. Combining TRAC and LAI-2000 is recommended to ensure that TRAC quantified the clumping information while LAI-2000 measures LAIe without knowledge of the LAD (Chen et al. 1997; Leblanc et al. 2005a).

### 2.4.2 TRAC

The portable TRAC (3rd Wave Engineering, Nepean, ON, Canada) instrument allows quantifying the clumping effect and thus providing the true LAI rather than LAIe (Chen and Cihlar 1995a; Leblanc et al. 2005a). The TRAC Photosynthetically Active Radiation (PAR) sensors measure the transmitted direct light in the sun direction. It provides "gap-size" distribution, in addition to the canopy gap fraction. (Chen and Cihlar 1995a; Leblanc 2002)

Measurements should be performed under cloudless conditions, at different times during the day to cover a wide range of zenith angles. At least, half a clear day is recommended for TRAC measurement to obtain an accurate LAI value using TRAC alone (Leblanc et al. 2005a).

### 2.4.3 DEMON

DEMON (CSIRO, Canberra, ACT, Australia) measures direct solar beam transmission through a directional narrow angle of view (0.302 sr) at a band near 430 nm because leaves have less than 5% transmission and reflectance in this band (Lang et al. 1985; Ross 1981). It measures transmission along the transect and accommodates clumping effect using the finite-length averaging model (Lang and Xiang 1986).

Measurements should be performed under cloudless conditions with unobscured sun. The operator holds it by hand and walks along the transect while keeping the sensor pointed directly at the sun. Gap fraction is computed in the sensor's data logger by log that averages the transmittances of subgroups of the data using a prior reference reading of uninterrupted beam radiation.

Half a clear day is also needed to collect data over a range of zenith angles by repeating measurements at various times. This requirement may be a limiting factor in certain climates (cloudiness) and at high latitudes in winter (too narrow range of sun angles). Aiming the detector at the sun while walking is not convenient and a traversing system is needed in some conditions (Welles 1990).

### 2.4.4 Line Quantum Sensors

Line quantum sensors utilize several individual sensors on a probe to measure canopy light transmission. Representative commercial instruments include AccuPAR LP-80 Ceptometer (Decagon Devices, Pullman, WA, USA) and SunScan Canopy Analysis System (Delta-T Devices, Cambridge, UK). AccuPAR consists of 80 PAR sensors embedded in a 0.84 m long probe, and SunScan consists of 64 PAR sensors embedded in a 1 m long probe. They are mainly designed for PAR measurements, but they also provide information about LAI from PAR interception.

Measurements made above and below the canopy are used to calculate canopy light interception. Below-canopy measurements are conducted with the probe, whereas above-canopy measurements are performed using the probe or an external PAR sensor.

Uniform canopy with randomly distributed leaves is assumed because LAI calculation is only based on Beer-Lambert law. The line quantum sensors also provide sunfleck information, but they are insufficient for quantifying the clumping effect. SunScan is officially suggested to obtain LAI measurement in low and uniform canopies (e.g., cereal crops and trial plots) or high, uniform, and non-clumped canopies (e.g., some timber plantations) (Webb et al. 2016). AccuPAR suggests collecting numerous spatially distributed samples of transmitted PAR to alleviate clumping-associated errors in LAI estimation.

### 2.4.5 Imaging Devices

Imaging devices are early instruments used for indirect LAI measurement. They can be categorized as hemispheric and directional by directional sampling, and visible band and near infrared band by spectral bands. The images permanently conserve the most comprehensive information. They provide details, such as gap distribution and gap-size distribution. Thus, they are attractive for implementing different algorithms to quantify clumping effect.

#### 2.4.5.1 Hemispherical photography

Hemispherical photography is one of the earliest methods and is still widely used today (Rich 1990). Hemispherical photography initially used films and was gradually replaced by digital photography, namely digital hemispherical photography (DHP) (Chianucci and Cutini 2012; Jonckheere et al. 2004). The system generally consists of a high-resolution digital camera, an extreme wide-angle fisheye, and a self-leveling system to ensure that it is held horizontally. HemiView Forest Canopy Image Analysis System (Delta-T Devices Ltd, Cambridge, UK) and WinSCANOPY (Regent Instruments Inc., Quebec, Canada) are representative commercial hemispherical photography instruments. Their viewing angle approaches are equal to 180°, which provides a complete view of all sky directions.

Images are manually taken under the canopy with the camera oriented toward the zenith or sometimes above the low canopies with the camera downward, and data are analyzed externally on a computer. Several software packages are developed to analyze hemispherical images, including commercial software, such as HemiView, WinSCANOPY, and Hemisfer (Schleppi et al. 2007) and freeware, such as CAN-EYE (Weiss and Baret 2016), GLA (Frazer et al. 1999), and CIMES (Gonsamo et al. 2011).

Distinguishing leaf and sky area is an important procedure for processing hemispherical photography, where user subjectivity remains a significant issue. The use of DHP is flexible but brings perceived sensitivity of the results to several factors, including photographic exposure, gamma function, and classification threshold (Chianucci and Cutini 2012; Leblanc et al. 2005b; Macfarlane et al. 2014; Zhang et al. 2005). The blue channel is generally recommended to reduce the influence of light transmission and reflectance of leaves (Leblanc et al. 2005b). Manual thresholding was replaced gradually by automatic classification methods to avoid subjectivity, and different classification methods do not greatly differ from each other (Macfarlane 2011). Photographic exposure and gamma correction still affect the magnitude of the gap fraction of canopy. Automatic exposure is unreliable, and a manual setting is sometimes needed (Zhang et al. 2005). Gamma correction has a considerable impact on the estimates of forest canopy properties in film and digital cameras and should be back-corrected to 1 (Chianucci and Cutini 2012; Macfarlane 2011; Macfarlane et al. 2007b). The sensitivity of the results to photographic exposure and gamma function is understandable because light distribution is rather complex in the large view of hemispherical photography. Thus, DHP should be generally applied under a uniform overcast sky or alternatively close to sunrise or

sunset (Breda 2003; Chianucci and Cutini 2012; Jonckheere et al. 2004). Distinguishing leaf and soil area is even more difficult for downward photography above the low canopies due to the misclassification of shaded leaves and soil (Demarez et al. 2008), therefore, cloudless conditions at noon with less shadows are recommended for data acquisition.

DHP is more time consuming than other indirect instruments because it requires time to analyze images in the laboratory (Garrity 2014).

#### 2.4.5.2 Directional photography

Directional photography uses a normal rather than the fisheye lens (Baret et al. 2010; Chianucci et al. 2014; Macfarlane et al. 2007b; Ryu et al. 2012; Song et al. 2015). Directional photography is mainly taken at nadir (Digital Cover Photography) or 57.3°. Directional photography does not provide a hemispherical view, but it is less sensitive to camera settings, such as exposure and threshold, and is thus superior to hemispherical photography in performance.

Directional photography has a narrow viewing angle and maximizes the full frame, which brings several advantages. First, the cover images have fewer mixed pixels because they have higher resolution than hemispherical photography (Macfarlane 2011; Macfarlane et al. 2007a). Second, sky luminance is even and cover images are less sensitive to photographic exposure and gamma function (Macfarlane et al. 2007a; Macfarlane et al. 2007b). Thus, directional photography could be applied in all light conditions (Baret et al. 2010) and used for long-term monitoring (Ryu et al. 2012). Third, the restricted field of view and the rectangular shape of the cover images better suit small rectangular experimental plots (Macfarlane et al. 2007b).

The use of raw images was emphasized recently. Raw image acquisition has significant advantages. The raw format stores original information in bit depth (10 to 32 bit) higher than the lossy JPEG format (8-bit), has controls of the gamma function, and has the potential of largely eliminating the influence of photographic exposure (Hwang et al. 2016; Macfarlane et al. 2014). The use of a blue channel is highly recommended in raw images (Hwang et al. 2016; Macfarlane et al. 2014).

#### 2.4.5.3 Multi-angle photography

Multi-angle photography is a special directional photography using multi-angle platform. It combines the hemispherical view of hemispherical photography and full-frame images of directional photography. Its multi-angle platform enables camera systems to provide images in several zenith and azimuth angles to cover the hemispherical view (Hu et al. 2016a; Mu et al. 2017; Yan et al. 2012; Zou et al. 2009). Multi-angle data are also helpful for solving the inversion problem. The acquisition of multi-angle images is slower than hemispherical photography, but the multi-angle photography provides consistent high resolution in all zenith angles. It has similar advantages to directional photography because they take the same full-frame images as cover photography.

#### 2.4.5.4 Multispectral Photography

Most photography instruments are in visible band and provide only RGB images. Multiband vegetation imager (MVI) is an early zenith-pointing instrument with a near-infrared band of 720 nm to 950 nm; this instrument can distinguish woody components from canopy components (Kucharik et al. 1997). Multispectral canopy imager (MCI) introduces the multi-angle platform to obtain multispectral images in the hemispherical space (Zou et al. 2009).

Multispectral cameras or filters, typically with additional near-infrared bands, are used to capture multiband images in addition to traditional visible images. Near-infrared information helps classify woody components from leaf components (Kucharik et al. 1998a; Zou et al. 2009). These instruments were employed in field measurements and improved LAI estimations because they consider the impact of woody components (Fu et al. 2011; Kucharik et al. 1998a, 1999; Tian et al. 2011).

### 2.4.6 Light Detection and Ranging (LiDAR)

LiDAR, also known as laser scanning, is an emerging active remote sensing technology for indirect LAI measurement. LiDAR directly measures the 3D data and has the potential to provide additional detailed information on canopy structure. LiDAR can derive canopy vertical

profiles from waveform. Discrete return LiDAR is of particular interest. Multi-scale platforms, including ground-based, airborne, and space-borne LiDAR, were employed in relative studies.

However, the first studies exploiting the LiDAR signal were based on allometric methods empirically established between LAI and some structural parameters directly derived from the LiDAR signal, such as the canopy volume and height (Lefsky et al. 1999; Lim et al. 2003a; Riano et al. 2004; Roberts et al. 2005). However, these relationships are applicable only for a single species in a given geographical area (Richardson et al. 2009). Gap fraction-based methods were introduced in LiDAR measurements in the past decade (Heiskanen et al. 2015; Luo et al. 2015; Morsdorf et al. 2006; Richardson et al. 2009; Tang et al. 2014a; Zhao et al. 2011). Their theoretical basis, namely, Beer-Lambert law, provides the potential for consistent LAI estimation using multi-platform and multi-scale LiDAR. LiDAR LAI estimation has two common issues, namely, gap probability estimation and clumping effect correction.

The advantage of LiDAR in gap probability estimation is its ability to operate in all time and is not limited by the light environment because LiDAR uses active lighting (Jupp et al. 2009). The intercepted and un-intercepted lights can be easily distinguished. The disadvantage is that a laser pulse has a relatively large size and sometimes has multiple returns and faces problems in identifying small gaps (Lovell et al. 2003; Seidel et al. 2012), especially in airborne and spaceborne LiDAR with footprints from tens of centimeters to tens of meters. Laser penetration metrics (LPM), ground-to-total energy ratio, or waveform data are used as a proxy of gap probability to accommodate the large footprints for airborne and space-borne LiDAR (Luo et al. 2015; Morsdorf et al. 2006; Tang et al. 2014b).

For clumping effect correction, traditional clumping correction methods are only applicable for ground-based LiDAR. Airborne and space-borne LiDAR should employ empirical values, ground measurements, or regression analyses (Jensen et al. 2008; Tang et al. 2014b; Tang et al. 2012; Thomas et al. 2011; Zhao and Popescu 2009), which is better than none but is not accurate because the clumping index is highly variable and changes with observation direction, location, scale, and season, even in the same forest (Chen and Black 1991; Pisek et al. 2013a; Yan et al. 2016b; Zou et al. 2015). However, observing complete gap-size distributions using airborne LiDAR systems is difficult because their footprints are generally too large to resolve numerous small gaps in the canopy. The detailed gap distribution data are the essential input for traditional clumping correction methods but are only available in ground-based LiDAR. Airborne and spaceborne LiDAR is technically incapable of capturing the gap-

size distribution data given that their footprints are larger than most small gaps in forests. The path length distribution model provides the potential for quantifying clumping using airborne and spaceborne LiDAR because it utilizes path length distribution (Hu et al. 2014), which is available in airborne LiDAR (Hu et al. 2018) and potentially in waveform data of spaceborne LiDAR. Some efforts were exerted to differentiate between and within tree crown gaps, and some clumping information can be acquired that way (Hu et al. 2018).

Similar to other measurements using passive optical instruments, the woody components and LAD are rarely considered in LiDAR, especially for airborne or spaceborne LiDAR due to their large footprint, low point density, and single-direction observation mode. Theoretically, airborne and spaceborne LiDAR are less affected by woody components than ground-based LiDAR because of smaller proportions of woody component in downward field of view.

The multi-platform and multi-scale LiDAR have some principles and issues in common, but their data acquisition, instrument performance, and processing still differ considerably. Ground-based LiDAR is the most similar to traditional passive optical instruments; thus, it is suitable for applying traditional methods. Airborne and spaceborne LiDAR also differ in terms of applications. For example, tree crown is identifiable in airborne LiDAR with a footprint size of 0.1 to 1 m, but not for spaceborne LiDAR with a footprint size of ~70 m. Therefore, different methods are developed for these platforms.

#### 2.4.6.1 Terrestrial Laser Scanner (TLS)

TLS is a ground-based laser scanning technology that acquires the finest 3D characterization. Several commercial TLS companies, such as RIEGL, Leica, and FARO, have a series of TLS products that include discrete return and waveform. A special waveform-recording LiDAR system called Echidna validation instrument, which covers the field of view with no gaps in laser illumination, is of significant interest (Jupp et al. 2009; Strahler et al. 2008; Yao et al. 2011; Zhao et al. 2011). LAI retrieval using TLS can be classified into two categories, namely, gap-based and the voxel-based methods.

The gap-based method uses the same theory, namely, Beer-Lambert law, as other passive indirect methods for LAI measurements (Calders et al. 2015; Lovell et al. 2003; Zhao et al. 2011). This method is not limited by the uneven point cloud density or incomplete point cloud of a tree because it is based on the gap probability. However, TLS also has some limitations for gap probability measurement. TLS resolution is higher than airborne and spaceborne laser

scanning, but lower than imaging devices. Moreover, the scanning geometry of TLS leads to a more frequent sampling of near-range than far-range objects. A maximum likelihood estimator was also introduced to accommodate these laser scanning geometries (Lovell et al. 2003; Seidel et al. 2012).

The voxel-based method voxelizes the cloud points and counts the beam-contact frequency in each layer for LAI retrieval using a point-quadrat method (Beland et al. 2011; Hosoi and Omasa 2006). The horizontal layers of the tree should be fully and evenly scanned from several locations surrounding the tree to minimize the influence of uneven laser penetration and point density (Hosoi and Omasa 2007; Van der Zande et al. 2006; Zhang et al. 2016a). However, several theoretical problems should be considered regarding the voxel-based method. Sampling frequency decreases with the scanning distance, and the inner-canopy point density is relatively low due to the obstruction, which causes bias in estimation (Hosoi and Omasa 2007; Zhao et al. 2015). The results are sensitive to voxel size, and the choice of voxel size is also influenced by occlusion (Beland et al. 2014).

Several theoretical problems must be resolved regarding LAI estimation using TLS, including the clumping effect, woody component, extinction coefficient (mainly the G function), and the blocking effect (Beland et al. 2014; Ma et al. 2017; Zheng and Moskal 2009). Recent efforts were exerted on some of these issues. Several traditional clumping algorithms were implemented in TLS by grouping TLS returns in voxels to identify occupied and non-occupied ones, but results were influenced by voxel size (Garcia et al. 2015). A triangle reconstruction method, which is based on 3D point cloud, was developed for LAD for the rapid measurement of LAD (Bailey and Mahaffee 2017). Additional efforts are needed on these issues.

#### 2.4.6.2 Airborne Laser Scanner (ALS)

ALS provides an opportunity to accurately map the LAI at landscape or regional scales due to its capability to penetrate canopies and its fast coverage over large areas. The ALS systems record data downward over a swath and cover a large area by several flight lines (Bouvier et al. 2015). Several commercial ALS systems are also available, including discrete return and waveform ones. Footprint size depends on the laser beam divergence and the flight altitude. Size approximately ranges from 0.1 to 1 m for the discrete return ones and may vary from 1 to 80 m for the waveform ones (Bouvier et al. 2015; Lim et al. 2003a; Vincent et al.

2012). LAI retrieval using ALS can be classified into two categories, namely, Beer-Lambert law-based and the empirical allometric methods.

Beer-Lambert law-based ALS method uses the same theory as other passive indirect methods for LAI measurement and the input is slightly different from gap fraction (Alonzo et al. 2015; Morsdorf et al. 2006; Solberg et al. 2006). ALS cannot precisely capture the traditional gap fraction because its footprint is generally larger than leaves and a laser pulse generally encounters both leaves and ground. Therefore, the LPM, which is also called the laser penetration index, is used as a proxy of gap probability. Several LPMs were proposed and validations showed that LPMs with both first and last returns perform best because they balance the contributions of the first and last returns (Heiskanen et al. 2015; Korhonen et al. 2011). An energy-based method using small-footprint, full-waveform ALS, was recently proposed to improve the total canopy transmittance estimation (Milenković et al. 2017).

The need for modeling and quantifying the clumping effect was highlighted in airborne LiDAR research (Hopkinson et al. 2013; Hosoi and Omasa 2007; Lovell et al. 2003; Riano et al. 2004; Schneider et al. 2014; Zheng and Moskal 2009). However, airborne LiDAR footprints (tens of centimeters or larger) are excessively large to capture small gaps and the have detailed gap-size distribution for the application of traditional clumping algorithm. The empirical values of clumping index (Tang et al. 2012; Zhao and Popescu 2009), ground measurements (Jensen et al. 2008), and regression analyses with vegetation indices (Thomas et al. 2011) were adopted for comparison with true LAI, but their uses are limited. Traditional clumping algorithms are also implemented in TLS and ALS data, but the results of ALS are generally worse because the ALS footprint is excessively large for detecting small gaps (Garcia et al. 2015). Therefore, the quantification of clumping effect remains an ongoing task in ALS. Recently, Hu et al. (2018) proposed a grid cell method based on path length distribution model to calculate the clumping-corrected LAI using airborne LiDAR data. This method separates the within- and between-crown areas to consider between-crown clumping, and uses the path length distribution as estimated by local canopy height distribution to consider 3D foliage profile and within-crown clumping. Given it does not require additional field measurements, this method provides an opportunity to map the clumping-corrected LAI operationally and to strengthen the ability of airborne LiDAR to validate the remote sensing products and to monitor vegetation changes.

#### 2.4.6.3 Spaceborne Laser Scanner (SLS)

SLS with high vertical resolution provides an opportunity to map the vegetation structure at global scales. Geoscience Laser Altimeter System (GLAS) on board ICESat (Ice, Cloud, and Land Elevation Satellite), operated between 2003 and 2009, is the first long-duration spaceborne LiDAR that provides a view of the earth in three dimensions with unprecedented accuracy (Schutz et al. 2005). Although the primary objective was to monitor polar ice sheet mass balance (Harding and Carabajal 2005; Zwally et al. 2002), GLAS measurements were also extended to vegetation vertical structures and LAI (Harding and Carabajal 2005; Tang et al. 2014b). GLAS is operated at the 600 km height in polar-orbiting platform at day and night at 40 Hz frequency and a 1064 nm wavelength for surface and vegetation measurements. Beam divergence is 0.5 mrad and produces a footprint of ~70 m in diameter, separated along-track by ~170 m. GLAS Level 1 altimetry product, namely, GLA01, typically contains waveforms digitized in 544 bins with a vertical resolution of 1 ns or equivalently 15 cm.

LAI retrievals that use GLAS were generally based on Beer-Lambert law and gap probability from waveform data. The information of GLAS returns is highly complex due to its large footprint given that GLAS laser pulse interacts with vegetation and ground in a large area. Physical model, regression, and empirical values were used for LAI retrieval using GLAS. Studies on GLAS are considerably fewer than those on ALS and TLS. Luo et al. (2013) computed the ground-to-total energy ratio from waveform energy and established a regression model between the ratio and the field-measured LAI based on Beer-Lambert law. Their results showed a strong linear relationship between the field-measured LAI of LAI-2000 and the log-transformed inverse of the ground-to-total energy ratio. Moreover, the inversed results of SLS are also LAIe, which does not consider clumping, because the results of LAI-2000 are LAIe. Tang et al. (2014b) derived LAI and vertical LAI profile through a recursive analysis of GLAS waveforms based on a physical geometric optical and radiative transfer model (Ni-Meister et al. 2001), which was previously implemented for a high-altitude waveform ALS (Land, Vegetation, and Ice Sensor, LVIS) (Tang et al. 2012). To correct the clumping effect, Tang et al. (2014b) built a clumping look-up table by assigning each MOD12Q1 land cover class an average clumping index from the multi-angular satellite POLDER. However, quantifying clumping using spaceborne laser scanner remains unsolved because the clumping index is highly variable and changes even in the same forest.

## 2.5 Recent Advances and Future Perspectives

Indirect LAI measurement is particularly important because it is the most feasible means to retrieve LAI at field and landscape scales. Various indirect methods and instruments were developed to estimate LAI from passive or active optical data. Moreover, these methods rely on different amendments to the Beer-Lambert law and on different assumptions, which might not hold true under certain circumstances, because of the limited gap information provided in optical data. On the one hand, attaining further significant progress in theory with traditional gap distribution data will be difficult considering the significant progress in recent decades and the rigorous theoretical derivation of indirect LAI measurement. On the other hand, several technical and specific problems, including sampling, instrument setting, photography processing, gap identification, leaf angle and woody component measurement, and individual tree measurement, remain uncertain and are still crucial in practical measurements. Slope effect is also a direction worth pursuing. Exploring new ideas and introducing new information are necessary to overcome the limitation of traditional gap data. Progress can be expected in developing new methods for LAI estimation by utilizing 3D information from laser scanner.

### 2.5.1 3D Modeling Using Multi-Platform Laser Scanners

The amount of information is always the main limitation for indirect LAI measurement. Separating and resolving all the factors, including LAI, LAD, and clumping using Beer-Lambert law, remains difficult because gap probability information is the only input. Improved retrieval requires additional information. The introduction of gap distribution information promotes the modeling and correction of clumping effect. However, gap distribution is a 2D information, which can be regarded as an irreversible lossy compression of 3D vegetation structure. Theoretically, the 2D gap distribution cannot fully resolve the 3D vegetation structure. Several clumping correction methods model and correct the clumping effect successfully, but some assumptions remain.

The laser scanner provides 3D point cloud information, which is a relatively appealing new data source. New data sources are often the driving force behind innovation. The use of LiDAR can assess information inside the canopy and facilitate the retrieval of vegetation structure parameters. Several new methods were proposed based on 3D point cloud information,

including LAD measurement on the basis of leaf surface reconstruction, canopy height profile estimation, and voxel-based method (Bailey and Mahaffee 2017; Hosoi and Omasa 2006; Lovell et al. 2003). Moreover, 3D information is always converted to 2D gap information to apply Beer-Lambert law in most LiDAR research. The use of Beer-Lambert law is reasonable because 3D reconstruction methods based on point cloud still have several theoretical problems that need to be solved, especially occlusion. LAD measurement is less limited by occlusion because measuring some samples is enough to represent the LAD of the whole canopy. By contrast, LAI measurement based on leaf, tree reconstruction, or voxels is extremely sensitive to occlusion, voxel size (Beland et al. 2014) and point cloud density for shoots. All elements should be fully scanned to avoid missing parts and LAI underestimation, which is difficult for dense trees and forests. In addition, the TLS acquisition takes time and is generally not as convenient as portable instrument such as LAI-2000 and DHP.

Thus far, Beer-Lambert law remains a reliable and rigorous theory because it is not limited by the uneven point cloud density and the occlusion. However, the 3D information of point cloud data should be explored further. The use of path length distribution model can facilitate the application of 3D point cloud.

Multi-platform laser scanners also provide an opportunity for consistent LAI retrieval at multiple scales. The data acquisition mechanism of terrestrial, airborne, and spaceborne laser scanners is similar, but their resolutions and footprint sizes are different. Beer-Lambert law-based methods are mostly used and perform best in LAI estimation using terrestrial, airborne, and spaceborne laser scanners, whereas the clumping effect correction are not efficiently solved using airborne and spaceborne laser scanners. Clumping effect correction using airborne and spaceborne laser scanners could be an important research direction in the future.

### 2.5.2 Individual Tree Measurement

Measuring LAI of individual trees attracts attention for analyzing and modeling urban forests. Allometric method was first used, but it is laborious, destructive, species dependent, and sometimes not feasible (Peper and McPherson 1998; Peper and McPherson 2003; Simioni et al. 2004). LiDAR-based estimates of tree and crown dimensions were attempted to estimate LAI in combination with allometric relationship (Roberts et al. 2005). This method is less

laborious and more efficient than traditional allometric methods, but its accuracy is mostly limited by LiDAR-based estimates of crown dimensions (Roberts et al. 2005). Voxel-based 3D modeling method was also proposed with extremely high-resolution LiDAR and an extremely small-voxel element size of 1 mm × 1 mm × 1 mm. This precise voxel model computes LAD and LAI by directly counting the contact frequency in each layer of the experimental trees (Hosoi and Omasa 2006). Fully and evenly scanned data from several stations are important for this method, and sensitivity to voxel size and occlusion should be considered (Beland et al. 2014). The Beer-Lambert law-based method is more explored than other methods because its theory is well developed and its measurement is operational and efficient (Chianucci et al. 2015; Lin and West 2016; Moorthy et al. 2008). However, most indirect methods at stand scale should be adjusted for individual tree because the continuous canopy assumption is typically not satisfied and the measurement is influenced by surrounding urban infrastructure, such as buildings.

The physical meaning of Beer-Lambert law's results is the first thing that need to be considered. The general formula of Beer-Lambert law [Eq. (1.1)] with an adjustment factor $1/\cos(\theta)$ is developed for continuous canopy layers to consider the path length, which is not directly suitable for individual trees. The observations on different zenith angles have different path lengths and represent different projected areas. The leaf area in a continuous canopy layer or a forest stand increases with the projected area. The LAI of different projected areas could be regarded as different samples and are generally consistent. However, an individual tree has a certain leaf area, and the leaf area does not change with the projected area. The LAI of an individual tree is inconsistent in different projected areas. Therefore, the path length and the projected area should be explicitly considered when using the general formula of Beer-Lambert law for individual tree measurement.

The leaf area and the combination of leaf area density and volume are two alternatives for describing individual trees. Considering that the LAI of an individual tree is ambiguous unless the size and position of the ground area is also given (Li-COR 2011), the leaf area is a better description than the LAI because the leaf area of an individual tree is fixed and independent. Leaf area density is closely related to Beer-Lambert law, whereas a volume is necessary to fix the leaf area. The corresponding surface area or the volume at the same time should be defined when using LAI or leaf area density for individual trees. Otherwise, the LAI or leaf area density is incomplete and not comparable. We recommend using the leaf area density and the path

length within the individual tree for indirect LAI estimation and use the leaf area for validation and comparison.

### 2.5.3 Clumping Effect from the Perspectives of Sampling and Scaling

Clumping effect, which may underestimate LAI of 30% to 70% in heterogeneous canopies, is an important factor influencing indirect LAI measurements. Corrections from the clumping effect are generally successful by reducing the LAI underestimation. However, all of the clumping correction methods, although based on the Beer-Lambert law, have their own assumptions and therefore provide different results. Users must choose the optimal methods by considering physical principles, sensor characteristics, data resolution, and available information.

From the perspectives of sampling and scaling, the clumping correction methods could be regarded as the application of Beer-Lambert law on different scales with different sampling strategies (Yan et al. 2016b; Zeng et al. 2014). The clumping effect of leaves causes the leaves to be aggregated and deviate from the random distribution assumption, which results in large gaps, especially large gaps between crowns. However, the leaves still tend to be randomly distributed within tree crowns and crop rows or on a smaller scale. Clumping correction methods basically apply Beer-Lambert law on these small scales where leaves are close to random distribution (Fig. 2.8). Therefore, all the existing methods (LX, CC, CLX, Path Length) are subject to errors when foliage distribution deviates from random distribution at this scale. Non-randomness within the LX segments will underestimate LAI, and the LX segments are not long enough to meet infinite canopy requirement of Poisson theory, which will overestimate LAI. The choice of 10 times the characteristic width of a leaf is a compromise, but not a physical solution. The CC method applies Beer-Lambert law on the remaining gaps after removing large gaps in excess of the random gap-size distribution. The deviation of the remaining gaps from the random situation is a source of error. Moreover, a random gap-size distribution does not necessarily correspond to a homogeneous canopy with randomly distributed leaves. The non-randomness within a crown envelope is a source of error for PATH method, but it considers the non-randomness caused by the variable path length through a crown envelope. Several

approaches for obtaining path length distribution can be employed. Inversing from traditional gap transect measurement with a sliding window can consider non-randomness within a crown envelope because its path length distribution is inversed from the measured gap probability distribution, which reflects the information of variable path length and variable leaf area density. By introducing the relative path length in the PATH method, the error of utilizing a finite-size sliding window is minimized in comparison with the LX method. For instance, the sliding window size is 20 times the characteristic width of a leaf, which overestimates absolute path lengths for 2.6% systematically. Non-randomness within the sliding window underestimates and smoothens absolute path lengths. After converting absolute path lengths to relative path lengths, the systematic error will be completely corrected, and the error caused by non-randomness within the sliding window will be minimized, especially when non-random degrees are similar in all windows.

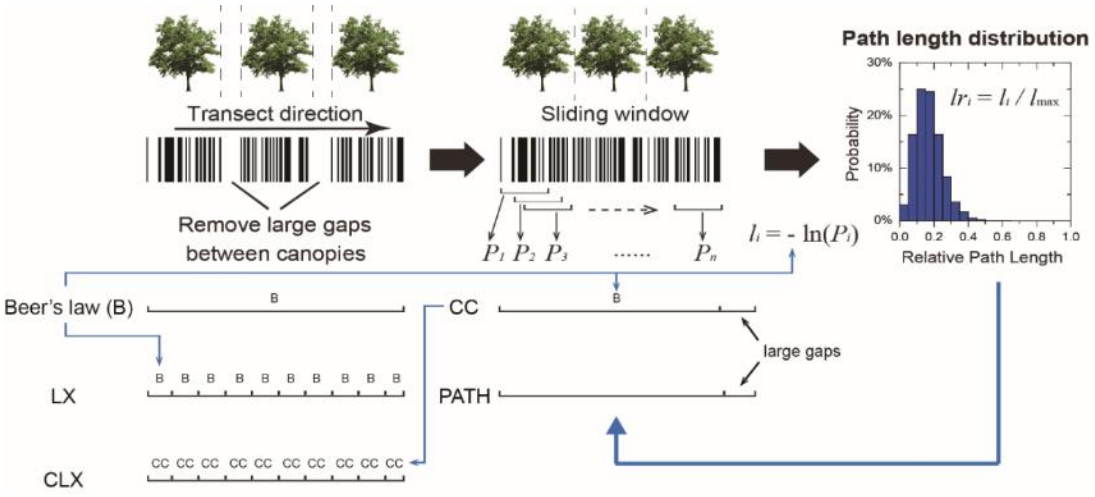


Fig. 2.8 Illustration of various clumping correction methods, including Beer-Lambert law (B), the finite-length averaging method (LX), the gap-size distribution method (CC), combination of the finite-length averaging and the gap-size distribution method (CLX), and the path length distribution method (PATH)

Clumping effect is highly related to the scale where Beer-Lambert law is applied. Foliage clumping effect leads to an inconsistent path length through canopies, which results in the spatial heterogeneity of gap fraction. Scale effect arises when applying the exponential Beer-Lambert law to the spatially heterogeneous gap fraction data. Different segmentation lengths show different results with the identical gap transect data; thus, the clumping effect of Beer-Lambert law in indirect LAI measurement is also a scale problem (Yan et al. 2016b). Different methods for correcting the clumping effect show different trends with the change in calculation

scale. The finite-length averaging method, the combination of gap-size distribution and finite-length averaging methods, and the path length distribution method that involve a segmentation process, are insensitive to a segment scale; these methods stabilize when the segment scale is larger than 20 m. The gap-size distribution method and Beer-Lambert law prefer a large segment scale, which is larger than a full period of a row in row crop scenes and 100 m in forest scenes. Computing the average LAI of all the short segments, which is commonly performed, is not as good as merging these short segments into a long segment and computing the LAI value for the merged segment. In situ measurement always requires certain amounts of observations to represent the sample plot due to the limitations of plot boundary and instrument. Therefore, we recommend merging several observations for calculation, especially when the sample plot is small.

In general, the clumping effect is closely related to scales and sampling strategies. The perspectives of sampling and scaling are also helpful for analyzing the scopes of application and limitations of different clumping effect methods. Much progress has been achieved on the modeling clumping effect, but some assumptions and simplifications remain, which could be directions for future research.

### 2.5.4 LAD: Measurement and Integration

The influence of LAD has been well modeled physically for decades in theory. However, LAD correction is not often applied because of the lack of a convenient measurement method.

The G function corresponding to six typical LADs varies from 0.27 to 0.84 (Fig. 2.4). However, the spherical LAD (G=0.5) is often adopted for calculation given the difficulty of measuring LAD. The G value is close to 0.5 regardless the LAD near the zenith angle of 57.3° (Fig. 2.4), which happens to be the average leaf angle of spherical LAD (Table 2.3). Measuring at the zenith angle of 57.3° is thus a compromise (Baret et al. 2010); otherwise, the spherical LAD approximation should be used with caution, especially near the zenith angle of 0°, where the G value of 0.5 brings an error of up to 68% in LAI estimation.

The current methods for LAD measurement should be analyzed and improved for operational use. Methods for measuring LAD could be classified into three categories. The first is the contact measurement method, which measures a certain amount of leaves with a 3D

protractor, a protractor with a plumb bob, or an electromagnetic digitizer and then calculates the distribution by statistics (Hutchison et al. 1986; Lang 1973; Thanisawanyangkura et al. 1997). This method is relatively accurate, but is difficult to implement for tall trees. (Hutchison et al. 1986). The second method is the indirect non-contact measurement method, which retrieves LAI and averages leaf inclination angles using Beer-Lambert law with multi-angle measurements of gap fractions (Kucharik et al. 1998b; Welles and Norman 1991). This method assumes random or similar foliage spatial distributions in different viewing angles, which are often not satisfied. Mu et al. (2017) improved this method by introducing additional information, including bidirectional fractions of vegetation and soil and the clumping index using a portable multi-angle observation system (Ren et al. 2013; Yan et al. 2012). The improved integration of this information can potentially improve LAD's inversion accuracy; thus, this method should be automated. The third method involves taking digital photographs around the canopy using a leveled camera, which selects leaves oriented approximately parallel to the viewing direction of the camera and measures the inclination angle manually in an image processing software (Pisek et al. 2011b; Ryu et al. 2010b). Although this method still needs manual operations, it is moderately efficient and greatly improves the feasibility of measuring tall trees; thus, it was applied to UAV platform (McNeil et al. 2016). This method also needs to be automated for operational use. A new method that triangulates laser-leaf intersection points to reconstruct the leaf surface for rapid LAD measurement is appealing and requires further evaluation (Bailey and Mahaffee 2017). The latter two indirect methods, together with gap fraction measurements have potential application, and automation is particularly important for practical and operational LAD measurement.

Improved integration of LAD will improve the accuracy of the indirect LAI measurement because leaf projection function $G(\theta)$ is a continuous curve. In previous studies, the $G(\theta)$ value is only calculated in several discrete angles, such as in the middle zenith angle of each zenith layer. Although the G values do not differ significantly in a small zenith layer that uses the integration forms of Beer-Lambert law (Hu et al. 2014); this method can use the accurate $G(\theta)$ curve and reduce the error as much as possible.

### 2.5.5 Slope Effect in a Complex Terrain

Most field indirect LAI measurements were carried out in flat areas. Thus, the slope effect

is relatively less studied. The slope effect of indirect LAI measurement has been gradually highlighted in the past 20 years with the development of remote sensing in a complex terrain. The necessity of correcting the slope effect remains controversial. The consensus of the present study is that the slope effect is relatively small and negligible with a slope less than 30° but becomes a moderate source of error with a slope larger than 30° (Duursma et al. 2003; España et al. 2008; Gonsamo and Pellikka 2008).

LAI on slopes is defined on a horizontal surface in consideration of consistency with remote sensing products and independence from the slope. Measurement methods on slopes have two types, namely, leveled (oriented to local zenith) and tilted (oriented perpendicular to slope) acquisitions, both of which need a conversion or correction to obtain the LAI on slopes (España et al. 2008; Gonsamo and Pellikka 2008; Schleppi et al. 2007). Leveled acquisition refers to the same projection direction as LAI definition, but has variable path lengths and gap probabilities azimuthally. The slope effect leads to a small gap fraction upslope and large gap fraction downslope due to the differences of the path lengths (España et al. 2008; Walter and Torquebiau 2000). Tilted acquisition has relatively even path lengths and gap probabilities azimuthally, but the vegetations observed are shifted, tilted, and referred to the sloping surface. Both acquisitions should consider the topographic masks, which include in upslope directions for leveled acquisition and in downslope directions for tilted acquisition.

Several correction methods were proposed based on DHP. Leveled acquisition has different processing approaches; one approach is converting the reference to sloping surface as tilted acquisition for retrieval (Gonsamo and Pellikka 2008; Montes et al. 2007; Walter and Torquebiau 2000); another approach is transforming the slope gap fraction to the flat gap fraction by accounting for variation with the azimuth of the path length due to the slope (España et al. 2008). Tilted acquisition directly provides the data for retrieval referring to the sloping surface and its LAI adjusted to horizontal by dividing with the slope cosine (Gonsamo and Pellikka 2008). When the slope is less than 30°, the downslope and upslope effects approximately compensate for leveled acquisition (España et al. 2008); these two acquisition methods are not significantly different (Gonsamo and Pellikka 2008). When the slope is greater than 30°, the LAI from the leveled acquisition is systematically lower than that from the tilted acquisition; the larger the slope is, the higher the difference becomes (Gonsamo and Pellikka 2008). A comparison shows that the methods of España et al. (2008) and Gonsamo and Pellikka (2008) perform the best for spherical LAD, and España et al. (2008)’s method is preferred for

nonspherical LADs (Cao et al. 2015).

No preference is suggested for leveled or tilted acquisition technique (Gonsamo and Pellikka 2008). Leveled acquisition is preferably employed in DHP and can be easily implemented with a bubble level. Tilted acquisition has broad applicability because it does not require additional information other than slope cosine, but holding the sensor perpendicular to slope cannot be easily ensured. Tilted acquisition is recommended for LAI-2000 series (Li-COR 2011) and LAI can be adjusted horizontally by dividing with the slope cosine. The transect parallel to the slope is preferred for TRAC (Leblanc et al. 2005a) and the reported LAI is referred to sloping surface. The LAI referred to sloping surface can be adjusted horizontally by dividing with the slope cosine. Theoretically, other correction methods based on angular information can be applied to TRAC if transect azimuth direction, slope cosine, and aspect are known. Several TRAC transects may be necessary for a representative result.

### 2.5.6 Coupled Effects and 3D Real Scene Validation

The study and validation of these factors are usually conducted individually by simplifying or controlling other factors. However, these factors are often coupled, which increases the difficulty of modeling and validation dramatically. A fully controlled and known 3D real structure simulation scene might be the best solution for validating these factors individually.

Validating each factor accurately with field validation has always been a problem. For example, the clumping effect and the woody components influence the result in field measurements. Attributing the error source is difficult. If the woody components are not considered, the PAI of indirect measurement is compared with the LAI of direct measurement. The clumping effect is then underestimated. If the clumping effect is not considered, the LAIe of indirect measurement is compared with the LAI of direct measurement. The woody components are then underestimated. Moreover, if the woody components are underestimated, the clumping effect is also underestimated and vice versa. Therefore, a fully controlled environment should be identified where all factors can be quantified separately for validation.

The computer simulation technique can provide a 3D canopy with a controllable structure and an accurate leaf area (Qi et al. 2017; Widlowski et al. 2013), which provides a potential for validating the LAI indirect measurement method (Hu et al. 2014). Thus, the coupled effects

should be analyzed quantitatively based on the computer-based real structure simulation. In addition, clumping parameterization through 3D model, the use of artificial intelligence and machine learning algorithm might be helpful for solving these complex coupled problems and relate directly true LAI to gap fraction.

## 2.6 Gaps of Current Methods and Possible Solutions

After several decades of development, the Beer-Lambert law-based leaf area index measurement theory has been continuously enriched and improved, providing an effective means for the rapid measurement of the ground leaf area index. The emergence of new requirements, new technologies and new data sources has brought new opportunities and challenges to the indirect measurement of leaf area index.

(1) The within-crown foliage clumping becomes an unavoidable problem, as the accuracy requirement of leaf area index measurement increases. The clumping effect has always been the most critical problem in Beer-Lambert law-based leaf area index estimation. Previous algorithms correct the clumping effect to a large extent by separating the large gaps between crowns or by applying Beer-Lambert law in short segments. On a segment where gaps are relative randomly distributed, the clumping effect is largely avoided. However, there are some differences between the results of different clumping index correction algorithms, and some degree of underestimation still appears in some validations. One of the reasons is that the existing methods have not explicitly considered the clumping effect caused by the inconsistent path length of the light penetrating crowns. This limitation is gradually revealed and becomes an unavoidable problem as the accuracy requirements increase, although the within-crown clumping is usually weaker than the between-crowns clumping caused by the between large gap.

(2) Estimating leaf area index of an individual tree needs additional consideration. Previous work on leaf area measurement mainly focused on the stand level, although the presence of individual trees is more common than forests in urban areas. Traditional indirect LAI measurement theory, which uses the cosine of observation zenith angle for path length correction, is incompatible for an individual tree because the representative projected area of LAI changes as the observation zenith angle changes, making the results incomparable and ambiguous. In addition, traditional instruments are not applicable to urban individual tree LAI

measurement, because its light path is always intercepted by the surrounding buildings or other objects. Therefore, it is necessary to explore new instruments and methods to separate the individual tree from the urban environment.

(3) The airborne LiDAR estimation of leaf area index lacks an effective clumping effect correction method. Airborne LiDAR can provide 3D point cloud, which brings opportunities and challenges for leaf area index inversion research. Airborne LiDAR shares the same principle Beer-Lambert law with indirect measurement, making it possible for airborne LiDAR inversion to learn from the research progress and experience of indirect measurement of the ground leaf area index for more than half a century, but it also faces similar problems with ground indirect measurement. The clumping effect is still the key factor, and it is also one of the most concerned issues in the current airborne LiDAR estimation of leaf area index. The large footprint and low point density of airborne LiDAR are two major constraints for applying the traditional ground method to correct the clumping effect, as airborne LiDAR footprints (tens of centimeters or larger) are too large to capture the small gaps and the detailed gap size distribution, which is necessary input for traditional ground method. In addition, the three-dimensional (3D) information is also not utilized efficiently.

This thesis will focus on the modeling and correction of the clumping effect. (1) To characterize the inconsistent path length in the canopy, the path length distribution is introduced, and the leaf area index estimation model based on the path length distribution is established to correct the crown shape-induced clumping. (2) Path length distribution model is implemented for individual tree leaf area measurement by replacing the traditional cosine path length correction for continuous canopy with real path length distribution. TLS point cloud is used to reconstruct the tree crown envelope and calculate real path length distribution through laser pulse-envelope intersections. (3) Clumping effect correction using airborne LiDAR is realized based on the path length distribution acquired from ALS three-dimensional point cloud information.

# Chapter 3 Modelling Leaf Area Index Based on Path Length Distribution

The clumping index has been used to modify effective LAI for decades. However, the change in path length within canopies is often the most uncertain factor in indirect LAI estimation using Beer-Lambert law. A simple clumping index is incapable of describing the heterogeneity of a canopy and may cause large errors in calculating true LAI values. Beer-Lambert law is originally a function related to the path length, however, when Beer-Lambert law is applied to the indirect measurement of the leaf area index, the path length is eliminated, which implies the assumption that the path length is consistent.

In this chapter, the mechanism of the underestimation of the leaf area index caused by the inconsistent path length within crown is first analyzed. Then the path length distribution function is introduced to characterize the foliage clumping caused by the crown shape. We proposed a new LAI estimation method by using path length distribution functions in optical measurement. Both simulation and field measurements show that the path length-based method can effectively characterize the LAI values of heterogeneous canopies. Deviation is less than 10% for all the validations. One of the advantages of path length distribution theory is that it can characterize and handle crown shape-induced non-randomness within canopies. Such non-

randomness, which may cause underestimation of up to 25%, has not been well addressed by existing algorithms.

Different from the previous model, path length distribution model uses the path length distribution to describe the three-dimensional spatial distribution of leaves. It has the advantage of considering the three-dimensional crown shape and the height distribution of the tree, and it can deal with the non-random distribution of the gap probability within crowns. Through different forms of input, the model can be applied to existing ground and airborne instruments and platforms to effectively improve the accuracy of leaf area index measurement.

## 3.1 Beer-Lambert law

Beer-Lambert law, which is widely used in atmospheric science, relates the absorption of light to the properties of a material through which the light travels in optics (Beer 1852; Houghton 2002). The law states that a natural logarithmic dependence exists between the transmission of light through a substance, $T$, and the product of the absorption coefficient of the substance, $k$, the density (number per unit volume) of absorbing particles, $\rho$, and the distance the light travels through the material (i.e., the path length), $l$:

$$T = e^{-k \cdot \rho \cdot l} \quad . \tag{2.1}$$

When applied to vegetation, $k$ is substituted by leaf projection coefficient $G$, $\rho$ is substituted by foliage area volume density ($FAVD$), $G$ and $FAVD$ are both uniform in the scene, and $l$ is the function of the height of the foliage layer and the zenith angle (Chen and Leblanc 1997) given by

$$\rho = FAVD = \frac{LAI}{h} \tag{2.2}$$

$$l = \frac{h}{\cos\theta} \quad . \tag{2.3}$$

Eq. (2.1) can be written as

$$T = e^{-G \cdot FAVD \cdot l} = e^{-G \cdot LAI / \cos\theta} \quad . \tag{2.4}$$

The gap probability $P$ along a transect is introduced to substitute transmission $T$ because the transmission at each location cannot be measured directly.

If path length is constant along the transect (Fig. 3.1), the transmission at each location is also constant:

$$T_x = T_0 = e^{-k \cdot \rho \cdot l_0} \quad , \tag{2.5}$$

where $T_x$ is the transmission at the location $x$ of the transect and $l_0$ is the path length.

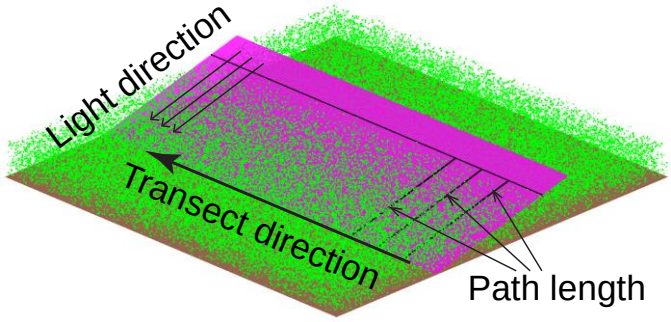


Fig. 3.1 Path length within the homogenous scene.

The gap probability of the whole transect can therefore be considered the statistical result of the same random transmission event repeated many times:

$$P = \overline{T_x} = T_0 = \exp\left(-G \cdot LAI / \cos\theta\right) \quad . \tag{2.6}$$

Eq. (2.6) is the general expression of Beer-Lambert law in the uniform distributed foliage layer, i.e., the Poisson model (Nilson 1971).

## 3.2 Essential Reason for LAI Underestimation: Inconstant Path Length

An important underlying assumption in Eq. (2.6) is the constant transmission along the whole transect.

This assumption is suitable for homogeneous vegetation scenes (Fig. 3.1). Hence, Beer-Lambert law is applicable and accurate for LAI retrieval in homogeneous canopy, which is

validated by quantitative simulation. Beer-Lambert law is also applicable for homogeneous canopies, such as crops, in many in situ experiments (Ross 1981; Welles and Norman 1991).

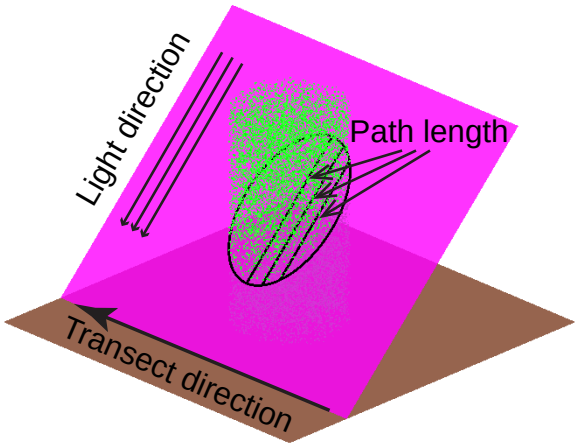


Fig. 3.2 Path length within a cylindrical canopy.

However, when applied to sparse row crops and forest canopies, the aforementioned assumption is no longer satisfied. To illustrate the structure clearly, the row crop or the tree is simplified as a cylinder with uniform foliage density. The path length $l$ is no longer constant within the canopy, as the cross section of the cylinder is an ellipse (Fig. 3.2). Therefore, the transmission $T_x$ at each point along the transect is also inconstant. The gap probability of the transect cannot characterize the transmission at each point in this case, but it is the mean of transmission along the transect:

$$P = \overline{T_x} \quad , \tag{2.7}$$

where $P$ is total gap probability of the transect, $T_x$ is the transmission at the location $x$ of the transect, which is inconstant.

Only the total gap probability of transect $P$ can be obtained in ground measurement; therefore, the LAI is always calculated as

$$LAI_e = -\ln(P) = -\ln\left(\overline{T_x}\right) \quad , \tag{2.8}$$

where $LAI_e$ is the effective LAI, defined as the product of the clumping index and LAI (Chen et al. 1991), i.e., the result of Beer-Lambert law, including clumping. $T_x$ is the transmission at

the location $x$ of the transect.

However, the true LAI is the mean of LAI along the transect:

$$LAI_{true} = \overline{LAI_x} = \overline{-\ln(T_x)} \ , \tag{2.9}$$

where $LAI_x$ is the LAI at the location $x$ of the transect.

Mathematical derivation proves $-\ln(\overline{T_x}) \le \overline{-\ln(T_x)}$, i.e., $LAI_e \le LAI_{true}$; the equality holds if and only if $T_x$ is constant. The inconstant transmission is the essential reason for the underestimation problem in LAI ground measurement. The large gap among canopies is the extreme case for inconstant transmission, as the transmission is 100%. The inconstant path length within canopies is another foremost cause, and it is particularly important because existing algorithms still cannot solve this problem completely.

## 3.3 New LAI Retrieval Method Based on Path Length Distribution

A new method based on path length distribution was developed for LAI retrieval to address the underestimation problem caused by inconstant path length.

### 3.3.1 Path Length Distribution

The path length distribution function is defined to describe the change of path length within the tree crown:

$$\int_0^{l_{\max}} p_l(l)\,dl = 1 \ , \tag{2.10}$$

where $l$ is path length, $l_{\max}$ is the maximum path length, $p_l(l)$ is probability density function of path length, and $p_l(l)dl$ is the frequency of $l$ falling within the infinitesimal interval, [$l$, $l$ + $dl$].

The path length distribution function can be calculated from frequency or relative probability of path length distribution.

$$p_l(l) = \frac{\hat{p}_l(l)}{\int_0^{l_{\max}} \hat{p}_l(l)\,dl} \quad , \tag{2.11}$$

where $\hat{p}_l(l)dl$ is the frequency or relative probability of $l$ falling within the infinitesimal interval, $[l, l + dl]$. Eq. (2.11) is used to normalize the path length distribution and make it meet Eq. (2.10).

For a more concise and consistent expression, a relative path length is introduced and defined as

$$lr = l / l_{\max} \quad , \tag{2.12}$$

where $l$ is the absolute path length at a location of transect and $l_{\max}$ is the max path length along the transect.

Second, the probability density function of a specific path length is defined as

$$\int_0^1 p_{lr}(lr)\,d(lr) = 1 \tag{2.13}$$

$$p_{lr}(lr) = \frac{\hat{p}_{lr}(lr)}{\int_0^1 \hat{p}_{lr}(lr)\,d(lr)} \quad , \tag{2.14}$$

where $lr$ is relative path length and $\hat{p}_{lr}(lr)d(lr)$ is the frequency of $lr$ falling within the infinitesimal interval, $[lr, lr + d(lr)]$.

### 3.3.2 Modeling Gap Probability for Discrete Canopy

Based on the Beer-Lambert law prototype, the exact expression of the discrete canopy gap probability can be theoretically derived by introducing the path length distribution function and the leaf area volume density.

The transmission at each location is a function of path length $l$ based on the Beer-Lambert law :

$$T(l) = e^{-G \cdot FAVD \cdot l} \quad , \tag{2.15}$$

where $G$ is the leaf projection coefficient, $FAVD$ is leaf area volume density, and l is the path length that a ray passing through the tree crown.

Thus, referring to Eq. (2.7), the total gap probability along the transect can be expressed as

$$\begin{aligned} \overline{P} &= \int_0^1 T(l) \cdot p_{lr}(lr)\, d(lr) \\ &= \int_0^1 T(l_{\max} \cdot lr) \cdot p_{lr}(lr)\, d(lr) \\ &= \int_0^1 e^{-G \cdot FAVD \cdot (l_{\max} \cdot lr)} \cdot p_{lr}(lr)\, d(lr) \\ &= \int_0^1 e^{-G \cdot (FAVD \cdot l_{\max}) \cdot lr} \cdot p_{lr}(lr)\, d(lr) \end{aligned} \quad . \tag{2.16}$$

Eq. (2.16) represents the canopy gap probability based on the path length distribution, where $T(l)$ and $p_{lr}(lr)$ is the transmission and proportion respectively of relative path length $lr$ and their weighted mean is the total gap probability $\overline{P}$. The total gap probability $\overline{P}$ and leaf projection coefficient $G$ are two necessary inputs for indirect LAI estimation based on Beer-Lambert law. The additional unknown parameters in Eq. (2.16) are $FAVD$, $l_{\max}$, and path length distribution function $p_{lr}(lr)$.

### 3.3.3 Modeling LAI for Discrete Canopy

LAI can be calculated as the product of $FAVD$ and canopy vertical height $H$ according to its definition, where the vertical height can be calculated from the path length $l$:

$$LAI(l) = FAVD \cdot H = FAVD \cdot l \cdot \cos\theta \quad . \tag{2.17}$$

Referring to Eq. (2.9), the true LAI along the transect can also be expressed as an integral form weighted by the path length distribution function:

$$\begin{aligned} LAI_{true} &= \int_0^1 FAVD \cdot (l \cdot \cos\theta) \cdot p_{lr}(lr)\, d(lr) \\ &= \int_0^1 FAVD \cdot (l_{\max} \cdot lr \cdot \cos\theta) \cdot p_{lr}(lr)\, d(lr) \\ &= \int_0^1 (FAVD \cdot l_{\max}) \cdot \cos\theta \cdot lr \cdot p_{lr}(lr)\, d(lr) \end{aligned} \quad . \tag{2.18}$$

Eq. (2.18) represents LAI for discrete canopy based on path length distribution, where $\rho \cdot \left( l \cdot \cos\theta \right)$ and $p_{lr}(lr)$ are LAI and proportion respectively of relative path length $lr$ and their weighted mean is true LAI. The observation zenith angle $\theta$ can be obtained from data and The additional unknown parameters in Eq. (2.18) are the same as those in Eq. (2.16), namely $FAVD$, $l_{\max}$, and path length distribution function $p_{lr}(lr)$.

The combined Eq. (3.16) and (3.18) are the core formulas for retrieving LAI based on path length distribution model:

$$\overline{P} = \int_0^1 e^{-G\cdot(FAVD\cdot l_{\max})\cdot lr} \cdot p_{lr}\left(lr\right) d\left(lr\right) \tag{2.19}$$

$$LAI_{true} = \int_0^1 \left( FAVD \cdot l_{\max} \right) \cdot \cos\theta \cdot lr \cdot p_{lr}\left(lr\right) d\left(lr\right) \ , \tag{2.20}$$

where observation zenith angle $\theta$, total gap probability $\overline{P}$, and leaf projection coefficient $G$ are basic inputs for retrieving LAI based on Beer-Lambert law. If path length distribution function $p_{lr}(lr)$ is known, the product of only two unknown quantities, $FAVD \cdot l_{\max}$, can be retrieved from Eq. (2.19). With the input of $FAVD \cdot l_{\max}$, the LAI can be calculated from Eq. (2.20).

Although the two parameters $FAVD$ and $l_{\max}$, are not separated, they are always in the form of product and can be regarded as an intermediate variable. The intermediate variables $FAVD \cdot l_{\max}$ and $lr$ have been combined in Eqs. (2.19) and (2.20), which means considering the accurate absolute values of $FAVD \cdot l_{\max}$ and $lr$ separately is unnecessary. Therefore, the use of relative path length does not introduce any simplifications and avoid the need of absolute path lengths without loss of precision. The relative value of $l$ is sufficient for LAI calculation, i.e., the accurate absolute value of $l$ is unnecessary, thereby making the theory more general and user-friendly.

## 3.4 Calculation of Path Length Distribution

Compared to the basic form of Beer-Lambert law for LAI estimation, the only addition input of path length distribution model is the path length distribution, which replaces the gap distribution required by traditional clumping index algorithm. The path length distribution can

also be obtained from the gap distribution, making it compatible with the data used by the traditional clumping index algorithm. In addition, the path length distribution can also be obtained directly based on elliptical hypothesis or three-dimensional measurement without the gap distribution, thereby further improving the applicability of path length distribution model. Among them, the three-dimensional measurement method can make full use of the unique three-dimensional information of the laser scanner. The use of the path length distribution is particularly meaningful for large-footprint airborne laser scanner that cannot obtain accurate gap distribution.

The acquisition of path length distribution function is currently available in the following ways: based on elliptical cross-section assumptions, based on measured gap distribution data, and based on three-dimensional data.

### 3.4.1 Path Length Distribution Calculation Based on Ellipse Section Assumption

Trees are generally shaped like a cylinder, cone, or ellipsoid, the sections of which are almost an ellipse. Therefore, characterizing the actual section as ellipse is reasonable. The path length through an ellipse is proportional to a circle (Fig. 3.3) and thus the relative path length, *lr*, of an ellipse makes no difference with that of a circle in reference to Eq. (2.12). The path length distribution of an ellipse or a circle is

$$\hat{p}_{lr}\left(lr\right) = lr / \sqrt{1-lr^2}, \quad lr \in \left[0,1\right) \ . \tag{2.21}$$

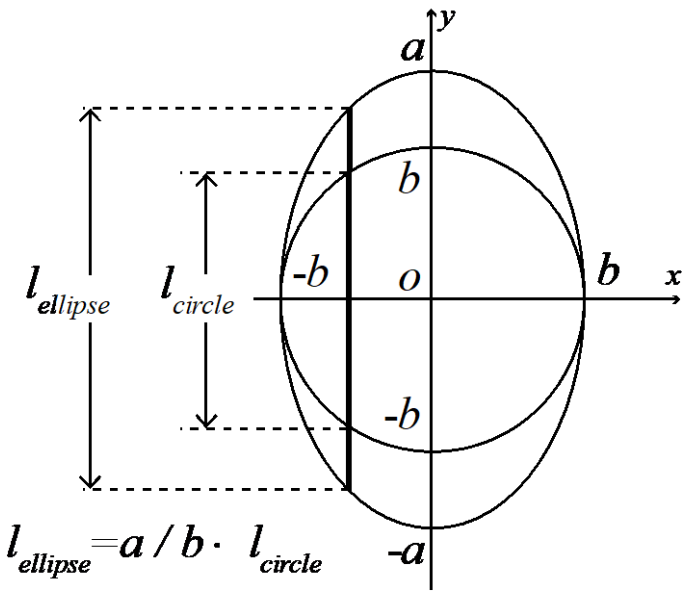


Fig. 3.3 Path length of the ellipse and circle. $l_{circle}$ is the path length through a circle with a radius of $b$, $l_{ellipse}$ is the path length through an ellipse, which is proportional to a circle, and the lengths of semi-major and semi-minor axes of the ellipse are $a$ and $b$, respectively.

This alternative requires less computation and can be combined with the CC method, which could remove the large gaps between canopies effectively.

### 3.4.2 Path Length Distribution Inversed From 3D Data

This method provides the possibility to obtain the absolute path length using 3D point cloud, which is mainly acquired by the terrestrial or the airborne laser scanners. With terrestrial laser scanner data, the crown contour can be reconstructed according to the point cloud, and the absolute path length can be directly obtained by calculating the distance that each laser pulse passing through the tree crown, which will be introduced in Chapter 4. With airborne laser scanner data, although the point cloud density is relatively low, the relative path length distribution can still be obtained by the canopy height model, which will be introduced in Chapter 5.

The advantages of using 3D data are: (1) it can obtain absolute path length, which provides the possibility of estimating leaf area density using terrestrial laser scanner; (2) it makes full use of distance data, which is the third dimensional information in addition to the traditional one-dimensional or two-dimensional gap probability information. The distance information has great advantages in describing the three-dimensional highly complex vegetation canopy structure. The introduction of new information sources helps to describe the three-dimensional spatial distribution of the leaves more accurately and accurately; (3) It solved the problem of clumping correction in airborne laser scanner retrieval. The airborne LiDAR footprint is larger than most of the gap in the canopy, therefore, the gap distribution information required by the previous clumping index algorithm cannot be obtained. The path length method does not depend on the gap distribution information and provides a possibility for the airborne LiDAR to correct the clumping effect.

### 3.4.3 Path Length Distribution Inversed from Measured Gap Data

In dense forests, light may travel through multiple levels of canopies in large zenith angles. In this case, characterizing the section with an ellipse is inexact. Path length distribution is thus inversed from measured gap data using a sliding window (Fig. 3.4).

First, the large gaps between canopies are removed to avoid the effect of large gaps on the sliding windows. For simplicity, a gap size threshold is used to detect large gaps, and 10 times the leaf width are used.

Second, a sliding window, which moves pixel by pixel, is used to obtain the gap probability at each location along the transect. As the canopies within the small window are relatively homogeneous, the path length in each window can be calculated using a concise expression given by

$$l_i = -\ln\left(P_i\right) \ , \qquad (2.22)$$

where $P_i$ is the gap probability in each window and $l_i$ is the path length in each window.

The size of the sliding window is set as 20 times the leaf width initially. If no gap is observed in the sliding window, the size of the sliding window is increased by one pixel until a gap appears. Assuming a sliding window is enlarged by n pixels, the sliding window is moved, skipping n pixels to balance roughly the weights of each pixel. As relative path length distribution is needed, slight non-randomness within the sliding window slightly affects the result. Thus, the result is not sensitive to the width of the sliding window.

Third, the relative path lengths in all windows are normalized and then the path length distribution can be obtained by statistical means.

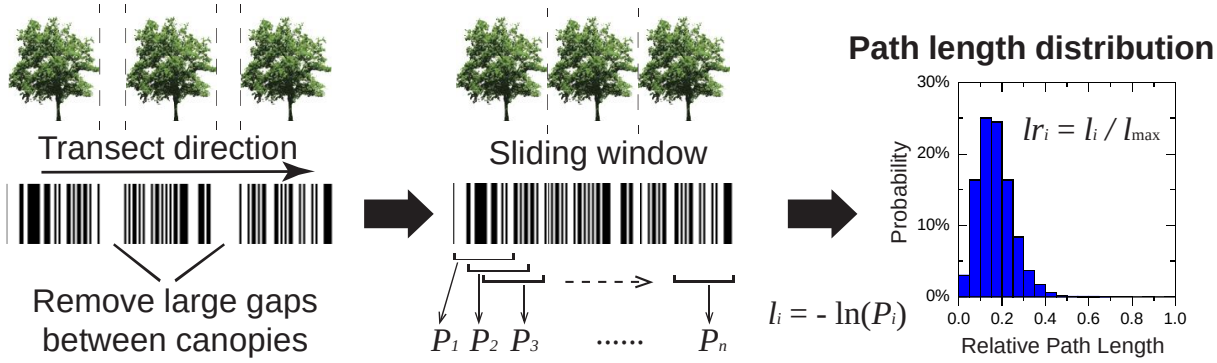


Fig. 3.4 Flow of obtaining path length distribution from measured gap data. $P_i$ is the gap probability in each window, $l_i$ is the path length in each window, $l_{max}$ is the max path length along the transect, and $lr_i$ is the relative path length in each window.

## 3.5 Materials

Field measurement is the ultimate means of model validation. However, ground true LAI is difficult to obtain. Different kinds of realistic structural scenes are used with a wide range of LAI for a comprehensive validation. In realistic structural scenes, parameters such as LAI can be controlled and both input (gap information) and output (ground true LAI) are accurately determined. By employing both realistic structural scenes and field measurement, the proposed path length distribution method is compared with the LX and CC methods.

### 3.5.1 Realistic Structural Scenes

Realistic structural scenes, including cylindrical row canopy scenes with varying LAIs and discrete broadleaf forest scenes, are selected from Radiation transfer model intercomparison (Pinty et al. 2001; Widlowski et al. 2011; Widlowski et al. 2007). The precise geometric and spatial information of the scenes are fully known.

One of the advantages of realistic structural scenes is that true LAIs can be calculated directly and accurately by definition, providing objective ground truth for validation and comparison of different indirect LAI measurement methods. As the size of each leaf is known, the true LAIs can be calculated by definition as

$$LAI_{true} = \frac{\sum A_i}{2A_s} , \qquad (2.23)$$

where $A_i$ is the total area of each leaf and $A_s$ is the area of horizontal ground surface. No approximation and assumption were made in calculating the true LAIs. The accuracy of true LAIs of the realistic structural scenes is better than 1%.

Cylindrical row canopy scenes (25 m × 25 m) are generated to represent row crop scenes. Leaves are randomly distributed in cylinders with a radius of 2 m and are close to row crops (Fig. 3.5). The *FAVD* is uniform in cylinders and the leaf projection coefficient, *G*, is known, whereas the path lengths within canopies are inconstant. Each scene is exclusively composed of disk-shaped leaves with a radius of 0.05 m. By controlling the number of leaves, different scenes are generated, with the LAI varying from 0 to 4 with a step of 0.2.

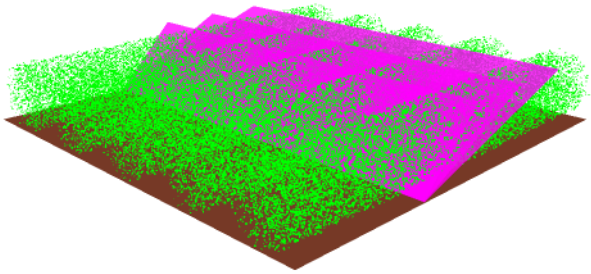

Fig. 3.5 Overview of the cylindrical row canopy scene. Disk-shaped leaves with a radius of 0.05 m are colored green, soil ground is colored brown, and observing angles are represented by pink planes.

Discrete broadleaf forest scenes (270 m × 270 m) are generated to represent natural forests (Fig. 3.6), containing a series of non-overlapped cylindrical or spherical volumes. The leaf angle distribution (LAD) of each scene is known. The cylindrical canopy scene is composed of 614 cylindrical plant crowns with various diameters and heights (Table 3.1). The spherical canopy scene is composed of 614 spherical plant crowns with various diameters (Table 3.2). Each plant crown is composed of circular leaves randomly distributed within the spherical or cylindrical volumes. In addition to large gaps between canopies and inconstant path length, the canopies are discretely distributed in the scene. The *G* and *FAVD* are both uniform and known in cylinders and spheres. The LAI of the scenes range from 1.19 to 6.35, covering the vast majority of forests in the world.

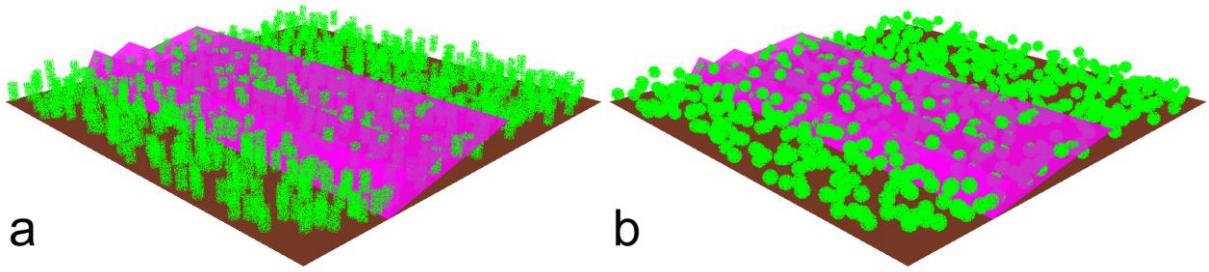


Fig. 3.6 Overview of discrete cylindrical (a) and spherical (b) tree canopy scenes

Table 3.1 Scene characteristics of broadleaf cylindrical canopies

| Scene | LAI = 1.19 | LAI = 4.23 | LAI = 6.35 |
|---|---|---|---|
| Scene dimensions: (m × m × m) | 270.0 × 270.0 × 24.0 | 270.0 × 270.0 × 36.0 | 270.0 × 270.0 × 48.0 |
| Leaf shape | Disc of negligible thickness | Disc of negligible thickness | Disc of negligible thickness |
| Leaf radius (m) | 0.05 | 0.05 | 0.05 |
| LAI of individual cylinder | 5.0 | 10.0 | 15.0 |
| Number of cylinders | 614 | 614 | 614 |
| Cylinder radius (m) | 3.0 | 4.0 | 4.0 |
| Cylinder height (m) | 12.0 | 24.0 | 36.0 |
| LAI of scene | 1.19 | 4.23 | 6.35 |
| LAD of scene | Uniform distribution | Uniform distribution | Uniform distribution |

Table 3.2 Scene characteristics of broadleaf spherical canopies

| Scene | LAI = 2.12 | LAI = 4.14 |
|---|---|---|
| Scene dimensions: (m × m × m) | 270.0 × 270.0 × 15.0 | 270.0 × 270.0 × 17.0 |
| Leaf shape | Disc of negligible thickness | Disc of negligible thickness |
| Leaf radius (m) | 0.05 | 0.05 |
| LAI of individual sphere | 5.0 | 6.25 |
| Number of spheres | 614 | 614 |
| Sphere radius (m) | 4.0 | 5.0 |
| LAI of scene | 2.12 | 4.14 |
| LAD of scene | Uniform distribution | Uniform distribution |

Eight transects are employed to obtain gap data and characterize the whole scenes sufficiently; the length of each segment depends on the width of the scene. In cylindrical row canopy scenes (25 m × 25 m), eight 25 m transects are used. In discrete broadleaf forest scenes (270 m × 270 m), eight 270 m transects are employed.

In each transect, gap data are measured in 7 zenith angles (10, 20, 30, 40, 50, 57.3, and 60°), which are generally employed in ground measurement (Welles and Norman 1991; Zou et al. 2009). The zenith angle 57.3° is used in this study because the G value is close to 0.5 (less than 5% error) for almost all types of leaf angle distribution.

The final LAI is the weighted average of all zenith angles given by

$$LAI = \sum_{i=1}^{7} LAI(\theta) \cdot W_i \quad . \tag{2.24}$$

The weight, $W_i$, is proportional to $sin(\theta)$; when normalized to 1.0, the values of $W_i$ are 0.0420, 0.0828, 0.1210, 0.1556, 0.1854, 0.2036, and 0.2096 for zenith angle 10, 20, 30, 40, 50, 57.3 and 60°, respectively.

Path length distribution method based on ellipse section assumption (PATH_ELL) and measured gap data are both evaluated. CC and LX methods are applied to the same gap data for comparison.

## 3.5.2 Field Measurement

### 3.5.2.1 TRAC

The LAI measurements were performed in a pear orchard (40.373° N, 115.723° E) in Huailai, Hebei province, China (Fig. 3.7, Table 3.3). The pear trees were planted approximately every 3.6 m in a north–south direction and every 3 m in an east–west direction. Indirect LAI measurement and destructive sampling measurement were conducted in a 30 m × 30 m sample plot on 5 June 2010.

Fig. 3.7 Pear orchard located in Huailai, Hebei province, China.

Table 3.3 Scene characteristics of the pear orchard in Huailai, Hebei province, China

| Scene | Pear orchard |
|---|---|
| Scene dimensions: (m × m × m) | 30.0 × 30.0 × 10.0 |
| Average leaf area: ($cm^2$) | 56.33 |
| Number of trees | 78 |
| Plant spacing (north–south) (m) | 3.6 |
| Plant spacing (east–west) (m) | 3.0 |
| LAI of scene | 2.04 |

The Tracing Radiation and Architecture of Canopies (TRAC; 3rd Wave Engineering, ON, Canada) instrument was used for indirect LAI measurement. It provides detailed photosynthetic photon flux density (PPFD) measurement along the whole transect, which is useful for foliage clumping research. TRAC measurements were conducted along several 30 m-long segments in the 30 m × 30 m sample plot. Markers were set every 7.5 m, and the TRAC instrument was operated by referring to the TRAC manual. Eight 30 m transects were employed in each of the two measurements performed.

Destructive sampling was performed on the same day. First, 229 leaves from different positions were harvested, and the average leaf area was obtained by photography. Second, the number of leaves in several trees was counted to represent the sample plot, as the plantation is relatively uniform. Third, the number of trees was counted in the sample plot, and the LAI was calculated by definition. The LAI of destructive sampling are taken as the ground truth to validate the indirect methods.

PATH_ELL and path length method from measured gap data (PATH_MES) were both evaluated on the basis of PPFD raw data measured by TRAC. The gap probability of each segment was obtained using integration approach described in the TRAC manual (Leblanc et al. 2005a), which ensures that the gap probability equals the mean beam transmittance. The results were compared with those processed by TRACwin software, which employed the CC method.

#### 3.5.2.2 Multispectral canopy imager (MCI)

The MCI was employed to obtain the gap data for the indirect LAI measurement in the four sites (Table 3.4) in the Saihanba National Forest Park in Chengde, Hebei Province, China in July 2014.

Table 3.4 Description of Study Sites and Results of The Indirect Measurement

| Site No. | Latitude | Longitude | Species | PAIe | PAI | LAI | α |
|---|---|---|---|---|---|---|---|
| 1 | 42°23'56"N | 117°18'15"E | larch (*Dahurian larch*) | 2.98 | 4.40 | 3.74 | 0.15 |
| 2 | 42°23'51"N | 117°18'59"E | white birch (*Betula platyphylla* Suk.) | 2.94 | 3.96 | 3.38 | 0.14 |
| 3 | 42°23'55"N | 117°19'01"E | larch (*Dahurian larch*) | 0.88 | 1.62 | 1.23 | 0.24 |
| 4 | 42°24'46"N | 117°14'44"E | pine (*Pinus sylvestris L.* var. *mongholica* Litv.*)* | 3.28 | 4.62 | 3.34 | 0.28 |

Multispectral images in the NIR and VIS bands were obtained in several zenith and azimuth angles (Table 3.6) for classifying canopy and woody components. Each image was clipped into a field of view of 20° vertically and 60° horizontally. The images were taken horizontally every 60° to cover an azimuth angle of 360°. Zenith observation angles of 30° and 50° were selected because these angles cover a zenith viewing angle of 20°–60°, which covers most of the site and does not contain numerous overlaps.

Table 3.5 Description of MCI Measurement

| Site No. | 2 |
|---|---|
| Observation Zenith Angles | 30°, 50° |
| Observation Azimuth Angles | Every 60° |
| Vertical Field of View | 20° |
| Horizontal Field of View | 60° |
| Bandwidth of NIR bands | 760–900 nm |
| Bandwidth of VIS bands | 390–690 nm |
| Average Diameter of Observation Area on Top of the Canopy (60°) | ~38 m |

VIS and NIR image pairs were registered and classified into canopy and woody components automatically (Fig. 3.8). We employed an automated image registration process to eliminate the slight offset between the VIS and NIR image pairs [Fig. 3.8(a) and (b)]. Control points were detected using normalized cross correlation, and the affine transformation was applied (Liu et al. 2011). The normalized difference vegetation index was calculated using registered multispectral images and then used to classify the canopy component and sky [Fig. 3.8(c)]. The NIR images were then used to distinguish the woody components [Fig. 3.8(d)]

from canopy components, which utilized the strong absorbance of woody components.

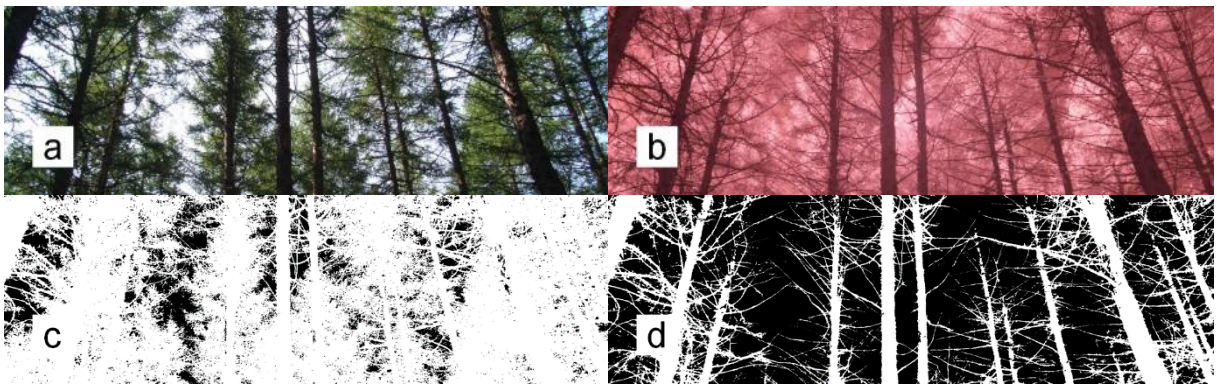


Fig. 3.8 Visible (a) and near-infrared (b) image pair and classified canopy (c) and woody (d) component in site 1

For each classified image, gap data were obtained and employed as input for the indirect LAI method. The gap data of canopy and woody components are used to calculate the PAI and WAI, respectively.

Destructive direct measurement and additional indirect LAI measurements with the MCI and LAI-2000 were conducted in August 2015 in site 2 (Table 3.6) for validation.

Table 3.6 Description of the Direct Measurement Site (White Birch) in Chengde, Hebei Province, China

| Site No. | 2 |
|---|---|
| Plot Size | 45.0 m × 45.0 m |
| Species | white birch (*Betula platyphylla* Suk.) |
| Number of Trees | 197 |
| Average Leaf Area | 13.4 $cm^2$ |
| Average Tree Height | 12.0 m |
| Average DBH | 61.9 cm |
| LAI of Scene | 3.81 |

First, a representative tree was cut down, and all leaves were manually collected into 18 bags and weighed. A bag of leaves (2,974 leaves) was then directly measured with a portable laser leaf area meter (CI-202) to determine the leaf area. The total leaf area (one side) of the tree is given by

$$LA_{tree} = \frac{LA_{sample}}{Weight_{sample}} \cdot Weight_{all} \quad , \tag{2.25}$$

where $LA_{sample}$ is the sum of the area (one side) of 2,974 leaves, $Weight_{sample}$ is the weight of 2,974 leaves, and $Weight_{total}$ is the total weight of all 18 bags of leaves of the tree.

Second, the trees of the site were counted, and several structure parameters, such as tree height and diameter at breast height (DBH), were measured with a laser rangefinder and a tape measure, respectively. As the number of leaves in each white birch could reach approximately 50,000, measuring the leaf area of all trees would be too time consuming and labor intensive. As the trees varied slightly in the sample plot, the leaf area was extended to the site by utilizing the relationship between the leaf area and the average heights and DBHs (Daughtry 1990; Gower et al. 1999). The total leaf area (one side) and LAI are calculated as

$$LA_{plot} = LA_{tree} \cdot \frac{Height_{avg} \cdot DBH_{avg}^{\ 2}}{Height_{tree} \cdot DBH_{tree}^{\ 2}} \cdot N \tag{2.26}$$

$$LAI_{plot} = LA_{plot} / Area_{plot} \quad , \tag{2.27}$$

where $LA_{plot}$ is the total leaf area (one side) in the sample plot; $Height_{tree}$ and $Height_{avg}$ are the height of the measured tree and the average height of the trees in the sample plot, respectively; $DBH_{tree}$ and $DBH_{avg}$ are the DBH of the measured tree and the average DBH of the trees in the sample plot, respectively; N is the number of trees in the sample plot; and $Area_{plot}$ is the area of the sample plot, that is, 45 × 45 m2. The $LAI_{plot}$ was calculated as 3.73 in this step.

Third, because it took six days to measure the 2,974 leaves, the leaves atrophied during the measurement. Hence, another 10 branches of 10 different trees were sampled, and each leaf was measured with CI-202. The results were used for the regression analysis of the changes in the leaf area per unit weight to refine the leaf area measurement. Afterward, the $LAI_{plot}$ was calculated as 3.81, which slightly differed from that in the second step.

## 3.6 Results and Discussion

### 3.6.1 LAI Retrieval in Cylindrical Row Canopy Scenes

LAI values were retrieved in 20 cylindrical canopy scenes with the true LAI ranging from 0 to 4 (Fig. 3.9). PATH_ELL and PATH_MES performed better than CC and LX methods.

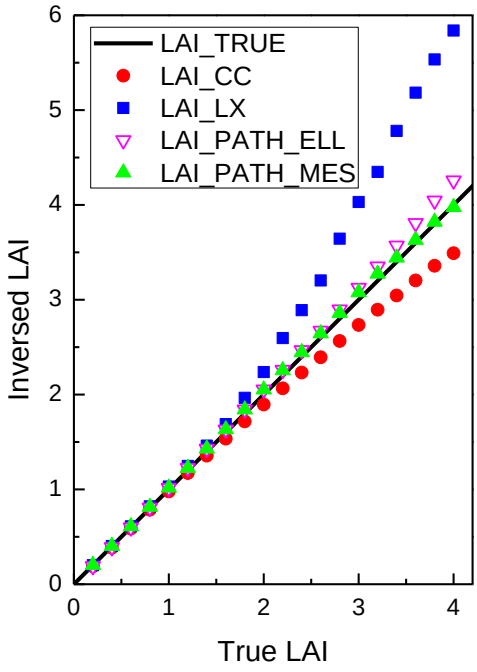


Fig. 3.9 Validation of the retrieved LAI in cylindrical row canopy scenes, using gap size distribution method (LAI_CC), finite length averaging method (LAI_LX), path length distribution method based on ellipse section assumption (LAI_PATH_ELL), and measured gap

All four methods show little difference with true LAI when LAI is low (<1.5). However, when the LAI increases, the CC and LX methods start to show deviation. The CC method shows a certain degree of underestimation (about 5%–15%) when the LAI is larger than 2. The underestimation is caused by inconstant transmission within cylindrical canopies although the CC method can largely eliminate the effect of large gaps between canopies. This finding indicates that spatial heterogeneity within canopies, which is caused by inconstant path length essentially, is another foremost and non-negligible cause for LAI underestimation. The LX

method shows a certain degree of overestimation, which can be explained by two reasons: (1) the simplification of binomial mode with Poisson model, (2) and the amendment to the sub-segment with no gaps. The deviation is more significant in dense canopies (larger LAI) because more gapless sub-segments are observed. The trend is also confirmed in previous studies, indicating the CC method always results in lower LAI and the LX method always gives higher LAI (Gonsamo and Pellikka 2009; Leblanc et al. 2005b; Pisek et al. 2011a).

The results of path length theory are in good agreement with true LAI, which proves path length distribution helps improve indirect ground LAI measurement. Path length distribution method can characterize canopies with inconstant path lengths effectively.

PATH_ELL is directly applied to the CC method result after which the large gaps are removed. The result shows little overestimation, for that matter the CC method might also correct a small part of the non-randomness within canopies. Although PATH_ELL shows a slight overestimation, the method remains attractive, as it can be applied to the result of the CC method directly and improves accuracy. PATH_ELL is easy to use and fast, as the path length distribution is built-in and without further computation.

PATH_MES is almost fully consistent with true LAI. It is even slightly better than that based on ellipse section assumption because it makes less assumption. Path length distribution calculated from gap data is thus more adaptable and accurate than that calculated from the ellipse section-based assumption.

### 3.6.2 LAI Retrieval in Discrete Broadleaf Forest Scenes

The LAI was retrieved in discrete broadleaf forest scenes in seven zenith angles (Fig. 3.10). The final LAIs (Fig. 3.11, Table 3.7) were weighted in these zenith angles as Eq. (3.24). PATH_MES shows the highest accuracy.

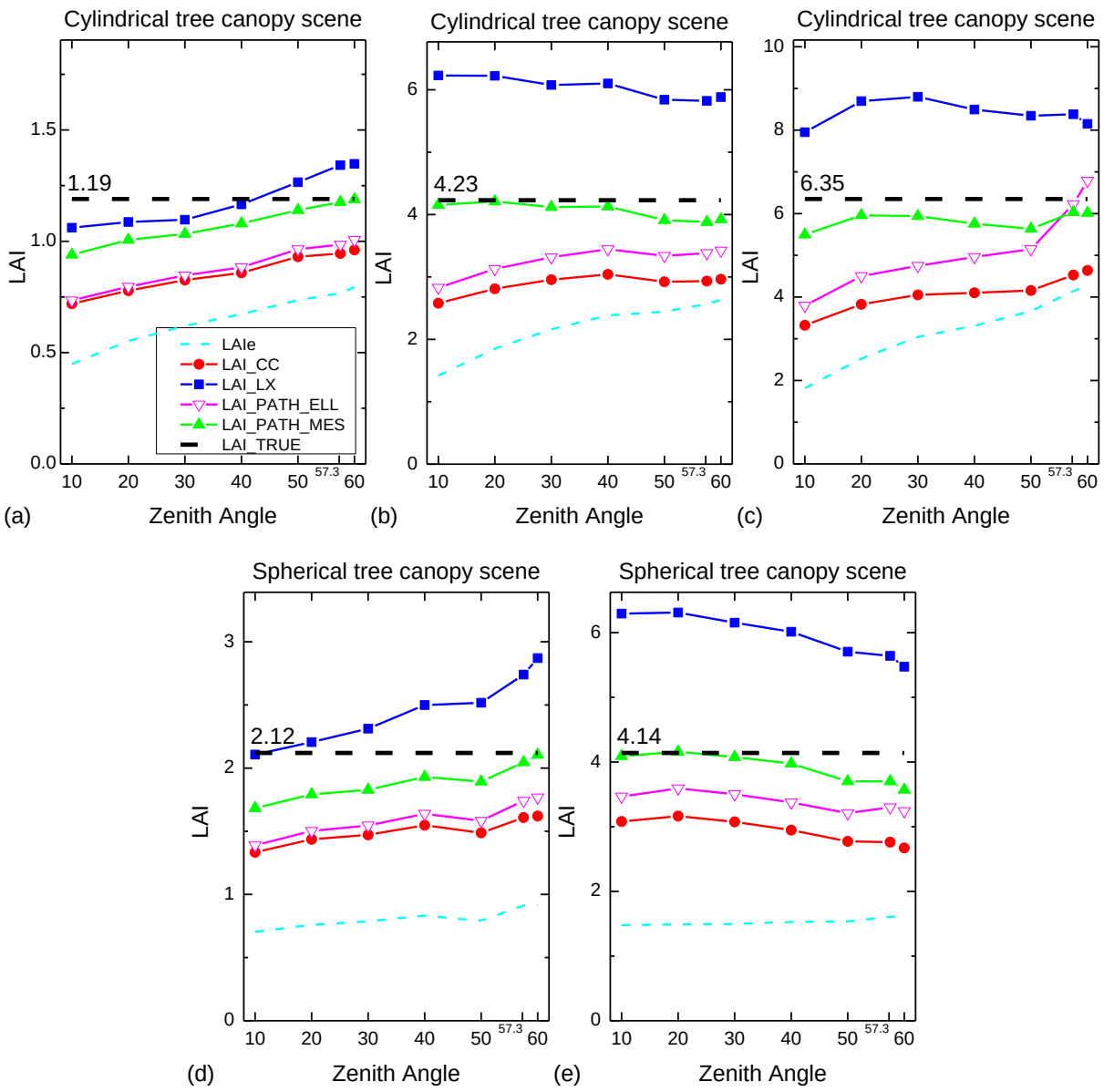


Fig. 3.10 Validation of the retrieved LAI in different zenith angles in discrete broadleaf forest scenes, using gap size distribution method (LAI_CC), finite length averaging method (LAI_LX), path length distribution method based on ellipse section assumption (LAI_PATH_ELL), and measured gap data (LAI_PATH_MES).

Table 3.7 Validation of the retrieved LAI weighted in seven zenith angles

| | Cylindrical tree canopy scenes | | | Spherical tree canopy scenes | |
|---|---|---|---|---|---|
| LAI_TRUE | 1.19 | 4.23 | 6.35 | 2.12 | 4.14 |
| LAIe | 0.70 (-40.9%) | 2.37 (-43.9%) | 3.59 (-43.5%) | 0.84 (-60.3%) | 1.56 (-62.4%) |
| LAI_CC | 0.89 (-24.8%) | 2.93 (-30.7%) | 4.25 (-33.1%) | 1.54 (-27.5%) | 2.86 (-31.0%) |
| LAI_LX | 1.24 (+4.1%) | 5.96 (+41.0%) | 8.40 (+32.3%) | 2.57 (+21.0%) | 5.82 (+40.6%) |
| LAI_PATH_ELL | 0.93 (-22.1%) | 3.34 (-21.0%) | 5.52 (-13.0%) | 1.64 (-22.5%) | 3.34 (-19.4%) |
| LAI_PATH_MES | 1.10 (-7.7%) | 4.00 (-5.4%) | 5.87 (-7.5%) | 1.92 (-9.5%) | 3.82 (-7.8%) |

*LAIe - Beer's law, LAI_CC - Gap size distribution method, LAI_LX - Finite length averaging method, LAI_PATH_ELL - Path length distribution method based on ellipse section assumption, LAI_PATH_MES - Path length distribution method based on the measured gap data

The CC method shows a consistent underestimation (about 24.8%–33.1%), although it improves the LAIe to some extent. Previous experiments also found 21%–33.3% underestimation of the CC method in forests (Kucharik et al. 1998a; Leblanc et al. 2005b), which agree with our results. The underestimation of CC method is smaller in larger zenith angles for both LAI and LAIe. The reason is that large gaps have less chance to be observed in large zenith angles and thus the gap probability distribution is closer to a random situation.

The LX method provides good result in sparse scenes (LAI = 1.19) but the overestimation is large (21.0%–41.0%) in dense scenes (LAI = 4.14, 4.23, 6.35). Even in sparse scenes (LAI = 1.19, 2.12), the LX method shows overestimation in large zenith angles. A common denominator is that more gapless sub-segments are observed in dense scenes and large zenith angles. The finding confirms that the LX method will give erroneous results when numerous gapless segments are observed, which is found in previous studies (Chen and Black 1992b; Leblanc et al. 2005b).

PATH_ELL shows 13.0%–22.5% underestimation, which is slightly better than that of the CC method. The path length distribution is deviated from ellipse section assumption because of the mutual occlusion among the canopies. Thus, the result is unsatisfactory compared with that in cylindrical row canopy scenes.

PATH_MES exhibits high performance consistently. The overall bias is only -5.4% to -9.5% in five scenes (Table 3.7), which is smaller than the other four methods. PATH_MES also meets the relative accuracy (20%) requirement of the GCOS. The accuracy is stable in all zenith angles.

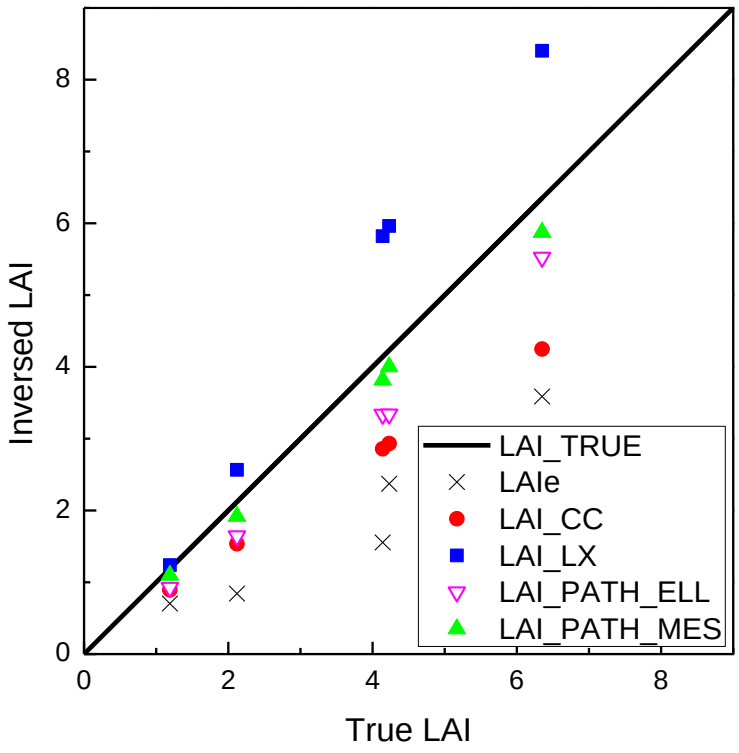


Fig. 3.11 Validation of the retrieved LAI in discrete broadleaf forest scenes, using gap size distribution method (LAI_CC), finite length averaging method (LAI_LX), path length distribution method based on ellipse section assumption (LAI_PATH_ELL), and measured gap data (LAI_PATH_MES).

The high accuracy and stability in discrete broadleaf forest scenes indicate that the proposed path length method based on the measured gap data is significantly better than existing methods. The method is universal because assumptions for path length distribution are unnecessary. Therefore, path length distribution theory can be promising for improving indirect LAI measurements.

### 3.6.3 LAI Retrieval in A Pear Orchard Using TRAC Data

The LAI was retrieved in a pear orchard using TRAC data (Table 3.8). The trends are consistent with those of realistic structural scene validation. PATH_MES characterizes the scene effectively in field measurement.

Table 3.8 In situ validation of LAI retrieval in the pear orchard

| | TRAC Sample 1 | TRAC Sample 2 |
|---|---|---|
| LAI_TRUE | 2.04 | 2.04 |
| LAIe | 1.31 (-35.8%) | 1.39 (-31.9%) |
| LAI_CC | 1.53 (-25.0%) | 1.79 (-12.3%) |
| LAI_PATH_ELL | 1.59 (-22.0%) | 1.88 (-7.8%) |
| LAI_PATH_MES | 1.98 (-2.7%) | 2.05 (+1.4%) |

*LAI_CC - Gap size distribution method, LAI_LX - Finite length averaging method, LAI_PATH_ELL - Path length distribution method based on ellipse section assumption, LAI_PATH_MES - Path length distribution method based on the measured gap data

The LAIe shows serious underestimations (31.9%–35.8%), which has been confirmed in many previous field measurements. The CC method modifies and improves the result largely by eliminating the large gaps between canopies. However, a 12.3%–25.0% underestimation remains because of the non-randomness within canopies caused by inconsistent path length. PATH_ELL slightly reduces the underestimation than the CC method. PATH_MES achieves the highest accuracy. The overall bias of LAI retrieved by PATH_MES is only -2.7% and +1.4% in two TRAC samples, smaller than the other methods.

PATH_MES also shows superior stability. In the two TRAC samples, the differences between the retrieved LAI values are large, as high as 0.26 for CC and 0.29 for PATH_ELL. By contrast, the results of PATH_MES are consistent with little difference (0.07). The consistency among different TRAC samples indicates that PATH_MES is a stable and practical approach for indirect LAI measurement.

### 3.6.4 LAI Retrieval in A Forest Park Using MCI Data

The LAI of the path length distribution model was compared with that of the three other methods in the four sites (Fig. 3.12). The result of Beer's law (LAIe) is the lowest in value because it does not consider the foliage clumping effect. The LAI_CC is larger than LAIe because the CC method can eliminate the large gaps between canopies. LAI_LX is the largest in value because many gapless sub-segments are observed in this measurement. A maximum LAI value was assigned to the gapless sub-segments because the logarithm of zero is undefined. This assignment causes the final LAI_LX to be overestimated. The overestimation of the LX method is also reported on several previous studies (Gonsamo and Pellikka 2009; Leblanc et al. 2005b; Pisek et al. 2011a). LAI_PATH is larger than LAI_CC because the PATH method modifies the non-randomness within and between canopies in comparison with the CC method. The trends are the same in all four sites.

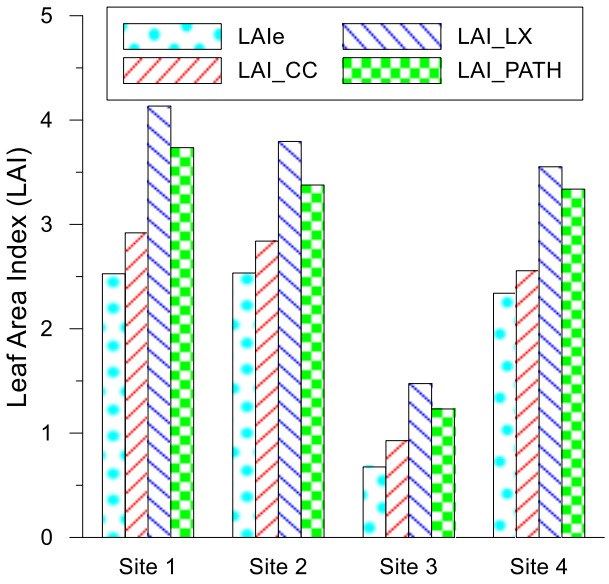


Fig. 3.12 Comparison of indirect leaf area index measurement in 2014 using Beer's law (LAIe), gap-size distribution method (LAI_CC), finite length averaging method (LAI_LX), and path length distribution method (LAI_PATH).

In comparing LAI_PATH and LAI_CC, a 16%–25% difference in the LAI can be noted. Such difference is caused by the non-randomness within canopies. The degree of underestimation is consistent with previous research (Hu et al. 2014). It is a considerable underestimation that influences the accuracy of the indirect LAI measurement.

Validations with a destructive direct measurement in the summer of 2015 confirm the abovementioned trends. The destructive direct measurement yields a LAI of 3.81 for site 2. The PAIe of LAI-2000 and MCI are 2.76 and 2.91, respectively, with a difference of approximately 5%. With the woody components removed from the MCI data, the results can be comparable to the directly measured LAI. The LAIe, LAI_CC, LAI_LX, and LAI_PATH of the simultaneous MCI measurements are 2.61, 2.90, 4.17, and 3.63, respectively. The LAI_PATH agrees with the directly measured LAI well, with the underestimation maintained within 5%. LAI_LX shows a 9.4% overestimation in this study. The results are consistent with the indirect measurement findings in 2014.

The mix of the opposing effects of spatial heterogeneity and woody components hinders their quantification and validation in forests.

If one of these factors is underestimated, the other is underestimated as well. For example, if the non-randomness within canopies is underestimated, PAI_CC, rather than LAI_CC, appears to be close to LAI_PATH. The effect of woody components is obviously underestimated. Ignoring woody components also results in the underestimation of spatial heterogeneity. LAIe underestimates 41% of the true LAI, whereas PAIe, which does not eliminate the effect of woody components, only underestimates 34% of the true LAI. PAIe seems to be better than LAIe, but it does not reveal true information. The underestimation of spatial heterogeneity is especially serious in forests with large woody-to-total area ratios.

In addition, the counteracting effects of woody components and non-randomness within canopies may be misleading. According to the results in the study area, woody components cause about 14%–28% overestimation, whereas non-randomness within canopies causes about 16%–25% underestimation. Such overestimation and underestimation lead to results that correct the effect of neither the non-randomness within canopies nor the woody components,

although in some cases, correction may appear to have been achieved. Fig. 3.13 shows that PAI_CC seems to agree with LAI_PATH well, especially in sites 2 and 3, even without considering the woody components and non-randomness within canopies. However, PAI_CC may not reveal real information because the degree of non-randomness within canopies and the proportion of woody components vary in different forests. The results show that PAI_CC is about 9% smaller than LAI_PATH in site 1 but about 7% larger than LAI_PATH in site 4.

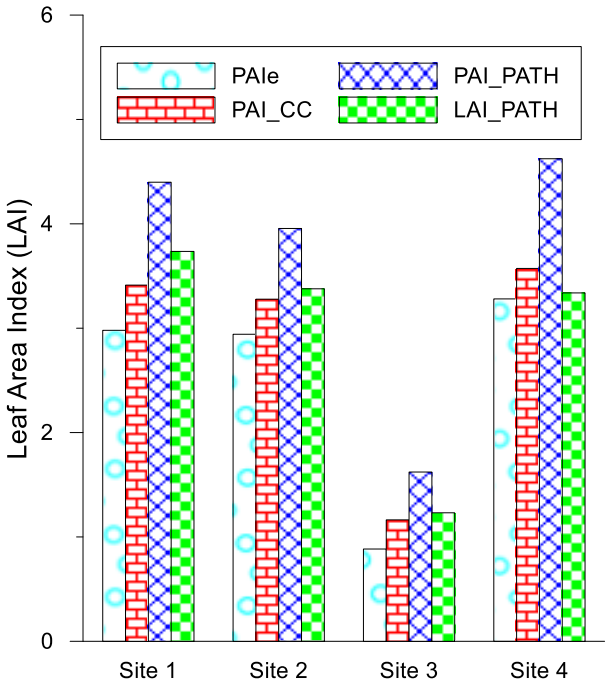


Fig. 3.13 Effect of woody components on the indirect leaf area index measurement. PAIe is the effective plant area index, PAI_CC is the plant area index of the gap size distribution method, and PAI_PATH and LAI_PATH are the plant area index and leaf area index of path length distribution model, respectively.

The mixed effect should be studied because it widely exists in indirect field measurements. Most optical instruments cannot distinguish leaf and woody components to provide the PAI or PAIe. By contrast, the destructive direct measurement provides LAI rather than PAI because only leaves are measured. The directly measured LAI is always utilized to validate the indirect measured PAI. The mismatch absolutely underestimates spatial heterogeneity, which consequently underestimates woody components. Thus, simultaneously quantifying spatial

heterogeneity and woody components is necessary because they can hardly be separated in forests.

## 3.7 Conclusion

A new theory based on path length distribution is proposed to improve indirect LAI measurement. Path length distribution theory can characterize and handle non-randomness within canopies, which may cause underestimation of up to 25%, and cannot be solved by existing algorithms. In our theory, path length distribution is introduced to expand Beer's law, avoiding the assumption of constant path length within canopies. Two methods for calculating path length distribution are presented.

Comprehensive validations consistently show that path length theory can characterize the inconstant path length within canopies effectively. Path length method based on measured gap data, which makes fewer assumptions, is accurate and stable in various scenes. The deviation is less than 10% in all scenes, which is better than that of widely employed methods and can meet the accuracy requirement of the GCOS. This method can be applied to commonly used instruments, such as TRAC, LAI-2000, and HemiView. The high accuracy, stability, and practicability of path length distribution theory are expected to benefit LAI indirect measurement tasks significantly.

# Chapter 4 Estimating Leaf Area of An Individual Tree in Urban Areas Using Terrestrial Laser Scanner and Path Length Distribution Model

Urban leaf area measurement is important for properly accessing the impact of urban trees on micro-climate regulation, heat island effect, building cooling, air quality improvement, and ozone formation. Previous work on leaf area measurement mainly focused on the stand level, although the presence of individual trees is more common than forests in urban areas. The only feasible ways for operational non-destructive leaf area measurement, namely optical indirect methods, are largely limited in urban areas because the light path is always intercepted by the surrounding buildings or other objects. Terrestrial laser scanner (TLS), which can extract the individual tree using its unique distance information, provides a possibility for indirectly measuring leaf area index (LAI) in urban areas. However, the indirect LAI measurement theory, which uses the cosine of observation zenith angle for path length correction, is incompatible for an individual tree because the representative projected area of LAI changes as the observation zenith angle changes, making the results incomparable and ambiguous.

In this chapter, the path length distribution model proposed in chapter 3 is modified for

individual tree leaf area measurement by replacing the traditional cosine path length correction for continuous canopy with real path length distribution. We reconstructed the tree crown envelope from TLS point cloud and calculated real path length distribution through laser pulse-envelope intersections. As a result, the foliage area volume density (FAVD) was separated from path length distribution model for leaf area calculation. Validations show that the TLS-derived leaf area using path length distribution is not sensitive to the scanning resolution and agrees well with the allometric measurement with an overestimation from $5m^2$ to $18m^2$ (3% to 10%). The results from different stations are globally consistent and the use of weighted mean of different stations by sample numbers further improves the universality and efficiency of the proposed method. Further automation of the proposed method can facilitate faster and operational leaf area extraction of an individual tree for urban climate modeling.

## 4.1 Introduction

Urban leaf area is particularly important and has attracted more and more attention, because of its important role in micro-climate regulation, heat island effects mitigation, buildings cooling (reducing energy consumption), air quality improvement, and ozone formation (Alonzo et al. 2015; Benjamin and Winer 1998; Najjar et al. 2015; Peper and McPherson 1998; Simpson 1998). Accurate leaf area measurement for urban trees is required for properly accessing the magnitude of these benefits.

Previous work on leaf area measurement mainly focused on the stand level, i.e. a contiguous community of trees (Leblanc and Fournier 2014; Nowak et al. 2008; Strahler et al. 2008; Weiss et al. 2004). Leaf area measurement for an individual tree is rarely explored although isolated trees are more common than forests in urban areas. Traditional optical instruments are not applicable to urban individual tree LAI measurement, because its light path is always intercepted by the surrounding buildings or other objects. Therefore, it is necessary to explore new instruments and methods to separate the individual tree from the urban

environment.

Terrestrial laser scanning (TLS) has advantages of good directivity, high angular resolution, and strong anti-interference ability, which facilitate the measurement of vegetation structure information. One of the advantages of TLS for individual tree measurement is that TLS can separate the studied tree from the urban environment using its unique distance information. However, the commonly used gap probability-based methods at the stand level need adjustment for an individual tree, because the continuous canopy assumption is typically not satisfied. There are two theoretical problems in Beer-Lambert law for individual tree measurement: 1) the representative projected area changes with the change of observation zenith angle (Nilson 1999), and 2) a large proportion of laser pulses are distributed in large zenith angles near 90° due to the relative position and height between TLS station and the tree crown, which can hardly be used in traditional methods (Demarez et al. 2008; Gonsamo and Pellikka 2009). Moreover, the 3D LiDAR data is not fully explored in gap probability-based method because gap probability or gap size distribution is only 2D information.

PATH method proposed in chapter 3 is not limited by observation zenith angle because it replaces the traditional cosine path length correction for continuous canopy with a real path length distribution. In chapter 3, it derives the relative path length distribution from the gap probability distribution measured by photography instrument using a sliding window for continuous canopy (Hu et al. 2016a; Yan et al. 2016b; Zeng et al. 2015). In this chapter, the unique distance information of TLS provides a potential to obtain the accurate path information directly for PATH model, making it possible to separate the path length and FAVD. Moreover, it can be used to get rid of the influence of the laser pulses reflected by objects other than the target tree. Inspired by the above findings, the PATH method is adjusted to an individual tree to calculate FAVD and leaf area by building an envelope from LiDAR data to get the absolute path length.

## 4.2 Modeling Leaf Area of a Single Tree

### 4.2.1 Beer-Lambert Law for A Forest Stand

The general formula [Eq. (1.1)] of Beer-Lambert law-based method is developed for a forest stand. Assuming the height is $h$, the path length passing through the stand is $h/\cos(\theta)$ and its representative projected area is $h \cdot \tan(\theta)$ (Fig. 4.1a) (Nilson 1999). For a forest stand, although the representative projected areas in different zenith angles are different, LAIs calculated in different zenith angles are comparable and compatible because the canopy is continuous. The leaf area per unit ground calculated in different zenith angles can be regarded as similar, because the leaf area increases with the representative projected area. The measurement in different zenith angles can be regarded as different samples representing the stand. It is noteworthy that continuous canopy is an assumption in almost all indirect LAI measurement methods, including the traditional clumping correction methods, because all of them use Eq. (1.1) or $\cos(\theta)$ for path length correction.

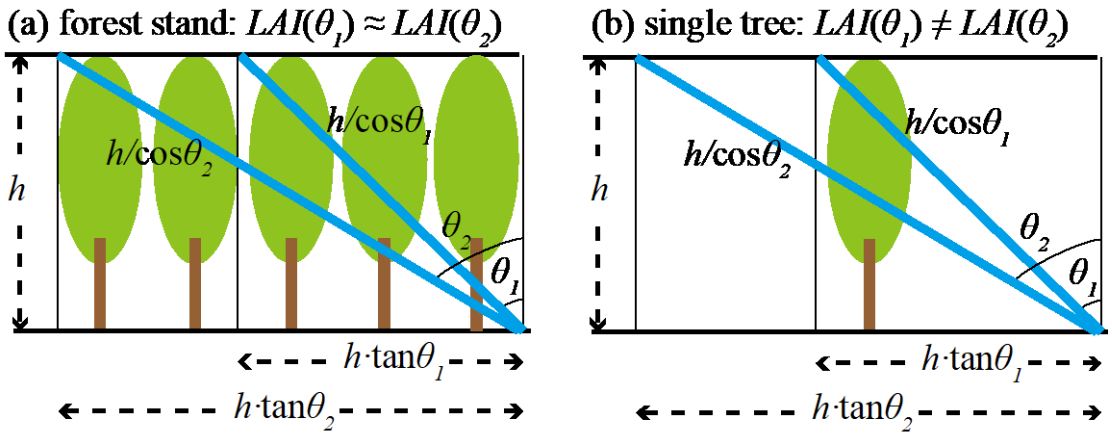


Fig. 4.1 Illustration of Beer-Lambert law-based method for a forest stand (a) and for a single tree (b).

### 4.2.2 Beer-Lambert Law for A Single Tree

For a single tree, however, the LAIs calculated from Eq. (1.1) in different zenith angles are incomparable and incompatible because the representative projected area changes while the total leaf area does not change (Fig. 4.1b). Therefore, these LAIs are ambiguous and cannot be averaged directly.

Considering that the LAI of an individual tree is ambiguous unless the size and position of the ground area is also given, the use of FAVD is suggested (Li-COR, 2011). However, FAVD alone is still not enough to characterize a tree crown, because its leaf area still varies with the volume. The total leaf area maybe be the best variable to characterize an individual tree because it is fixed and independent. For leaf area estimation, FAVD is more closely related to Beer-Lambert law than leaf area, whereas a volume is necessary to fix the leaf area.

$$LA = \rho \cdot V \quad , \tag{3.1}$$

where LA is the leaf area of a tree, $\rho$ is the FAVD, and V is the volume of the tree crown.

Path length distribution model is modified to model the FAVD of an individual tree by introducing a tree crown envelope with a known volume.

### 4.2.3 Path Length Distribution Model for A Single Tree

Path length distribution model (PATH) was proposed to consider crown-shape-induced clumping effect within crowns by introducing path length distribution to the theoretical prototype of Beer-Lambert law. Foliage clumping, namely nonrandom foliage distribution is a description of spatial distribution of leaves. The path length distribution describes the thickness distribution of crowns which is filled with leaves and the thickness distribution is also a description of spatial distribution of leaves. Assuming the random foliage distribution within the crowns, the path length distribution becomes the main factor to describe the spatial distribution of leaves.

PATH was originally developed in traditional optical instruments, which can only obtain

relative path length distribution from gap distribution data rather than absolute path length distribution. The relative path length distribution and relative FAVD are used as intermediate variables, which are enough for LAI estimation in a forest stand but absolute FAVD is unavailable.

TLS provide 3D point cloud data, which facilitate acquiring absolute path length distribution directly and separate the path length and FAVD. The PATH model is modified for an individual tree as:

$$P = \int_0^{l_{\max}} e^{-G\cdot\rho\cdot l} \cdot p_l(l)\, d(l) \ , \qquad (3.2)$$

where $P$ is the average gap probability in the tree crown, $G$ is the leaf projection function, $\rho$ is FAVD, $l$ is the path length, and $p_l(l)$ is the path length distribution function, where $\int_0^{l_{\max}} p_l(l)\, d(l) = 1$. The P and G are basic inputs for Beer-Lambert law-based method, $p_l(l)$ can be calculated based on intersections between laser pulses and the tree crown envelope constructed from point cloud data. Detailed calculations will be described in the method section. With all these variables known, the FAVD can be retrieved with root-finding algorithms.

## 4.3 Materials

### 4.3.1 Studying Site

The studying site is located in the historical garden of university of Strasbourg (Fig. 4.2) (48°35'4"N, 7°45'49"E). It is a part of a long term fieldwork experiment to measure and monitor the urban climate of the city of Strasbourg, with a particular focus on the role of vegetation in micro-climatic conditions (Najjar et al. 2015). The historical garden is a park with two rows of regularly spaced silver linden trees surrounded by 20 meters high university buildings. It is a typical urban environment where trees are isolated but are frequently blocked by buildings and other trees from different directions. Each silver linden tree is approximately 9 m high with an under-crown height of approximately 2 m. The diameter at breast height is approximately

0.3–0.4 m and the crown width is approximately 5 m. The foliage of a silver lime tree appears in April and remains until October. The data acquired during the leafy and leafless (branches alone) periods from 2013 to 2017 was used to characterize the tree structures.

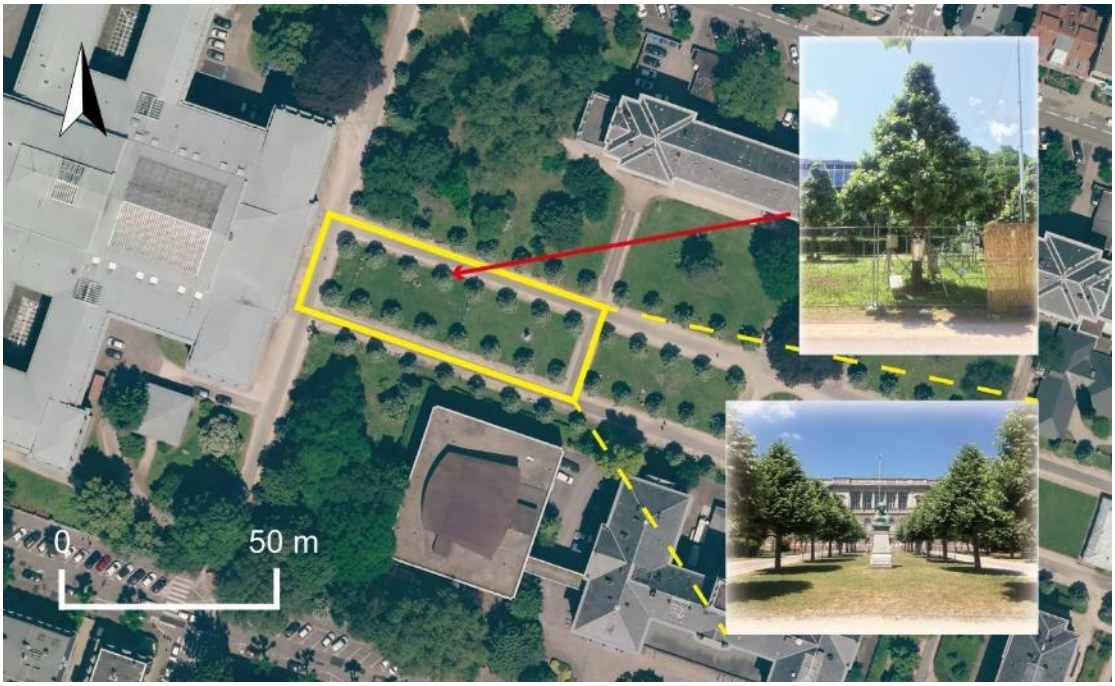


Fig. 4.2 Overview of the studied tree in the historical garden of the University of Strasbourg, France.

### 4.3.2 Terrestrial Laser Scanning (TLS) Data

TLS data was collected with a time-of-flight laser scanner (Leica ScanStation C10) on July 3, 2013 and a phase-shift laser scanner (FARO Focus 3D X330) on January 25, 2015, November 15, 2015, June 27, 2016 and July 6, 2017. At least seven stations were used in each experiment, within which at least four stations have a complete view of the studied tree (Fig. 4.3). The acquisition parameters were chosen in consideration of acquisition time and data amount (Table 1). Several target spheres were adequately positioned in the field before scanning, and point clouds acquired from different stations were registered into a same coordinate system based on them. For each station, point cloud was export as PTX format, which contains the scanner

location and the information (coordinates and intensity) of all emitted laser pulses no matter whether they have a return or not.


Fig. 4.3 Overview of the studied tree (red circle) and the seven TLS stations in June 27, 2016

Table 4.1 Technical parameters of the two TLS systems

| **Instrument** | Leica ScanStation C10 | FARO Focus 3D X330 |
|---|---|---|
| Ranging method | Time-of-flight | Phase-shift |
| Ranging error | 4 mm at 50 m | 2 mm at 10 m |
| Resolution | 0.2 mrad | 0.6 mrad |
| Spacing between points | ~ 2 mm at 10 m | ~ 6 mm at 10 m |
| Beam divergence | 0.1 mrad | 0.19 mrad |
| Beam waist diameter (1/e) | 2.5 mm | 2.25 mm |

### 4.3.3 Allometric Data

Allometric measurements on leafy shoots were carried out during the leafy period. Approximately 25 shoots of different length were sampled in each measurement to represent

existing shoot length. For each shoot, the shoot length, the number of leaves, the distance between leaf nodes, and the petiole length were measured manually with a measuring tape. All leaves were cut and placed on a piece of red paper with a reference square of 4 cm × 4 cm, then the area of each leaf was extracted by an automatic image processing. Based on these measurements, allometric statistics related to leaf surface area, number of leaves and shoot length were established (Sonohat et al. 2006) using the VégéMaker tool (developed by INRA laboratory of Clermont-Ferrand, France) (Fig. 4.4).

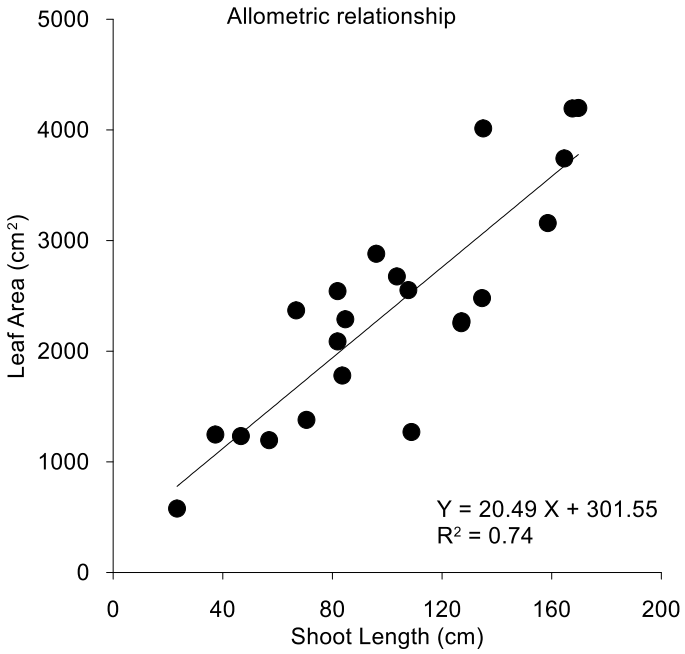


Fig. 4.4 Allometric relationship between leaf area and shoot length

Similar allometric statistics were obtained for four different dates: August 2013, September 2014, July 2017 and August 2017. With these allometric statistics, it is possible to have a reliable estimation of the total leaf area of a tree if the lengths of all its shoots are known. The skeletons of all shoots of the studied tree were reconstructed based on the 3D point cloud to have complete tree structure and the length of all shoots. For the year of 2013, the shoots were reconstructed by manual digitalization, which takes three months but is very accurate. For other years, the shoots were reconstructed by automatic 3D reconstruction using the Boudon et

al. (2014) method (Bournez et al. 2017) (Fig. 4.5). Then the length of each reconstructed shoot was obtained and was used for leaf area calculation based on allometric statistics. The total leaf area in the summer of 2013 was considered to be the most accurate because both the allometric statistics and shoot lengths were measured manually. The leaf area of the studied tree was 187.39 $m^2$, 182.47 $m^2$, and 179.86 $m^2$ on July 3, 2013, June 27, 2016 and July 6, 2017, respectively. The three measurement dates are similar with a difference of approximately a week and their results are close. Therefore, we think these results are reasonable and consider them as validation data in this study.

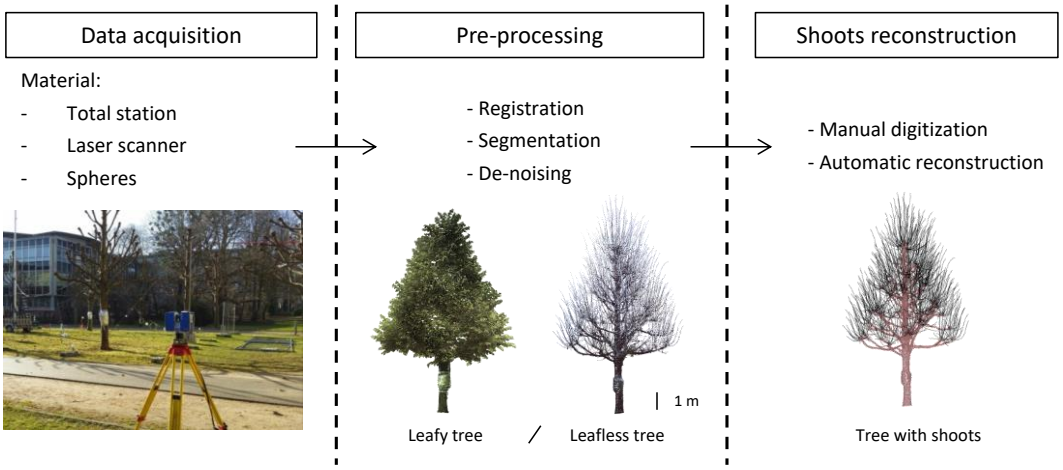


Fig. 4.5 Terrestrial laser scanning data acquisition, pre-processing, and reconstruction of the studied tree (Source : E. Bournez).

### 4.3.4 Leaf Angle Distribution Measurement

The leaf angle distribution was obtained from leaf normals computed using high-resolution point cloud (Table 4.1) and an open source software CloudCompare (www.cloudcompare.org). The trunk and the branches were removed before computation. The leaf normals were computed using plane surface model (Bailey and Mahaffee 2017). The computed leaf inclination angles were validated with the method proposed by Ryu et al. (2010b) and Pisek et al. (2011b) that measures selected leaves oriented approximately parallel to the viewing direction. The point

clouds were visualized and inspected in CloudCompare using leveled camera setting. Validations show that the computed leaf inclination angles using CloudCompare agree well with those using manual measurement. The leaf projection functions [Eq. (1.7)] computed from the point cloud of each station and the merged point cloud of four stations were compared and a small difference (< 3%) was found (Fig. 4.6). The G function of merged point cloud was used for further calculation.

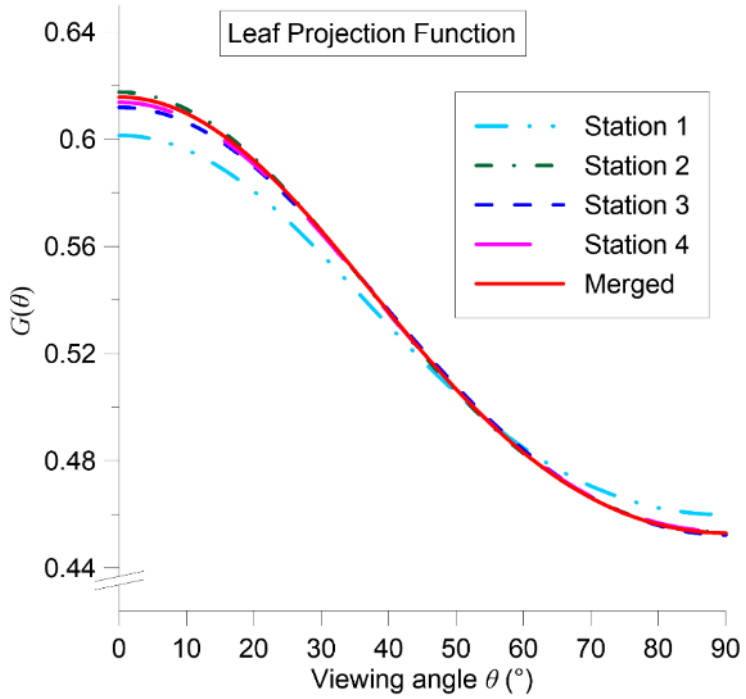


Fig. 4.6 Leaf projection functions (G) computed from the point cloud of each station and the merged point cloud of four stations in July 3, 2013

## 4.4 Methods

FAVD is estimated using the path length distribution and the gap probability within the studied tree crown by Eq. (3.2). The leaf projection function G is calculated from the leaf angle distribution measured in the high-density point cloud. An envelope was reconstructed for path length distribution calculation and a tree crown mask was used to limit the calculation within

the studied tree crown. The envelope is reconstructed based on the merged point cloud obtained from multiple stations, while the tree crown mask, the path length distribution, the gap probability and the FAVD were calculated for each station separately.

### 4.4.1 Envelope Reconstruction

Point cloud data from multiple stations were merged together to characterize the complete envelope of each tree. The point cloud is thinned to one tenth of the complete point cloud to speed up processing. The thinning process hardly affects the path length distribution as the thinned point cloud still have enough information to characterize the outline of the tree crown. Then the crown of the studied tree was segmented manually using CloudCompare. Alpha shape algorithm (Edelsbrunner and Mücke 1994) was then applied to the segmented point cloud to reconstruct the envelope of the tree crown using MATLAB. This algorithm can reconstruct both convex and concave envelopes (Fig. 4.7). Convex envelope, which is composed of hundreds of triangular facets, is the smallest convex region enclosing all points, whereas concave envelope, which is composed of thousands of triangular facets, fits the tortuosity of the tree crown better. In the concave envelope, the outline is refined by removing the large gaps in the edges. In this study, both convex and concave envelopes will be tested.

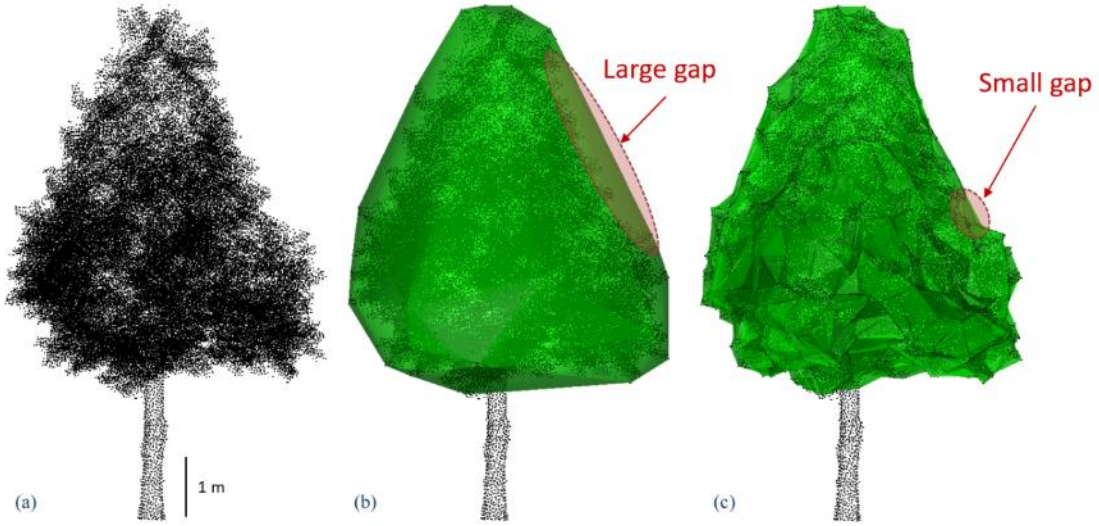


Fig. 4.7 The merged point cloud (a), convex envelope (b), and concave envelope (c) of the studied tree crown.

### 4.4.2 Tree Crown Mask

For each station, a tree crown mask is used to filter the laser pulses which do not enter the tree crown because these laser pulses do not contribute to retrieval. Intersections were calculated between the tree crown envelope of the studied tree and each emitted laser pulse no matter whether it has a return or not (Fig. 4.8). The laser pulses without any intersections with the envelope were first filtered (Fig. 4.8, laser pulse a). The laser pulses, those have intersections but were blocked by objects between the studied tree and the laser scanner (Fig. 4.8, laser pulse b), also do not contribute information to retrieval. These laser pulses were filtered by distance. If the distance from the laser scanner to the return is shorter than that to the envelope, it means that this pulse is blocked by other objects and does not reach the envelope. All further processes only concern the laser pulses within the tree crown mask, which is composed of emitted laser pulses c, d and e in Fig. 4.8.

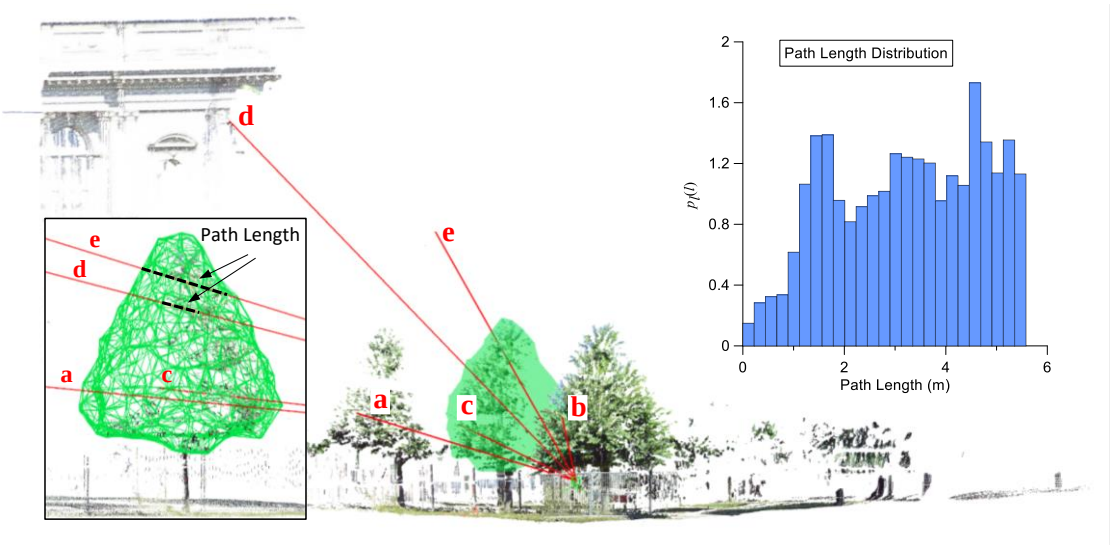


Fig. 4.8 Illustration of laser pulses, gap probability and path length calculation for the studied tree using its envelope. Approximately 43% of the studied tree (green) is visible from TLS station in the illustration. Emitted laser pulses are classified into 5 types: a - do not intersect the tree crown envelope, b – blocked by the objects in front of the tree. c – intersect within the tree crown envelope and have a return within the envelope, d – pass through the envelope and have a return behind the tree, e – pass through the envelope and have no return. Only emitted laser pulses c, d, and e are used to calculate the gap probability and path length distribution within the tree crown.

Specifically, the coordinates of a laser pulses without returns are (0,0,0) in PTX file, it is necessary to know its direction for determining whether it has intersections with the envelope. Considering the TLS acquires data with a consistent zenith and azimuth angular spacing, its direction can be interpolated accurately. The data in PTX file is formatted as an image, and each record in PTX file can be regarded as a pixel in the image. First, we calculated the zenith and azimuth angles of the pixels with known coordinates. Second, the zenith and azimuth angles of remaining pixels are interpolated based on the zenith and azimuth angles of surrounding pixels and the zenith and azimuth angular spacing of TLS (Table 4.1). Once the directions of these laser pulses are known, they could be used for tree crown mask and path length distribution calculation as the same as the other laser pulses with known coordinates.

### 4.4.3 Path Length Distribution

The path length distribution is calculated for each station using the tree crown mask. The path length represents the distance a laser pulse travels through the studied tree crown. Each laser pulse is a ray emitted from TLS and regarded as having an infinite length. The intersections of each laser pulse with each triangular facet of the tree crown envelope are calculated. If a laser pulse encounters the tree crown envelope, it generally has two intersections, with one entering and the other exiting the envelope. The path length is calculated as the distance between the two intersection points. It is noteworthy that the emitted laser pulses with a return within the envelope (Fig. 4.8, laser pulse c) also employ this manner for path length calculation, even though it does not actually pass through the envelope. Finally, the path length distribution is obtained from statistics of all the path lengths.

### 4.4.4 Gap Probability

Gap probability is calculated from the TLS data of each station separately using the tree crown mask. Leica C10 and FARO Focus 3D X330 are both single return TLS, therefore, gap probability of the studied tree is calculated as the ratio of the number of laser pulses passing through the tree crown to those entering the tree crown. The surrounding objects should be considered additionally for a single tree compared to a forest stand. First, the number of laser pulses entering the tree crown was calculated by using the tree crown mask, where the laser pulses that are blocked by instruments or other trees are omitted from the calculation (Fig. 4.8, laser pulse b). Second, the laser pulse with no return or with a return from the object behind the studied tree is regarded as a gap (Fig. 4.8, laser pulse d). Therefore, in addition to laser pulses without returns, the laser pulses, whose returns are farther than envelope, are also gaps for the tree crown.

### 4.4.5 Weighted Mean of Multi-Station FAVD

The studied tree is scanned from several stations (Fig. 4.3), and FAVD is calculated from each station for the same tree separately using path length distribution model [Eq. (3.2)] with root-finding algorithm. Specifically, Brent's method of GNU Scientific Library was chosen as the root-finding algorithm in our programming and it can solve the FAVD of a tree in a few seconds. Different stations are at different distances and have different fields of view of the studied tree. We averaged the FAVDs calculated from different stations with weighting factors, to use more samples and achieve a higher confidence. The weighted mean and the weighted standard deviation of FAVD are:

$$\bar{\rho}_w = \frac{\sum_{i=1}^{N} \rho_i \cdot w_i}{\sum_{i=1}^{N} w_i} \tag{3.3}$$

$$\sigma_w = \sqrt{\frac{\sum_{i=1}^{N} \left(\rho_i - \bar{\rho}_w\right)^2 \cdot w_i}{\sum_{i=1}^{N} w_i}} \quad , \tag{3.4}$$

where $\bar{\rho}_w$ is the weighted mean of FAVD, $\sigma_w$ is the weighted standard deviation, $\rho_i$ is FAVD calculated from each station, $w_i$ is the weighting factor. Both the number of laser pulses and the sum of path lengths are tested as the weighting factor. The number of laser pulses is related to the number of samples in scanning direction, while the sum of path lengths contains the additional depth information and is related to the volume proportion.

### 4.4.6 Leaf Area and Woody Area

The result of allometric method is leaf area. However, both leaf area and woody area contribute to the result of gap probability-based method during the leafy period, because both of them block the laser beam. To compare the results of allometric method and gap probability-based method, it is necessary to make sure their results have the same physical meaning.

For gap probability-based method, data acquired during the leafless period (branches alone)

was used to quantify the woody area using the same model as during the leafy period. The leaf area of gap probability model is:

$$LA = PA - WA \ , \tag{3.5}$$

where *LA* is the leaf area, *PA* is the plant area which is the result of gap probability-based method during the leafy period, *WA* is the woody area which is the result of gap probability-based method during the leafless period.

## 4.5 Results

### 4.5.1 FAVD Retrieval from Different Stations Using Path Length Distribution Model

In each measurement, FAVD was retrieved from different TLS stations separately (Table 4.2), and the weighted mean of different stations was calculate using Eq. (3.3). Station 3, 4, 6, and 7 are in the range of 7.2 to 11.2 meters away from the studied tree and there is almost no object occluding the scanning (Fig. 4.3). Almost 100% of the studied tree can be observed from these stations and a large number of laser pulses reach the tree crown. The path length distributions obtained from these four stations are similar (Fig. 4.9). The results of station 3, 4, 6, and 7 are closest to the weight mean of the seven stations. Station 1, 2 and 5 were not set specifically for studied tree but for the whole garden. These three stations are farther away from the studied tree than other stations and cannot observe the whole tree due to occlusion. Only 9%–27% of the studied tree is visible from station 1, 2 and 5 because the field of view of TLS is blocked by other trees or objects. The path length distributions of these three stations are various and different from other stations (Fig. 4.9), because different parts of the tree crown are observed. The station 1, 2 and 5 have small number of laser pulses entering the tree crown, which is only approximately 5% or less of that of another station. The difference between the weight mean and the result of station 1 or 2 is larger than that between the weight mean and the

results of other stations. The FAVD mean weighted by number of pulses and by sum of path lengths are consistent, indicating either number of pulses or sum of path lengths is a good weighting factor.

Table 4.2 Foliage Area Volume Density retrieved from seven TLS stations using path length distribution model and concave envelope in June 27, 2016

| Station | Distance (m) | Zenith angle (°) | Gap probability | Number of pulses | Sum of path lengths (cm) | Visible proportion | FAVD |
|---|---|---|---|---|---|---|---|
| 1 | 21.8 | 74.0-89.3 | 0.0375 | 24636 | 7723208 | 22% | 4.18 |
| 2 | 21.2 | 73.2-88.9 | 0.0428 | 32224 | 8964874 | 27% | 4.35 |
| 3 | 8.2 | 51.0-87.2 | 0.0390 | 733266 | 240238600 | 100% | 3.69 |
| 4 | 9.6 | 55.1-88.1 | 0.0379 | 564733 | 173408250 | 100% | 3.89 |
| 5 | 25.9 | 76.1-89.3 | 0.0506 | 7388 | 2192861 | 9% | 3.62 |
| 6 | 11.2 | 61.1-89.3 | 0.0435 | 388309 | 122030813 | 97% | 3.40 |
| 7 | 7.2 | 49.0-88.1 | 0.0392 | 945730 | 299908200 | 100% | 3.56 |
| FAVD mean (SD) weighted by number of pulses | | | | | 3.655 (0.181) | | |
| FAVD mean (SD) weighted by sum of path lengths | | | | | 3.653 (0.178) | | |

SD – Standard Deviation

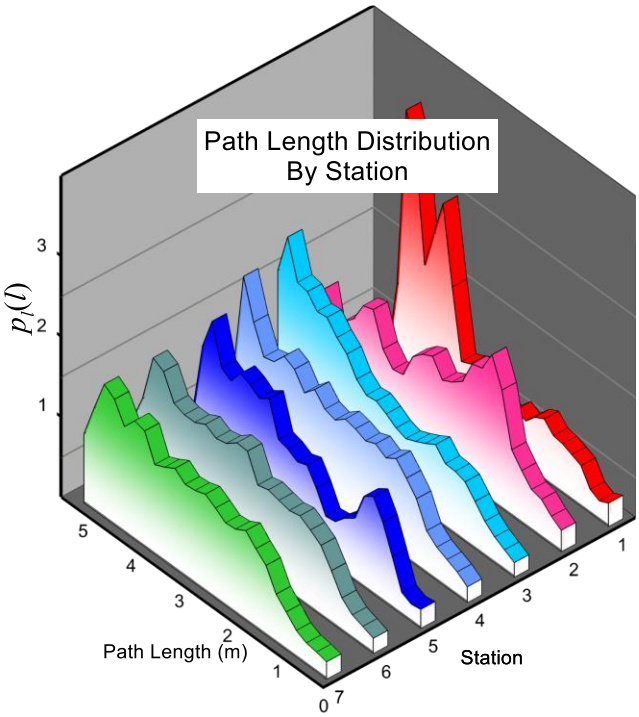


Fig. 4.9 Path length distributions from seven TLS stations using a concave tree crown envelope in June 27, 2016.

### 4.5.2 Plant Area, Leaf Area and Woody Area

FAVD was then converted to leaf area for comparison (Fig. 4.10). The result of Beer-Lambert law-based method during the leafy period is plant area, because the leaves and woody components intercept laser pulses equally. The result in winter when all the leaves have fallen, is woody area. Both the plant area during the leafy period and the woody area during the leafless period were retrieved by the consistent method using TLS data and path length distribution. The results of the three measurements around the early July of 2013, 2016, and 2017 are close. Among the tree measurement, the weighted standard deviation of leaf area in 2013 is the smallest. One possible reason is that the angular resolution of TLS in 2013 is the highest. The woody area retrieved from two measurements during the leafless period are close (Fig. 4.10), and their mean was used as woody area for all years.

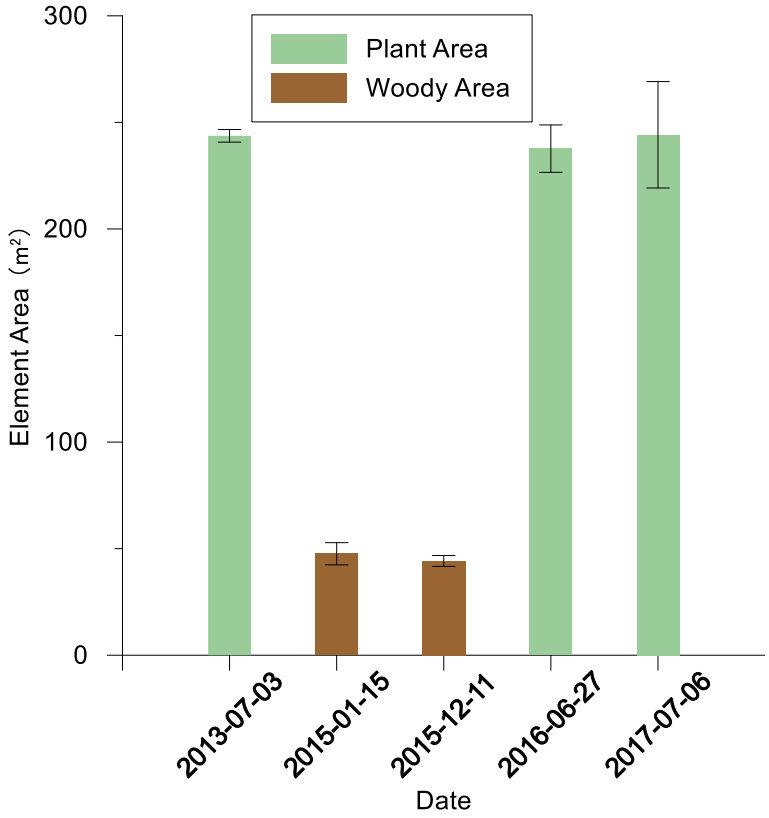


Fig. 4.10 Plant area or woody area of the studied tree retrieved using TLS data and path length distribution model at different dates and seasons. The results are weighted mean of several stations and the error bars donate weighted standard deviation.

The leaf area of the studied tree during the leafy period was calculated by subtracting the woody area from the plant area [Eq. (3.5)]. The leaf area retrieved using TLS data and path length distribution model was validated using allometric measurements (Fig. 4.11). The results retrieved using refined concave envelope generally agree with the allometric measurement, with an overestimation from 5m$^2$ to 18m$^2$ (3% to 10%) approximately. The convex envelope underestimates the results by 50m$^2$ to 80m$^2$ (29% to 43%) approximately during the leafy period. The relative difference between the woody areas calculated based on a concave envelope and a convex envelope is approximately 10% (Fig. 4.12), much smaller than the difference of leaf area (approximately 50%). Considering the tree crown during the leafy period is denser than that during the leafless period, the larger difference during the leafy period between the results calculated based on convex and concave envelopes indicate that the choice of envelope has a larger impact on a dense tree crown than a sparse tree crown.

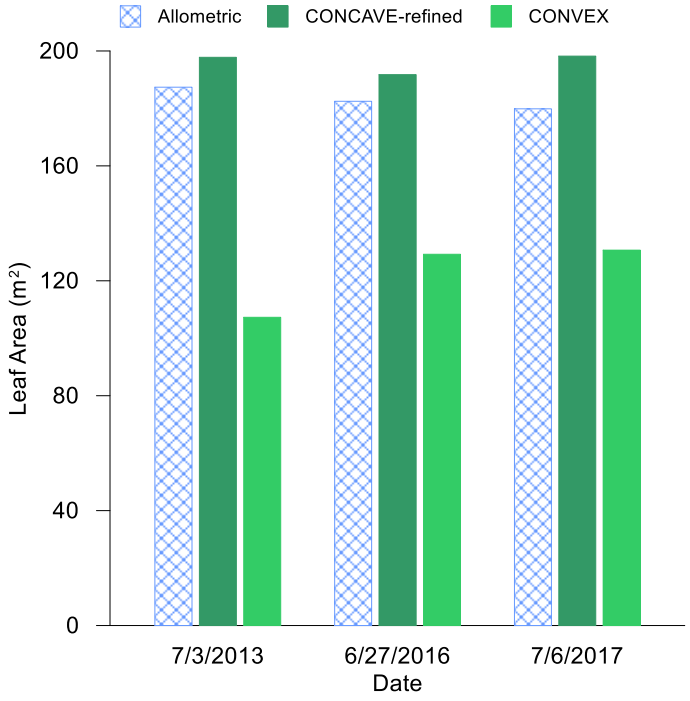


Fig. 4.11 Validation of the retrieved leaf area using TLS data and path length distribution model. Both refined concave envelope and convex envelope were tested.

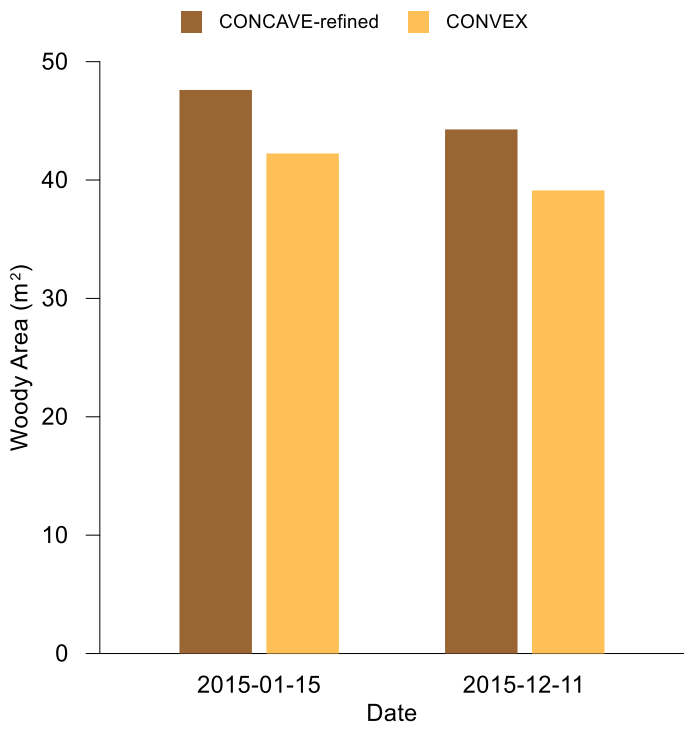


Fig. 4.12 Comparison of woody area retrieved using refined concave envelope and convex envelope.

### 4.5.3 Plant Areas of Ten Trees Retrieved from Seven TLS Stations

Plant areas of ten trees in the studying area were retrieved using the same TLS data from seven stations (Table 4.3). Although there is no allometric measurement available for these ten trees, the results show that the proposed method can characterize different plant areas with low standard deviation. Seven results for each tree were retrieved from seven TLS stations at different distances separately. The plant area of the ten trees range from 184.38 $m^2$ to 234.21 $m^2$. The relative proportion of weighted standard deviation to the weighted mean of the seven results for the ten tree ranges from 4.87% to 16.71%, indicating that the proposed method is generally stable in plant area estimation.

Table 4.3 Plant Area of ten trees retrieved from seven TLS stations in June 27, 2016

| Tree number | Distance (m) | Plant Area ($m^2$) | |
|---|---|---|---|
| | | Weighted mean | Weighted standard deviation |
| 1 | 14.9-37.8 | 186.10 | 10.03 (5.39%) |
| 2 | 9.1-33.2 | 192.97 | 17.43 (9.03%) |
| 3 | 5.9-29.0 | 184.38 | 11.01 (5.97%) |
| 4 | 7.2-25.9 | 234.21 | 11.41 (4.87%) |
| 5 | 8.9-26.6 | 225.82 | 28.07 (12.43%) |
| 6 | 13.5-46.5 | 184.41 | 18.62 (10.10%) |
| 7 | 8.5-42.6 | 197.83 | 27.72 (14.01%) |
| 8 | 5.4-39.3 | 189.22 | 9.90 (5.23%) |
| 9 | 5.3-37.6 | 228.49 | 15.35 (6.72%) |
| 10 | 7.6-37.3 | 231.14 | 38.63 (16.71%) |

### 4.5.4 Leaf Area Retrieved Using TLS Data at Different Resolutions

In order to analyze the influence of scanning resolution on leaf area estimation, the TLS data in July 3, 2013 with a resolution of 0.2 mrad was sampled every 2, 3, 5, 10, 15, and 20 points to build the TLS dataset with resolutions of 0.4, 0.6, 1, 2, 3, and 4 mrad, respectively. The same method and process were applied to the TLS data to estimate leaf area at different resolutions, and the differences of leaf area only result from different scanning resolutions (Fig. 4.13). The leaf areas at different resolutions are generally consistent, with a maximum difference of 6.6% between 0.2 mrad and 4 mrad. The leaf area slightly increases with resolution. The weighted standard deviation of leaf area increases with the decrease of resolution. The gap probability of the studied tree crown decreases with the decrease of resolution. Considering that smaller gap probability corresponds to a larger leaf area, the increase of leaf area is generally correlated with the decrease of gap probability.

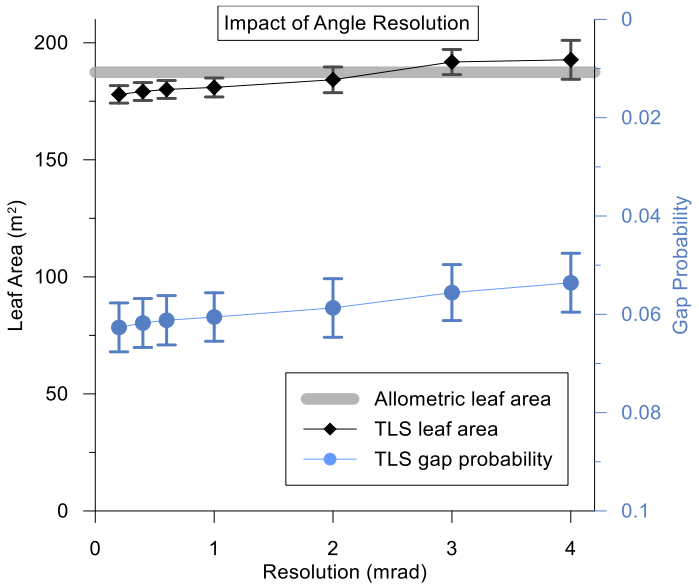


Fig. 4.13 TLS-derived leaf area and gap probability of the studied tree crown at different resolutions. The Results are weighted means of multi-station results retrieved using PATH model. The error bars donate weighted standard deviation of multi-station results.

## 4.6 Discussion

### 4.6.1 Consistency of Using FAVD And Path Length Distribution

The results of different stations are generally consistent, especially when there are enough samples (Table 4.2). It is reasonable because large visible proportion and number of pulses correspond to a high confidence. The results of station 1 and 2 differ more from the weighted mean, because these two stations are farther away from the studied tree and their fields of view are blocked by other trees. The number of laser pulses from station 1 or 2 reaching the studied tree is only about 5% of that of other stations, resulting in an inadequate sampling and low confidence. After introducing the number of pulses as a weighting factor, the contribution of station 1 or 2 is only 1% approximately and its uncertainty to the weighted mean is largely limited.

The relative proportion of standard deviation to weighted average of leaf area (1.5% to 3.8%) is found to be smaller than that of gap probability (7.9% to 11.2%) (Fig. 4.13), indicating that the uncertainty is reduced after using the path length distribution model. It is because the gap probability varies with path length distribution which varies at different parts of the tree crown scanned from different stations (Fig. 4.9). The use of path length distribution compensates the difference of gap probability in different parts and provides a more consistent leaf area.

The use of path length distribution also gets rid of the limitation of observation zenith angle. Traditional methods generally do not use the data at zenith angle larger than 60° due to the limitation of data acquisition and quality (Demarez et al. 2008; Gonsamo and Pellikka 2009). The observations at large zenith angle around 90°, which cannot be used in traditional methods using Eq. (1.1) because 1/cos(90°) is undefined, can be used in path length distribution model (Table 4.2). The TLS laser pulses at zenith angles around 90° often account for a large proportion of the emitted laser pulses, due to the relative position and height between TLS station and the tree crown (Table 4.2). It is particularly important to make use of the data around 90° because most of the leaves are distributed in the bottom of the tree crown.

### 4.6.2 Advantage of Weight Mean of Different Stations for Leaf Area Estimation

The FAVD means weighted by number of pulses and by sum of path lengths are very close, indicating either the number of pulses or sum of path lengths is a good weighting factor (Table 4.2). Although it is possible to filter the data with low confidence, the use of weighted mean has the advantages of consistency, universality, and efficiency. First, the same TLS dataset can be used for each tree in the studying area, ensuring a consistent input for leaf area estimation. Second, no subjective process or threshold is needed for filtering bad data, ensuring all the calculations are quantitative and universal. That is why we take into account the results of all

stations, although some of them will enlarge the weighted standard deviation. Third, the use of weighted mean eliminates the requirement of several complete scans for each tree separately, which largely reduces the required scanning stations. The weighted mean method makes use of the data of all stations, regardless of the visible proportion. The only necessary input is a complete tree crown envelope, which is not sensitive to the point density. If the merged point cloud can characterize the envelope of a tree crown, the method will provide a leaf area and a weighted standard deviation to indicate its uncertainty. It is particularly useful for measuring the leaf area of several trees, because it only needs several shared stations with enough coverage of all the studied trees instead of several stations for each tree separately.

### 4.6.3 Influence of TLS Laser Beam Size on Leaf Area Estimation

Finite size of TLS laser beam was reported to underestimate canopy gap probability (Beland et al. 2011). The accurate gap probability is supposed to be the proportion of laser beams whose centers do not fall within the area of leaves. However, a laser beam has a finite diameter. The laser beams whose edge hit the leaf area while having its center outside the leaf area might also have returns. These returns are misclassified as canopy and underestimate the proportion of gaps. Beland et al. (2011) proposed a method to correct gap probability estimation by accounting for the laser beam size. With a 800-m long-range TLS (ILRIS-3D) who has a laser beam diameter of 7.7 mm at 20-m distance, results show that on the side of an elliptical leaf, a beam centered outside the leaf area but at a distance smaller than 2.3 mm from its edge will trigger a return; and the gap probability was reported to be underestimated by approximately 20% from zenith angle of 40° to 90°. This correction needs the accurate value such as minimum intensity required to trigger a return and the radius of the parabolic mirror, which are not available in the technical documents of the TLS used in this study. Therefore, we conduct a relative analysis of the effect of laser beam size on gap probability estimation. In this

study, we used a 330-m range TLS (FARO X330) who has a laser beam diameter of 4.15 mm at 20-m distance. First, the ranging distance represents the ability of a TLS to trigger a return. A 330-m range TLS is less likely to trigger a partial return, because its theoretical ability of triggering a low signal can be calculated as roughly 41% of that using an 800-m long-range TLS. Second, the laser beam diameter in this study is 4.15 mm, which is 53.9% of that in previous study. Therefore, the maximum distance between the laser beam center and the leaf edge for triggering a return should be less than 2.3 mm * 53.9% = 1.24 mm theoretically. Considering the mean leaf area in this study is 150 $cm^2$ to 250 $cm^2$, which is four times of that in previous study. The gap probability underestimation caused by laser beam size is less than 5% according to the method of Beland et al. (2011).

### 4.6.4 Influence of TLS Scanning Resolution on Leaf Area Estimation

The TLS scanning resolution influences leaf area estimation on two aspects: gap probability and path length distribution. The path length distribution is mainly decided by the envelope, which is not sensitive to the TLS resolution. Higher resolution results in denser point cloud and can better characterize the inner details of the studied tree, but has little impact on the outline of the tree which is always best scanned. The envelopes reconstructed from TLS data at different resolutions show almost no difference.

The similar trends of increase of leaf area and decrease of gap probability at different resolutions indicate that the TLS resolution mainly influences the leaf area estimation by influencing the gap probability (Fig. 4.13). TLS scanning resolution corresponds to sampling density for gap probability measurement. Theoretically, the gap probability will not change largely with the change of resolution if there are enough samples. In this study, the gap probability does not change largely but shows a decreasing trend, which might be explained by the edge effect. There are more gaps at the edge of the tree crown mask. When the resolution

becomes coarser, the edge part will be less sampled and this part of gaps will be less observed. The weighted mean of leaf area does not change largely when TLS angle resolution becomes coarser, while its weighted standard deviation increases (Fig. 4.13). The relatively small difference (6.6%) between the results of 0.2 mrad and 4 mrad resolution indicates this method is not sensitive to the scanning resolution. However, higher resolution is still preferred in order to provide a smaller uncertainty of leaf area estimation.

### 4.6.5 Comparison of Convex and Concave Envelope

The validations using allometric measurement show that concave envelope perform much better than convex envelope, which considerably underestimates leaf area. The concave envelope separates the tree crown and the gaps outside the tree crown better because it fits the tortuosity of the edge of the tree crow. However, convex envelope is the smallest convex with not pit so it also contains lots of empty spaces at the edge. Therefore, convex envelope contains more gaps in it. The underestimation of convex envelope is due to large gaps in the edge of the tree crown, which largely increase total gap probability within the tree crown. The difference between gap probability in the edge and within the tree crown is a typical clumping effect of Beer-Lambert law. The larger the difference, the more serious the leaf area underestimation. The gap probability within a tree crown is extremely small because trees always have nearly the most leaves in the beginning of July. However, when the gap probability within the tree crown is also large in winter, the underestimation becomes less obvious (Fig. 4.12).

The vegetation heterogeneity within the crown, including the clumping of needles in shoots in conifers (Stenberg 1996a, b) and non-uniform FAVD within crown, may lead to a significant underestimation of the leaf area. In this study, we chose broadleaf trees to avoid the shoot clumping in conifers. And we use path length distribution to account the crown shape-induced within-crown clumping caused by inconsistent path length (Hu et al. 2014) while assuming uniform FAVD within the tree crown envelope. The uniform FAVD assumption

within the tree crown envelope is generally met in the studied trees during growing season; thus, the results in this study is generally good. Accurate envelope reconstruction using a matrix of voxels (Beland et al. 2014) will be useful for more complex tree structures and could be tested to improve the results in the future.

### 4.6.6 Comparison of Time-of-flight and Phase-shift Laser Scanner on Leaf Area Estimation

The scanner laser sensors used in this study are all based on discrete returns. As Newnham et al. (2012) described, the time-of-flight scanner emits a laser pulse and measures the discrete time-of-flight of a return echo from intercepted target. The time-of-flight scanner provide high accuracy at large range and resolve gaps well. The phase-shift scanner employs a constant wave laser with a certain frequency of intensity. The shifts in phase of the returned modulations are used to determine range. The phase-shift scanners can sample at much higher frequencies and are generally lighter and cheaper than “equivalent” time-of-flight instruments. However, the data are noisy around the edges of objects and gaps are more difficult to resolve. Limited results show that the time-of-flight laser scanner performs more stable than the phase-shift laser scanner for leaf area estimation, because the weighted standard deviation of leaf area retrieved using a time-of-flight laser scanner in 2013 is much smaller than those retrieved using a phase-shift laser scanner (Fig. 4.10). Processing point cloud obtained from time-of-flight scanner is simple and robust because all the laser pulses that intercept objects will return accurate coordinates, making it easier to classify distinguish vegetation returns and gaps. Processing point cloud obtained from phase-shift laser scanner is more complex because some partial beam interceptions (at the edge of canopy components) do not have coordinate information although they have intensity information (Newnham et al. 2012). The directions of these records can be calculated by zenith and azimuth angle interpolations accurately because the TLS scans in a specific order and angle interval. However, it is still difficult to identify whether such a leafy

record is within the studied tree crown or in other trees because the distance cannot be interpolated very accurately. Therefore, the results of phase-shift laser scanner show larger uncertainties than the time-of-flight laser scanner on leaf area estimation. Nevertheless, the weighted mean of leaf area retrieved using a phase-shift laser scanner is close to that retrieved using a time-of-flight laser scanner. Therefore, the phase-shift laser scanner is still attractive due to its low instrument weight and high scanning speed.

## 4.7 Conclusions

Path length distribution model (PATH) is modified to estimate the leaf area of an individual tree in urban areas. Instead of the relative path lengths in the original model, accurate path lengths, which allow path length distribution model to retrieve FAVD, are obtained from 3D TLS data directly. The path lengths are obtained by calculating the interceptions between all the emitted laser pulses and the tree envelope reconstructed from multi-station point clouds. Validation shows that TLS-retrieved leaf areas using path length distribution model agree well with the allometric measurement for the studied tree.

The new model eliminates the limitation of observation zenith angle and is not limited by surrounding buildings or other objects in urban areas. It is able to make use of the laser pulses around 90°, which contain most of the leafy information due to the relative position and height between TLS station and the tree crown but cannot be used by traditional methods. In addition, leaf area estimation using TLS point cloud is not sensitive to scanning resolution.

The leaf areas of different stations are generally consistent, especially when there are enough samples. The use of weighted mean of different stations by sample numbers further improves the universality and efficiency of the proposed method, because it can make use of the data from all stations even if there are occlusions.

The concave envelope generally performs better than convex envelope because large gaps in the edge are removed. The concave envelope is preferred in summer when the tree crown is

dense and has few gaps. Further researches are needed to analyze the influence of envelope in other seasons. Accurate envelope reconstruction using a matrix of voxels will be useful for more complex tree structures. Existing data shows that the time-of-flight laser scanner generally performs more stable in leaf area estimation, but the phase-shift laser scanner is lighter and faster. Comparing the time-of-flight with phase-shift laser scanner in one measurement will be interesting to analyze their differences quantitatively. Nearly all the data processing is automatic except for the manual segmentation of the studied tree. Integrating automatic segmentation algorithms into the calculation will be appealing for faster leaf area extraction of multiple independent trees with several scanning stations in urban areas.

# Chapter 5 Quantifying Clumping Effect and Estimating Leaf Area Index Using Airborne Laser Scanner and Path Length Distribution Model

The Airborne Laser Scanner (ALS) provides great potential for mapping the LAI at the landscape scale using grid cell statistics, while its application is restricted by the lack of clumping information, which has been an unsolved issue highlighted for a long time. The ALS results are generally an effective LAI because the ALS footprint is too large to capture small gaps to apply traditional ground-based clumping correction methods. In this chapter, a grid cell method is presented based on path length distribution model to calculate the clumping corrected LAI using the ALS data without requirement of additional field measurements. We separated the within- and between-crowns areas to consider between-crowns clumping, and migrated the path length distribution model to consider 3D foliage profile and within-crown clumping. The path length distribution model takes advantage of the 3D information rather than the gap size distribution, thus avoid the limitation of large ALS footprint. With the 0.4 m-footprint ALS data, the results are generally promising and a multi-level clumping analysis is consistent with landscape flown. The ALS LAIs of different resolutions are consistent, with a difference of less

than 5% from 5 m to 250 m resolutions. Due to its consistency and simple configuration, the method provides an opportunity to map the clumping corrected LAI operationally and strengthens the ability of airborne LiDAR to monitor vegetation change and validate the satellite product. This grid cell method based on path length distribution worth further testing and application using more recent laser technology.

## 5.1 Introduction

LAI estimation has been achieved from ground to satellite levels, while its accurate estimation is still difficult at landscape or regional scales. Indirect ground-level methods based on Beer-Lambert law, which utilizes the gap probability measured by optical instruments, are convenient and fast for measuring the LAI at scales from tens to hundreds of meters (Chen 1996; Hu et al. 2014; Ryu et al. 2010a; Yan et al. 2016a; Yan et al. 2016b). However, they are impractical for measuring the LAI over larger scales due to time, cost and labor limitations. Spaceborne or airborne passive optical remote sensing, which is based on physical vegetation models or empirical relationships between vegetation indices, is able to map the LAI over larger scales (Baret et al. 2013; Liang et al. 2013; Myneni et al. 2002; Nagler et al. 2004) but its accuracy and consistency are limited by several other factors, such as atmosphere, soil, and underlying vegetation; thus, calibration and validation are always required (Abuelgasim et al. 2006; Fang et al. 2012; Ren et al. 2013; Yan et al. 2016c).

The airborne laser scanner (ALS), also commonly known as airborne LiDAR, provides a great opportunity to accurately map the LAI due to its ability to penetrate canopies and its fast coverage over large areas (Bouvier et al. 2015). Its penetrating ability allows it to better characterize the interior canopy, thus alleviating the saturation problem (Lefsky et al. 2002; Lim et al. 2003b; Riano et al. 2004). The similarity between LiDAR penetration rate and gap fraction also provides an opportunity to use the well-developed methods in indirect LAI measurements that are based on Beer-Lambert law. In the past decade, gap fraction-based methods have been

introduced in LiDAR measurements to derive the LAI and found to be superior to allometric or empirical methods (Heiskanen et al. 2015; Luo et al. 2015; Morsdorf et al. 2006; Richardson et al. 2009; Tang et al. 2014a; Zhao et al. 2011).

While much progress has recently been achieved, the vast majority of airborne LiDAR work estimates $LAI_e$ rather than the actual LAI. Correcting clumping effect is still an unsolved and highlighted issue in airborne LiDAR studies. For LAI mapping, 3-dimensional discrete airborne LiDAR data were generally gridded into an image with a grid size of tens of meters (Heiskanen et al. 2015; Lovell et al. 2003), which generally covers several tree crowns and large gaps between crowns. Thus, both between-crown and within-crown clumping exist in each grid cell. The need for modeling and quantifying the clumping effect has been highlighted for airborne LiDAR research for a long time (Hopkinson et al. 2013; Hosoi and Omasa 2007; Lovell et al. 2003; Riano et al. 2004; Schneider et al. 2014; Zheng and Moskal 2009). Very few attempts have been made to quantify the clumping effect using airborne LiDAR. Those that have include performing regression analyses with vegetation indices (Thomas et al. 2011) and implementing the traditional ground method with gap size information (Garcia et al. 2015). The correlations between airborne and ground measurements were found to be good. However, the LiDAR-based clumping index is still different from the ground clumping index and thus field measurements are still needed for regression in these methods (Garcia et al. 2015; Thomas et al. 2011). In addition, the results of airborne LiDAR are generally worse due to the low point density (Garcia et al. 2015). Although much progress has been achieved, these methods did not quantify the clumping effect using airborne LiDAR independently, which restricts airborne LiDAR from operationally monitoring vegetation.

The large footprint and low point density of airborne LiDAR are two major constraints for applying the traditional ground method to correct the clumping effect, as airborne LiDAR footprints (tens of centimeters or larger) are too large to capture the small gaps (Heiskanen et al. 2015) and the detailed gap size distribution, even if it is possible to resolve the average gap probability. In addition, the three-dimensional (3D) information is also not utilized efficiently. 3D information is often converted to a 2D binary image to use the traditional gap distribution-

based method (Garcia et al. 2015).

PATH model proposed in chapter 3 provides a potential solution for correct clumping effect without the gap size distribution. The distribution of path length, which models the clumping effect in a special view, might be useful for modeling clumping using airborne LiDAR. In this chapter, we proposed a new approach which obtains the path length distribution directly from the 3-D canopy height distribution information.

Through obtaining gap probability and path length distribution from airborne point cloud data, the PATH model is migrated on airborne LiDAR data to quantify the clumping effect and clumping corrected LAI. The data was analyzed using grids of varying cell size and perform the further calculations in each grid cell. First, we separated the crown area from large gaps in each grid cell and associate them with with-crowns and between-crowns areas of interest. This step was achieved by using Vertical Crown Cover (VCC), which can be estimated to a high precision using a simple proportion of canopy points in first-return data (Korhonen et al. 2011). Second, the with-crowns LAI was calculated using gap probability and path length distribution of with-crowns areas in each grid cell. The gap probability was estimated using laser penetration metrics (LPM), also called the laser penetration index (LPI) derived from the vertical and horizontal distribution of hits in the areas of dense cover. The path lengths were estimated by Canopy Height Model (CHM) which effectively measures the spatial distribution of canopy heights in each grid cell. Third, the LAI was calculated as the product of within-crowns LAI and the proportion of within-crowns area (VCC) in each grid cell. Finally, the LPMs and LAI were validated using in situ measurements (Fig. 5.1). It should be noted that the clumping corrections of both airborne retrieval and field validation in this chapter is focused on between-crown and within-crown clumping beyond the shoot level, because neither airborne retrieval nor indirect field measurement can quantify the needle-to-shoot level of clumping. The correction of leaf angle distribution and woody component was not applied because this information is unavailable from airborne LiDAR and does not influence the validation of clumping corrected LAI.

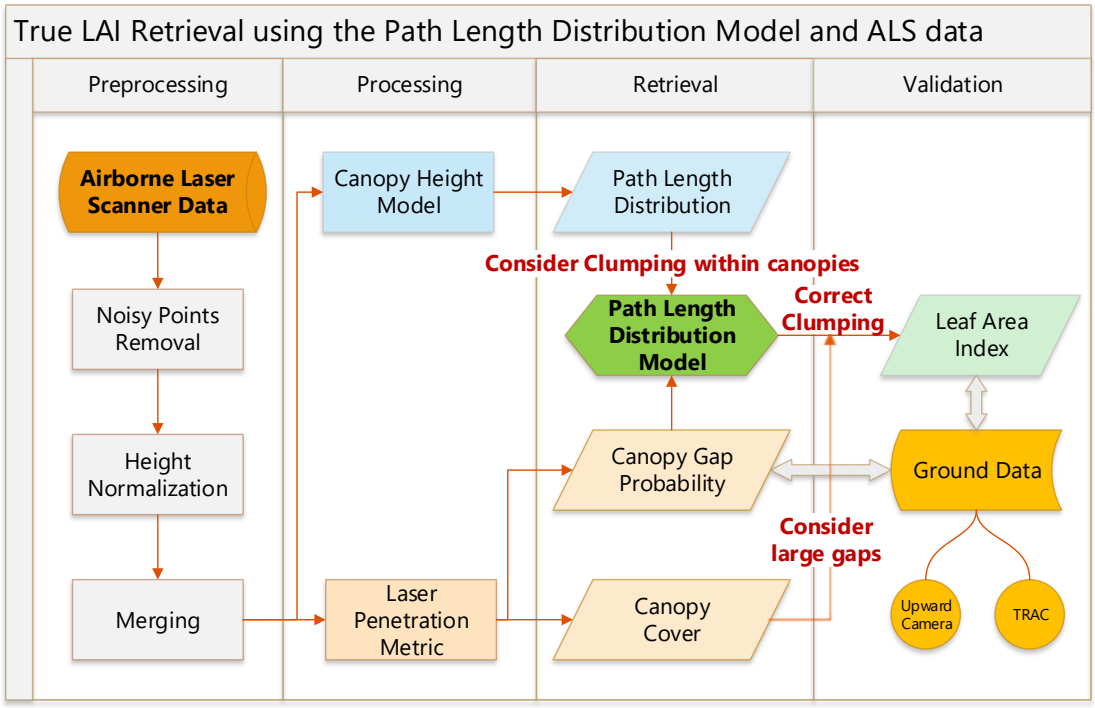


Fig. 5.1 Workflow diagram for estimating the clumping index and LAI by using the path length distribution model and airborne laser scanner data.

## 5.2 Materials

### 5.2.1 Study Area

The study area is located in the Genhe forestry reserve (120°12' to 122°55' E, 50°20' to 52°30' N), which is at the western face of north Greater Khingan (Fig. 5.2). The elevations range from approximately 775 m to 1300 m, and the slopes are less than 15° in 80% of the area. Located in the northernmost area of Inner Mongolia, Genhe has a monsoon-influenced subarctic climate and is officially designated the coldest city in China. The forest is mainly composed of *Larix gmelinii (Rupr.) Rupr.*, *Betula platyphylla Suk*, and *Pinus sylvestris var. mongolica Litv*. (Tian et al. 2015a).

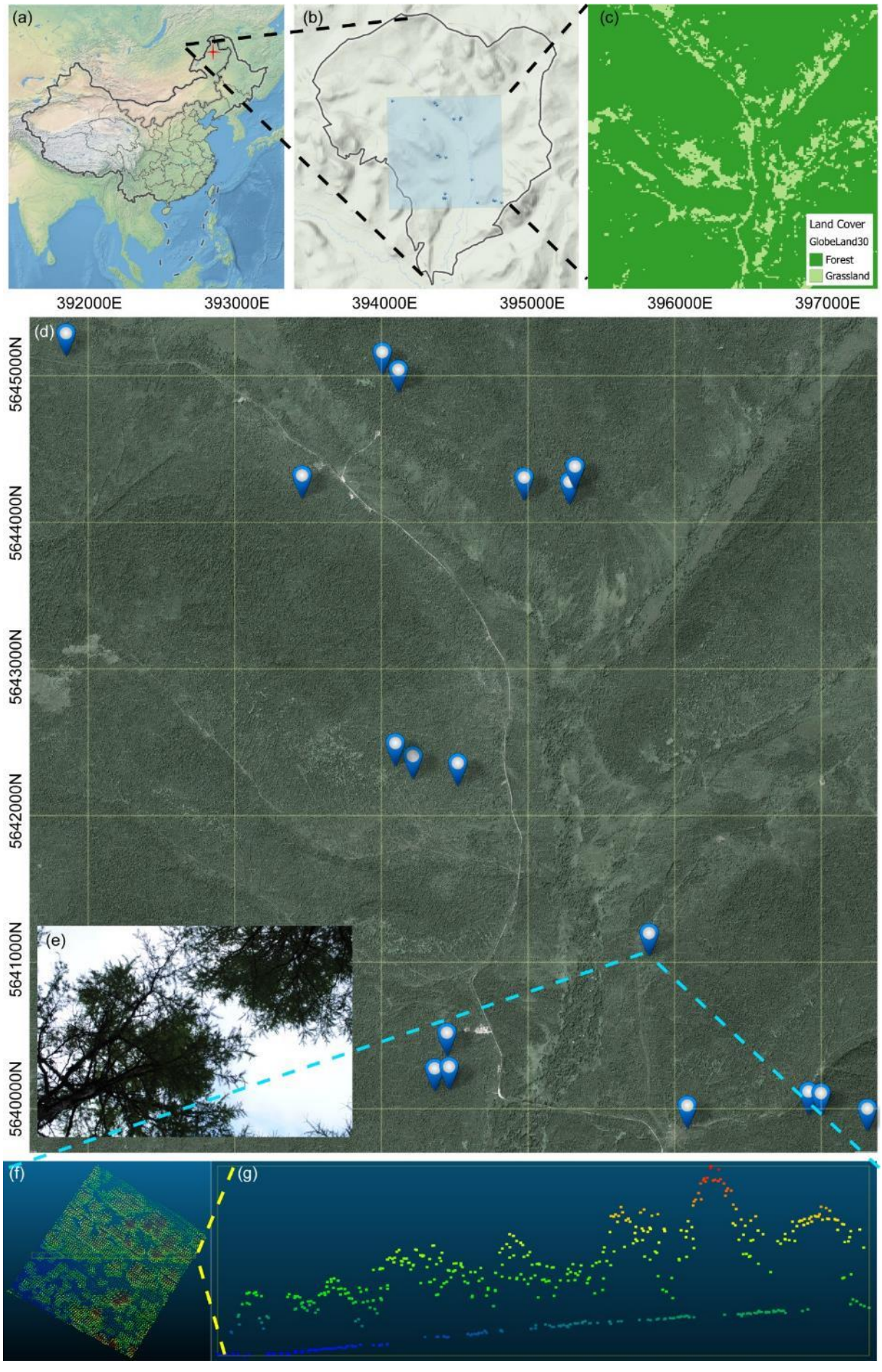
(a)
(b)
(c)
Land Cover
GlobeLand30
Forest
Grassland
392000E
393000E
394000E
395000E
396000E
397000E
(d)
5645000N
5644000N
5643000N
5642000N
5641000N
5640000N
(e)
(f)
(g)

Fig. 5.2 Airborne laser scanner data area and 18 field sites in the Genhe forestry reserve. (a) The position of the research area, (b) Google physical map of the research area, (c) Globeland30 Land Cover map of the ALS data area, (d) Google satellite map of the ALS data area and the positions of the 18 field sites, (e) upward photography and (f) point cloud data of site L1, (g) a transect of the point cloud data of site L1.

### 5.2.2 Airborne LiDAR Data

Airborne LiDAR data was collected using a Leica ALS60 system onboard a Yun-5 aircraft. This system works at a wavelength of 1064 nm and with a 0.22 mrad beam divergence. ALS60 was flown over the study area in the summer of 2012. It operated at a 166-kHz pulse rate at 1800 m Above Ground Level (AGL), with 97% of pulses falling within the 0-12° zenith angles and 99% of pulses falling within the 0-15° zenith angles. A maximum number of 4 returns were recorded per beam. The data used in this thesis is a subset of 20 flight lines, covering a 5700 m × 5800 m area (Fig. 5.2). The average pulse density was 5.91 pulses/$m^2$, and the average point density was 8.24 points/$m^2$.

### 5.2.3 Field Measurements

Field campaigns were conducted in 18 plots (45 m × 45 m) of the flight area (Fig. 5.2), using upward photography and Tracing Radiation and Architecture of Canopies (TRAC; 3rd Wave Engineering, ON, Canada). The field campaigns of vegetation monitoring were coordinated from 2013, and then the measurements were conducted during the same period of the year as for the flight in 2013. Upward photography measurements were conducted in all 18 plots, while TRAC measurements were conducted in 13 plots, with 200-300 m transects in each plot. The field measurement is a part of simultaneous satellite-borne, airborne, and ground-based experiments in addition to our study of LAI, and the other 5 plots were specially designed for the study of terrain effects and did not have TRAC measurement due to the limitations of

slope and accessibility.

The objective of this chapter is to correct the clumping beyond shoot level using airborne LiDAR. In field measurement, we also quantified the clumping and calculate the LAI beyond the shoot level in field measurement, in order to make the field data correspond to the airborne results. The needle-to-shoot level of clumping was not measured because it relies on manual measurements and is not available in airborne retrieval. Similarly, the woody components and the leaf angle distribution were not measured but considered in validation. Because the needle-to-shoot level clumping, the woody components, and the leaf angle distribution have the same contribution in airborne LiDAR retrieval and field measurement, the missing of these information does not limit the validation of the beyond shoot level clumping and the clumping-corrected area index.

Upward photography was employed for validation mainly because it provides a zenith-direction observation, similar to the ALS data. It was also found to outperform fisheye photography when correcting for the clumping effect and estimating the LAI (Macfarlane et al. 2007a). Approximately 50 upward photographs were taken using a Nikon D3000 in each plot along two diagonals across the sampling plot, generally under cloudy conditions, in JPEG format (Mu et al. 2015). The original images had a size of 2592 × 3872 pixels and a viewing angle of 66.4°×47.9°, and 60% of them were cropped to provide a viewing angle similar to that of airborne LiDAR. The k-means clustering method was employed to classify the images into sky and trees. Inspired by a previous work (Macfarlane et al. 2014), the two peaks of the blue channel histogram were detected as two initial inputs of the k-means clustering method for the automatic process. The histogram was also found to be helpful for overcoming exposure issues and scattering effects (Hwang et al. 2016; Macfarlane et al. 2014). The total gap probability was calculated using classified images and then used for validation of the ALS gap probability. Then, the clumping effect was corrected by dividing the gap probability into between-crowns and within-crowns gaps, which was first proposed by Macfarlane et al. (2007a) and was then successfully applied to continuously monitor the clumping-effect-corrected LAI at the ecosystem scale (Ryu et al. 2012). After image classification, the gap transects were sampled

from the classified images. For each image, several lines were sampled and combined into a long gap transect. We used an excessive sampling scheme so that all the pixels of the images were used. The large gaps between crowns were separated with a threshold of ten times the leaf width (Hu et al. 2014). The $LAI_e$ was calculated directly inverting Beer-Lambert law and the total gap probability. The LAI within crowns was calculated using the within-crown gap probability and then the LAI within crowns was multiplied by the fraction of the crown cover to calculate the LAI. A plagiophile leaf angle distribution, which was suggested to be more appropriate than a spherical distribution for temperate and boreal ecoclimatic regions (Pisek et al. 2013b), was used in both ground and airborne calculations, although the choice of leaf angle distribution do not influence the validation of clumping correction. The use of leaf angle distribution will be discussed in Section V.E.

As both the leafy component and woody component contribute to the ALS echo, the results of ALS data generally represent the Plant Area Index (PAI), which includes all the components of the plants. To match the results of the ALS data, the same classification was adopted in processing the photographs. The photographs were classified into the following two components: those of the sky and those of plants.

## 5.3 Methods

### 5.3.1 Preprocessing

The airborne LiDAR data was preprocessed using the *lasnoise*, *lasmerge*, *lastile* and *lasground* modules of LAStools (Isenburg 2016). First, the *lasnoise* module was used in each flight line to remove noise points (isolated points in the sky for example). Second, the *lasmerge* module was used to merge the flight lines together. Third, the *lasground* module was used to extract the ground points and then calculate the relative height above the ground for each point (Axelsson 2000). Because the ALS60 dataset for the whole research area is too big to execute the *lasground* module, the data were split into 1000 m × 1000 m tiles with a 50-m buffer in each

direction using the *lastile* module. The *lasground* module was applied to each tile, and the results were merged with the buffer removed. The buffer was used to avoid using the results at the edge of the data. Then, the height normalized ALS data were obtained for future processing. With a height threshold, points were classified as canopy and ground returns. The height threshold was set as 1 m to exclude the low grass and retain the relatively high underlying vegetation. Since all these preprocesses are commonly used in the LiDAR community, they could thus be achieved easily by using the batch-scriptable and friendly software LAStools or other similar tools or libraries.

### 5.3.2 Gridding

For LAI mapping, the 3-dimensional height normalized ALS data were gridded into an image. Grids with sizes of 5 m, 10 m, 30 m, 50 m, 100 m, 250 m, and 500 m were tested in this study. The LAI was retrieved for each grid cell. For each grid cell, two LiDAR metrics and a path length distribution were calculated for LAI retrieval (Fig. 5.3).

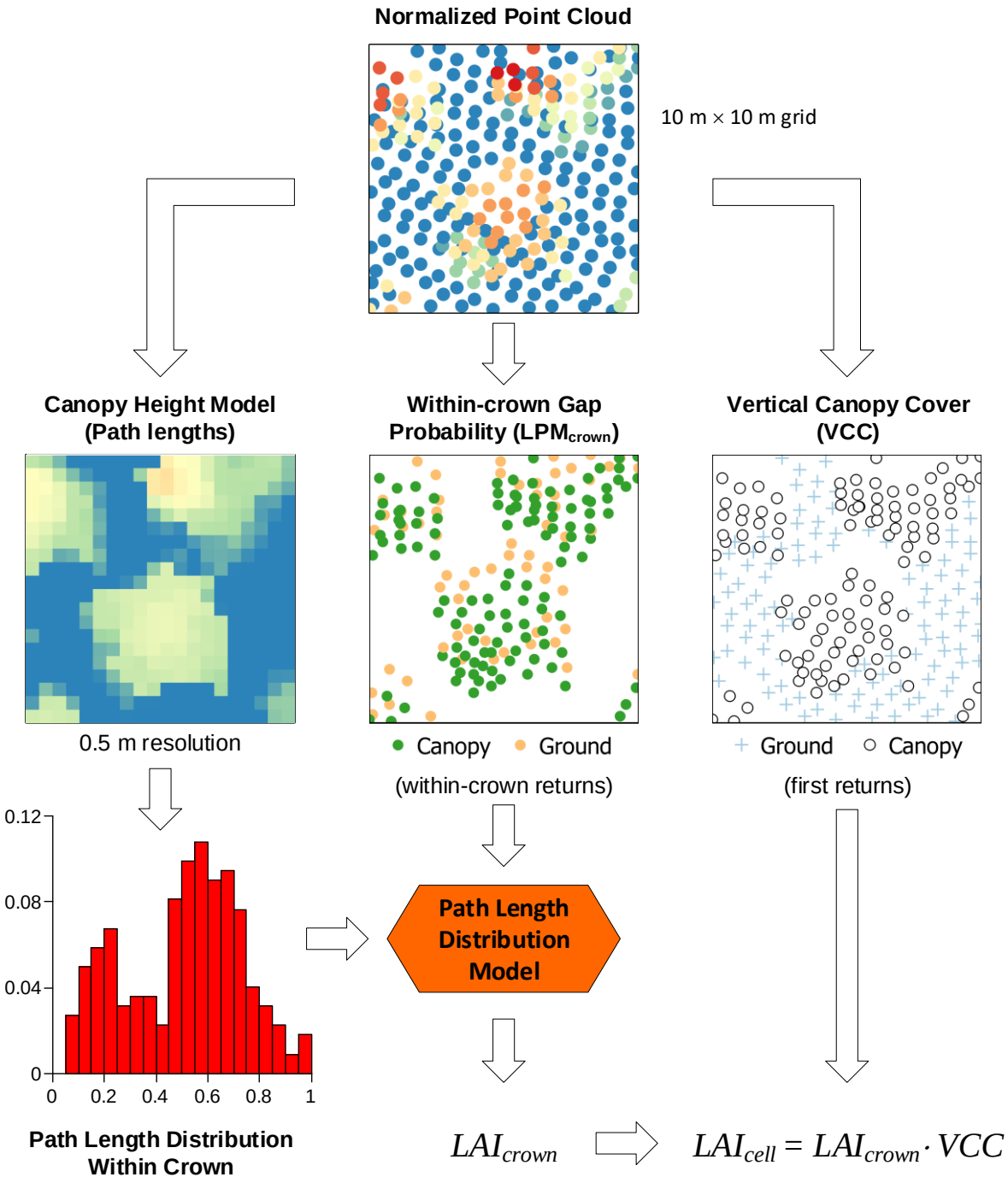


Fig. 5.3 Workflow diagram for processing the normalized point cloud data and calculating the LAI for each grid cell.

### 5.3.3 Theoretical Basis: Path Length Distribution Model

The path length distribution model was proposed in chapter 3 to address the clumping effect between crowns and the crown shape-induced non-randomness within crowns. It is based on the theoretical prototype of Beer-Lambert law and the path length distribution within crowns. The model is ideal for LiDAR, as it is able to take advantage of the 3D point cloud information of LiDAR data, and is thus able to provide path lengths directly, rather than via the traditional detailed gap distribution, which is inaccessible for large-footprint LiDAR data.

The Eqs. (2.19) and (2.20) of path length distribution model are mainly used to correct clumping within crowns in this chapter with the inputs of the average gap probability within crown ( $\overline{P_{crown}(\theta)}$ ) and the path length distribution within crown ( $p_{lr}(lr)$ ), and their results are clumping corrected LAI within crowns ( $LAI\_PATH_{crown}$ ). The clumping between crowns was corrected by fraction of large gaps in path length distribution model. All the calculations were made grid cell by grid cell. For each grid cell, the fraction of large gaps and the average within-crown gap probability were obtained from two LPMs, while the path length distribution was obtained from the path lengths from the CHM based on statistics.

### 5.3.4 Gap Probability from LiDAR Metrics

Two LiDAR metrics were calculated and combined for the LAI estimation in each grid cell. Within-crown Gap Probability was used to estimate the LAI within crowns ($LAI_{crown}$) in combination with path length distribution within crowns. Vertical Crown Cover, which is the proportion of tree crowns, ignoring within-crown gaps (Jennings et al. 1999; Korhonen et al. 2011), was used to quantify large gaps between crowns (i.e., correct horizontal clumping) and to convert the $LAI_{crown}$ to the LAI of the grid cell:

$$LAI_{cell} = LAI_{crown} \cdot VCC \quad . \tag{4.1}$$

The relationship between the total gap probability ($P_{cell}$), within-crown gap probability

($P_{crown}$), and VCC is:

$$P_{cell} = (1 - VCC) + P_{crown} \cdot VCC \quad , \tag{4.2}$$

where 1-*VCC* is the between-crown gap probability.

#### 5.3.4.1 Vertical Crown Cover (VCC)

VCC was calculated to quantify the proportion of tree crowns in each grid cell. First, a height threshold of 3 m was used to determine whether the grid has trees. If a grid cell contains no point higher than 3 m, it is regarded as a "no-tree" grid cell; otherwise, it is regarded as a "tree" grid cell.

For a "no-tree" grid cell, the VCC is not calculated and all points of the grid cell are used for calculating $LAI_{cell}$ using the path length distribution model (Section III.5.3.5).

For a "tree" grid cell, the VCC values are calculated as the crown proportions of first returns (Fig. 5.4):

$$VCC = N_{first\_canopy} / N_{first} \quad , \tag{4.3}$$

where $N_{first\_canopy}$ is the number of first returns classified as canopy and $N_{first}$ is the total number of first returns. Fig. 5.4 shows 9 grid cells in the grid and the analysis with the grid cells.

Then, only the returns from crowns are used to calculate the $LAI_{crown}$ using the path length distribution model, and the $LAI_{cell}$ is calculated by multiplying the $LAI_{crown}$ by the VCC [Eq. (4.1)].

It is reasonable to calculate the VCC using the first returns of ALS, as the ALS footprint is generally larger than gaps within a crown. It is convenient to distinguish and calculate the proportions of crowns and large gaps between crowns because the first returns from a crown are always canopy returns, and the first returns from large gaps between crowns are always ground returns. In this study, the ALS footprint had a diameter of 0.4 m, and there were rarely big holes larger than 0.4 m within crowns in the vertical direction; thus, a laser pulse could hardly pass through the canopy without any contact and hit the ground as the first return along

the vertical direction.

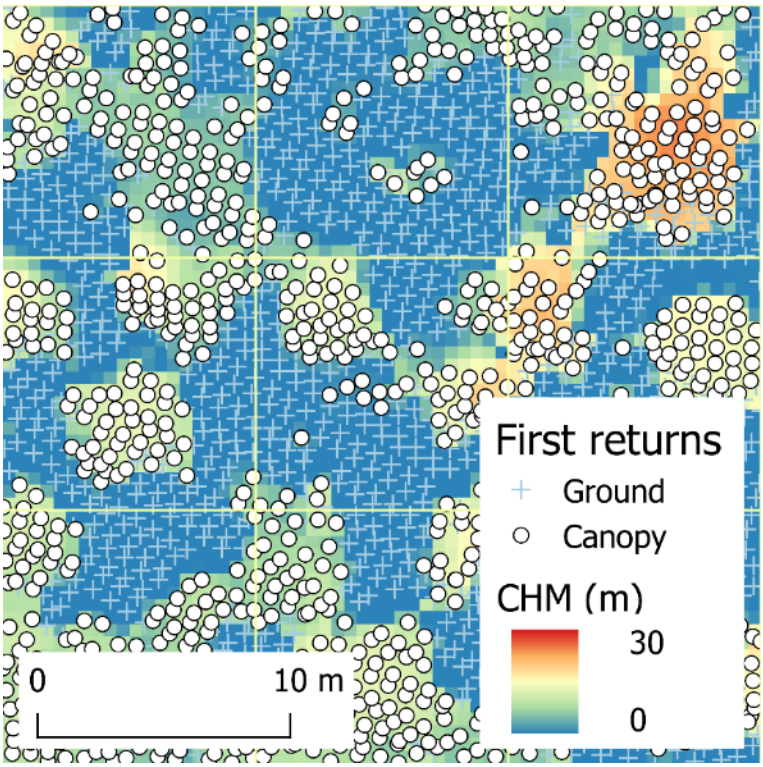


Fig. 5.4 Vertical crown cover from first-returns proportion.

#### 5.3.4.2 Within-crown Gap Probability from the LPM (for the LAIcrown)

After excluding the ground returns between crowns in each grid cell, the LPM were calculated as a proxy of within-crown gap probability. It is not easy to clearly define the gap probability because airborne LiDAR has finite-sized footprints. Several LPM have been constructed (Table 5.1), with only first returns, only last returns, all returns, or a combination of first and last returns (Korhonen et al. 2011; Morsdorf et al. 2006; Solberg et al. 2009). Field validations showed that using only first returns will underestimate the gap probability, while using only last returns will overestimate the gap probability (Korhonen et al. 2011; Morsdorf et al. 2006). In this study, four LPM (Table 5.1) were calculated and compared.

Table 5.1 Representative Laser Penetration Metrics (LPM)

| LPM | Canopy Cover = 1 - LPM |
|---|---|
| $LPM_{all} = \frac{N_{ground}}{N}$ | $ACI = \frac{N_{canopy}}{N}$ |
| $LPM_{first} = \frac{N_{single\_ground} + N_{first\_ground}}{N_{single} + N_{first}}$ | $FCI = \frac{N_{single\_canopy} + N_{first\_canopy}}{N_{single} + N_{first}}$ |
| $LPM_{last} = \frac{N_{single\_ground} + N_{last\_ground}}{N_{single} + N_{last}}$ | $LCI = \frac{N_{single\_canopy} + N_{last\_canopy}}{N_{single} + N_{last}}$ |
| $LPM_{Solberg} = \frac{N_{single\_ground} + 0.5\left(N_{first\_ground} + N_{last\_ground}\right)}{N_{single} + 0.5\left(N_{first} + N_{last}\right)}$ | $SCI = \frac{N_{single\_canopy} + 0.5\left(N_{first\_canopy} + N_{last\_canopy}\right)}{N_{single} + 0.5\left(N_{first} + N_{last}\right)}$ |

$N$ – number of all returns, $N_{ground}$ – number of ground returns, $N_{canopy}$ – number of canopy returns, $N_{first}$ – number of first returns, $N_{last}$ – number of last returns, $N_{single}$ – number of single returns, $N_{first\_ground}$ – number of first returns classified as ground, $N_{last\_ground}$ – number of last returns classified as ground, $N_{single\_ground}$ – number of single returns classified as ground, $N_{first\_canopy}$ – number of first returns classified as canopy, $N_{last\_canopy}$ – number of last returns classified as canopy, $N_{single\_canopy}$ – number of single returns classified as canopy, ACI – all echo cover index, FCI – first echo cover index, LCI – last echo cover index, SCI – Solberg's cover index.

### 5.3.5 LAI from the Path Length Distribution Model

The path length of each laser pulse is not known locally because LiDAR returns are always vertically inside the tree crowns rather than in the envelope of tree crowns. Therefore, we proposed to use a high-resolution Canopy Height Model (CHM) to represent the upper envelope of tree crowns. The CHM was generated as a proxy of the path length distribution, as path length is the distance covered when traveling through the canopies.

A pit-free CHM was generated via a multilevel method that combines the partial CHMs generated with points above certain heights (Khosravipour et al. 2014). This process can be achieved with a script using the *lastile*, *lasthin*, *blast2dem* and *lasgrid* modules of LAStools (Isenburg 2016). With an average point density of 5.91 pulses/m$^2$ and an average spacing of 0.41 m, the pit-free CHM was generated with a resolution of 0.5 m.

Then the path length distribution was obtained from CHMs in each grid cell by statistics. Grids with sizes of 5 m, 10 m, 30 m, 50 m, 100 m, 250 m, and 500 m were tested in this study. The minimum grid size was set to 5 m to take the representativeness and statistical requirements of the gap probability and path length distribution into consideration. In a 5-m grid cell, there were on average 206 points (yielding a gap probability precision of better than 0.005) and 100 path lengths. Only the CHMs in the crown area were used.

The LAI was retrieved for each grid (Fig. 5.3). First, the VCC, within-crown gap probability and within-crown path lengths were calculated for each grid cell. Second, the within-crown gap probability and within-crown path lengths were input into the path length distribution model to retrieve the $LAI_{crown}$ [Eqs. (3.19) and (3.20)]. Finally, the LAI of each grid cell was calculated by multiplying by the VCC [Eq. (4.1)].

### 5.3.6 Clumping

The LAIs and clumping indices were calculated for analyzing the clumping effect in different scales. All these clumping indices and effective LAIs are directional quantities, and were in the near vertical direction in this study.

First, the effective LAI of each grid cell ($LAI_e$) was calculated by directly inverting Beer-Lambert law to the total gap probability ($P_{cell}$) for each grid cell:

$$LAI_e = -\ln\left(P_{grid}\right)/G \quad . \tag{4.4}$$

Then, the total clumping index was calculated conveniently based on its definition,

$$\Omega_{All} = LAI_e / LAI_{cell} \quad , \tag{4.5}$$

where the $LAI_{cell}$, defined in Eq. (4.1), is the result of our method (Fig. 5.3) and takes into consideration both the between-crown clumping by the VCC and the within-crown clumping by the path length distribution model ($LAI_{crown}$).

Additionally, we defined a $LAI_e\_VCC$ between the $LAI_e$ and LAI and two clumping indices were used here to represent different sources of the clumping effect. The $LAI_e\_VCC$, which

considers the between-crown clumping by the VCC but does not consider the within-crown clumping, is defined as the product of the effective LAI within crowns and the *VCC*:

$$LAI_e\_VCC = -\ln\left(P_{crown}\right) / G \cdot VCC \quad . \tag{4.6}$$

The $LAI_e$, $LAI_e\_VCC$, and $LAI_{cell}$ are all values in each grid cell and have different degrees of clumping. We split the total clumping into two parts:

$$\Omega_{VCC} = LAI_e / LAI_e\_VCC \tag{4.7}$$

$$\Omega_{PATH} = LAI_e\_VCC / LAI_{grid} \quad , \tag{4.8}$$

where $\Omega_{VCC}$ represents the clumping effect between crowns; the difference between $LAI_e$ and $LAI_e\_VCC$ is due to the between-crown clumping, which is dominated by the VCC; $\Omega_{PATH}$ represents the clumping effect within crowns; the difference between $LAI_e\_VCC$ and LAI is due to the within-crown clumping, which is caused by the heterogeneous spatial distribution of vertical leaf profile and can be eliminated by the path length distribution model.

## 5.4 Results

### 5.4.1 Gap Probability from Laser Penetration Metric (LPM)

Several LPM were validated using field photography (Fig. 5.5). The total gap probabilities from the LPM for each grid cell were calculated for comparison with the field data.

The results show that $LPM_{all}$ and $LPM_{Solberg}$ perform the best against the field data, with an RMSE of 0.07. $LPM_{first}$ are generally lower than the field gap fraction, while $LPM_{last}$ are higher than the field gap fraction. Their trends and accuracy are consistent with previous studies (Heiskanen et al. 2015; Korhonen et al. 2011).

The underestimation of $LPM_{first}$ and overestimation of $LPM_{last}$ are understandable because certain laser pulses hitting canopies have canopy echoes as first returns and ground echoes as last returns, due to the large footprints. When a pulse has both canopy and ground returns, its footprint is occupied partly by the canopy and partly by the ground, rather than being pure

canopy or pure ground. $LPM_{first}$ actually regard these mixed areas as pure canopy and thus underestimate the fraction of ground, while $LPM_{last}$ regard these mixed areas as pure ground and thus overestimate the fraction of ground. Both $LPM_{all}$ and $LPM_{Solberg}$ utilize first and last returns, thus balancing the contributions of first and last returns. The difference between $LPM_{all}$ and $LPM_{Solberg}$ is very small, although $LPM_{all}$ also utilize the intermediate returns. This is because the proportion of intermediate returns is very small, being only 3.7%, 3.7%, and 5.7% of that of the first, last, and single returns, respectively.

The results show that both $LPM_{all}$ and $LPM_{Solberg}$ are capable of representing gap probability well and have very little difference; thus, $LPM_{all}$ can be used for further processing.

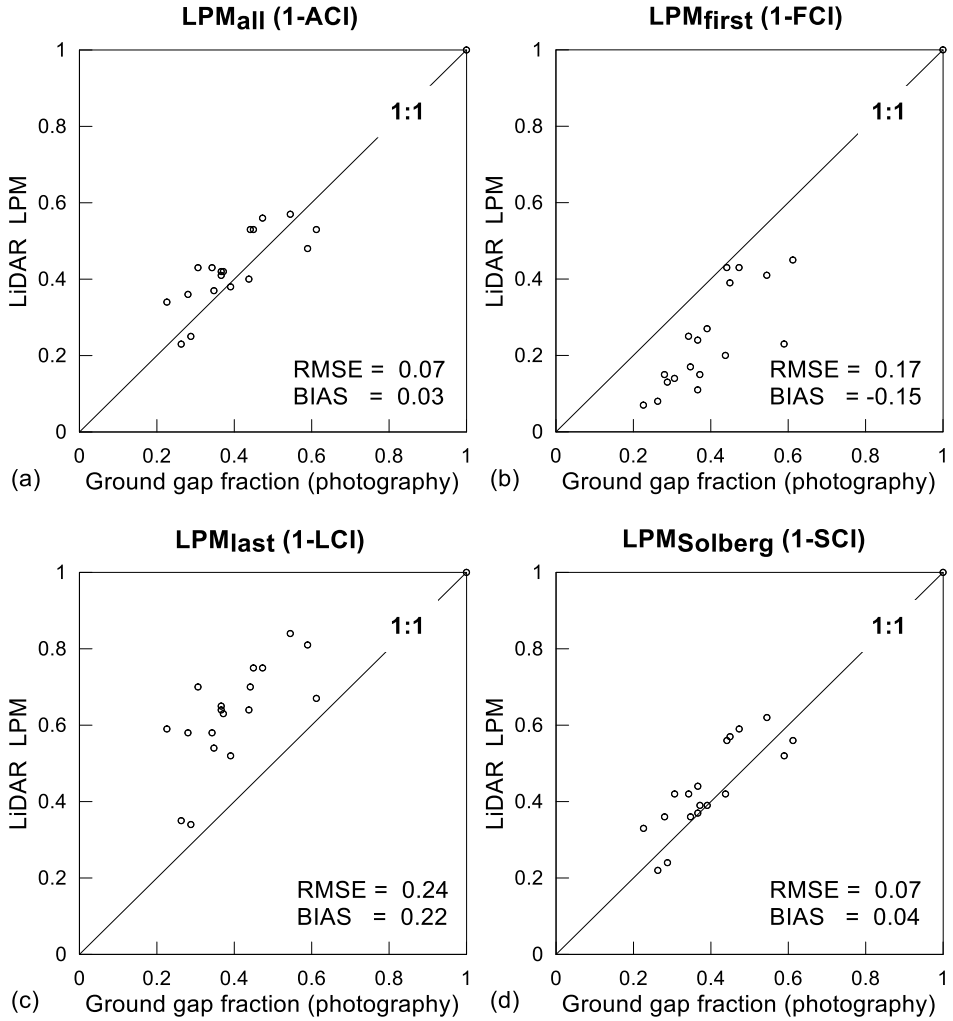


Fig. 5.5 Validation of the laser penetration metrics using field photography. (a) LPM calculated with all returns, (b) LPM calculated with only first returns, (c) LPM calculated with only last returns, (d) Solberg's LPM calculated with first and last returns.

## 5.4.2 Path length from Canopy Height Model (CHM)

The CHM was generated with a resolution of 0.5 m (Fig. 5.6). In total, 99.9% of pixels in the research area have a height of less than 30 m. The rivers, roads, and channels appear clearly on the map, with heights of approximately 0 m. Some traces of tree rotation can also be found, for example, in the bottom left part of the image. Tall trees are generally distributed deep in the mountains. The results show that the CHM is able to well characterize the upper envelope of

the forest. As the ALS data are near-nadir, with the scanning zenith angle generally less than 12° and a cosine larger than 0.978, the influence of the scanning angle is lower than 3%. Thus, the vertical height of the CHM is used as the path length of the laser pulse.

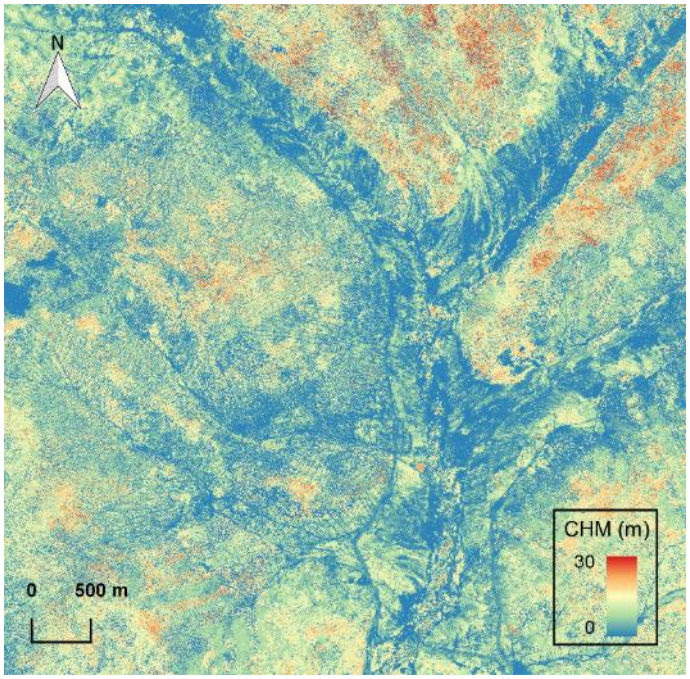


Fig. 5.6 The 0.5 m-resolution pit-free CHM generated using the ALS data.

### 5.4.3 LAI

The LAI was generated using the LPM and CHM in the path length distribution model (Fig. 5.7). The largest LAI was mainly distributed in dense forests in the mountains and in a forest-grassland transition zones. According to our field survey, we found that there is better underlying vegetation in the forest-grassland transition zones due to better lighting and watering. Meanwhile, in dense forests, most light is generally blocked by the trees, and there is less water in the mountains than in the wetlands. In the wetlands, the underlying vegetation is generally very dense and nearly 2 m in height, and the gap probability is much lower than that in the forests. In addition, there are also some trees in the wetlands, although not as many as in the forests. These trees and well-grown underlying vegetation lead to a high LAI in these areas.

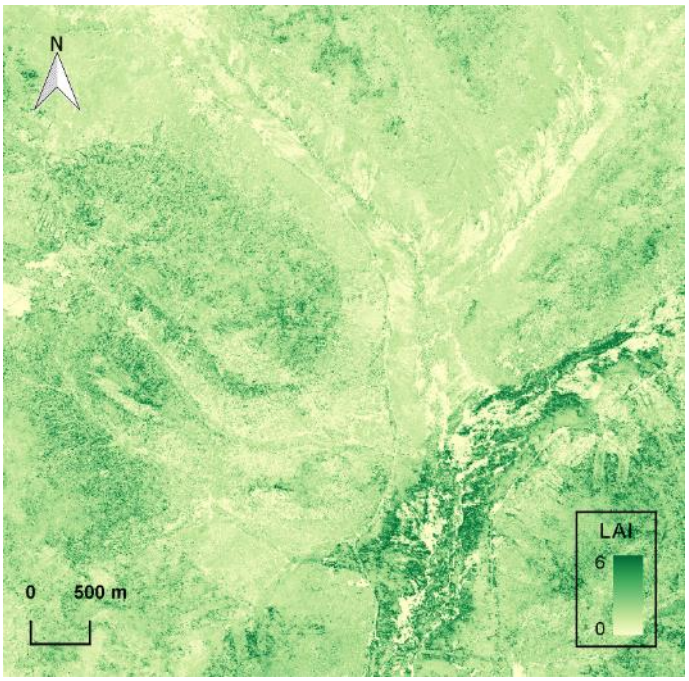


Fig. 5.7 The 5 m-resolution LAI generated using the ALS data using the path length distribution model.

ALS LAIs from the path length distribution model generally characterize the clumping corrected LAIs, with an RMSE of 0.41 (Fig. 5.8). The ALS LAIs of most sites are in good agreement with the field measurements, with a difference of less than 0.5, while a difference from 0.5 to 1 was found in several plots, which is not as good as expected. These differences might come from the differences in the mechanism and resolution between the ALS data and the upward camera. The pattern of LAI validation (Fig. 5.8) is similar to that of the LPM validation (Fig. 5.5) and will be discussed in Section V. A similar large error was also found in previous ALS studies of the $LAI_e$ estimation (Alonzo et al. 2015; Korhonen et al. 2011; Tang et al. 2014a).

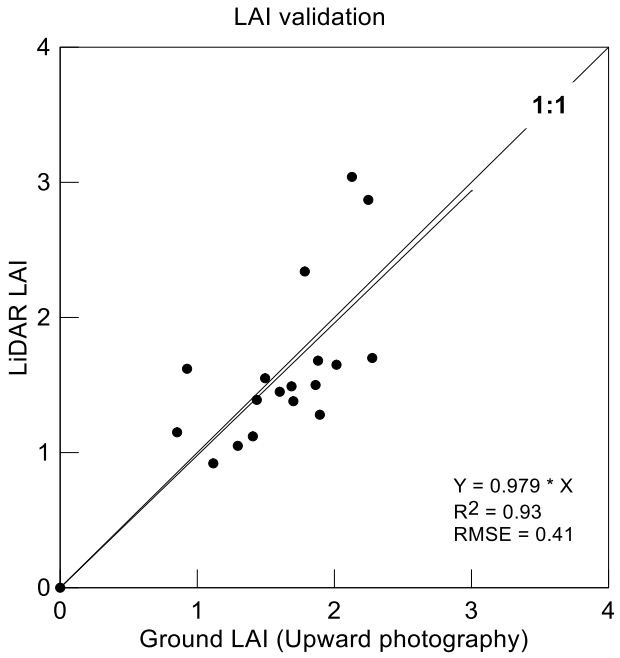


Fig. 5.8 Field validation of the LAI from the ALS data using the path length distribution model.

The LAIs of different resolutions were compared, and the results are generally consistent, especially when the LAI and the pixel size are not very large (Fig. 5.9). The differences are less than 5% from 5 m to 250 m resolutions (Fig. 5.9a-e) and 6% between 5 m and 500 m resolutions (Fig. 5.9f). The differences become larger when larger resolutions are compared. This could occur because the variation of foliage area volume density becomes greater for larger pixels. The consistency indicates that implementation of the path length distribution model on ALS data is not sensitive to the resolution. Note that the 5 m resolution data already have enough cloud points and path length distribution information for statistics for each grid cell, which is a requirement for obtaining reasonable results.

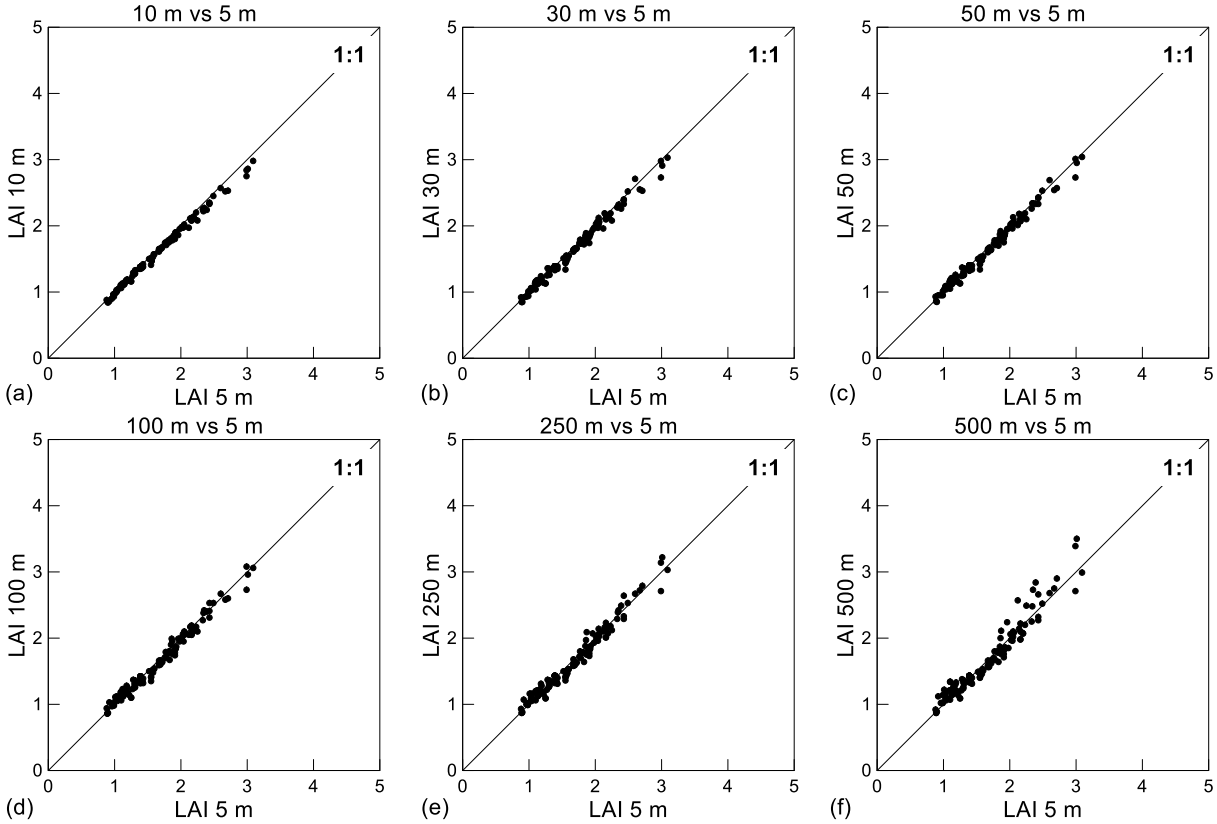


Fig. 5.9 Comparison of the LAIs with different resolutions. The LAIs of different resolutions are aggregated to 500 m pixels for comparison.

## 5.5 Discussion

### 5.5.1 Clumping Index at Different Scales

Three maps of the clumping index were then calculated to analyze the spatial pattern of the clumping effect at different scales. The clumping index between crowns $\Omega_{VCC}$ (Fig. 5.10b) contributes the most information to the spatial pattern of the total clumping index $\Omega_{ALL}$ (Fig. 5.10a), while the clumping index within crowns $\Omega_{PATH}$ (Fig. 5.10c) is more homogeneous spatially. This phenomenon is understandable, as the between-crown clumping is more related to the spatial distribution of canopies and the large gaps between crowns, while the within-crown clumping is more related to the shape of the tree crowns. The areas with fewer trees have

greater gaps between the crowns and thus are more clumped and have a smaller between-crown clumping index. The difference in the within-crown clumping index between the different land covers is less obvious (Fig. 5.10c), indicating the between-crown clumping contributes most of the spatial variance and the two clumping indices are well separated. The between crown clumping is influenced by the density and size of trees, which vary with different species and even different locations of the same species. The with-crown clumping is influenced by the collective effect of the crown shape and the leaf area density within crowns, which might vary with different species. The with-crown clumping is less variable because the variance of crown shape and leaf area density are generally smaller than that of the tree density on different land cover.

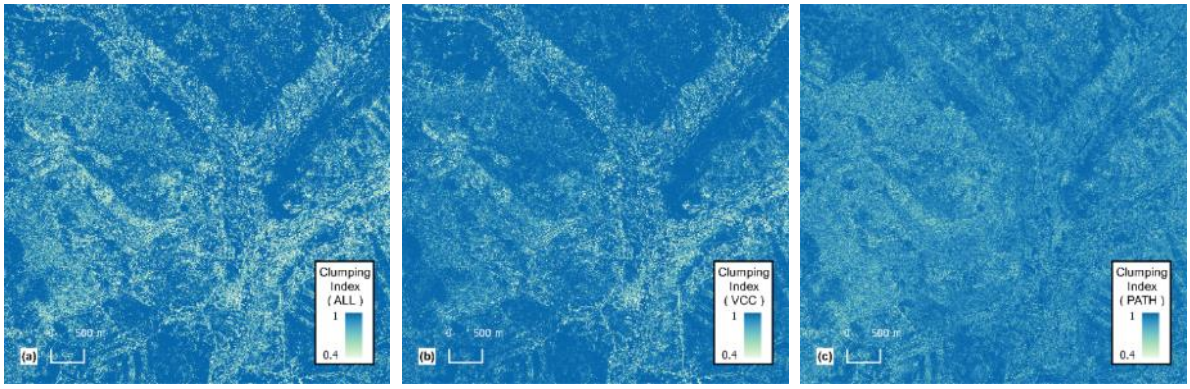


Fig. 5.10 Clumping index maps at different scales. (a) Clumping index in total, (b) clumping index between crowns, (c) clumping index within crowns.

### 5.5.2 Validity of Correcting Clumping Effect using the Path Length Distribution Model

The ALS Clumping index was compared with field measurement (Table 5.2). The ALS clumping index generally agrees with that of the field measurement, with an average difference of approximately 0.05. This difference is not large, since there is also a difference of 0.04 between field photography and TRAC measurement. These differences might mainly come from the differences in data acquisition mechanism between the ALS and the field

measurements, which result in different input data at different resolutions. The difference in the $LAI_e$, which comes from the gap probability (Fig. 5.5a), also propagated to the clumping index, because the $LAI_e$ is the numerator for calculating clumping index. There are observation towers for other instruments installed in some sites, which might have more influences on the field observations on large zenith angle than the near-nadir ALS measurement. Differences between the mechanisms of the ALS and upward camera do exist and are another source of the differences in validation. In addition, some of the field sites are on a sloping terrain with a slope of approximately 15°; thus, the slope effect might also bring some uncertainties to the field measurements and validation.

Table 5.2 Clumping Index of Airborne Laser Scanner (ALS), field photography and TRAC in 18 field sites. TRAC measurements were made on 13 sites.

| Clumping Index | ALS | Photography | TRAC |
|---|---|---|---|
| L1 | 0.89 | 0.86 | 0.88 |
| L2 | 0.92 | 0.84 | 0.95 |
| L3 | 0.93 | 0.92 | 0.92 |
| L4 | 0.98 | 0.98 | 0.93 |
| L5 | 0.99 | 0.93 | 0.92 |
| L6 | 0.97 | 0.93 | 0.88 |
| L7 | 0.69 | 0.79 | 0.81 |
| L8 | 0.94 | 0.85 | 0.88 |
| L9 | 0.98 | 0.88 | 0.94 |
| A1 | 0.78 | 0.87 | - |
| A2 | 0.87 | 0.89 | - |
| A3 | 0.93 | 0.82 | - |
| A4 | 0.96 | 0.94 | 0.93 |
| A5 | 0.84 | 0.85 | - |
| A6 | 0.75 | 0.79 | - |
| A7 | 0.96 | 0.81 | 0.89 |
| A8 | 0.90 | 0.86 | 0.95 |
| A9 | 0.95 | 0.89 | 0.92 |

The main advantage of using the path length distribution is that it is a physical model

utilizing the advantage of 3D information while avoiding the disadvantage of identifying small gaps with large-footprint ALS data. The path length distribution model itself does not have many parameters to adjust and is thus convenient and comparable for application. The consistency between the results at different resolutions also demonstrates its stability and potential for application.

### 5.5.3 Accuracy of the LPM as a Proxy of Gap Probability

The LPM data are important data sources for the LAI estimation. The pattern of the LAI validation (Fig. 5.8) is similar to that of the LPM validation (Fig. 5.5a).

There are still some differences in mechanism and resolution. First, the upward camera has a much higher resolution (higher than 0.01 m), which can be used to quantify the proportion of sky and trees more precisely, while the ALS has a much larger footprint (0.4 m). Second, their coverages are also different; the ALS generally has a full coverage of the whole plot, with hundreds of large footprints, while the upward photographs cover parts of the plot, especially after cropping. The upward photography and downward LPM are equally limited, but their agreement is comforting. Thus, there are still some differences between the LPM of ALS and the gap probability of upward photography (Fig. 5.5a); these differences further propagate to the LAI (Fig. 5.8). There is a maximum error of 0.13 in gap probability (Fig. 5.5a), which results in a maximum error of 0.8 in $LAI_e$ and will be further magnified after considering the clumping.

The use of small-footprint and high-density data should be helpful for better characterizing gap probability, as the canopy and ground returns will be less mixed and there will be more returns in each grid cell.

### 5.5.4 Accuracy of CHM as a Proxy of Path Length Distribution

The height in each grid cell was used as the path length in this thesis due to the limitations of the ALS footprint and point density. The CHM is able to characterize the relative path length distribution roughly, while there are still some differences. The returns at the top of the canopies and the ground are the most complete and informative and thus were used to extract the path length distribution in this study. Although we believe that the relative ratios of the path lengths are similar, the use of heights will underestimate the changes in path lengths. The impact of the CHM will be reduced by the VCC, as path length modeling is only used for correcting the clumping effect within crowns.

Extracting the lower envelope of the canopies in the ALS point data is difficult due to the much lower point density in the lower part of the canopies. In addition, the ALS pulses do not always have returns exactly within the lower boundary of the canopies. The waveform data might have the potential for extracting a more accurate path length, as the lower envelope is clearer in the waveform profile. Alternative methods, such as the Cloth Simulation Filter (Zhang et al. 2016b), could also be tested for extracting ground points.

### 5.5.5 Matching LiDAR and Field Measurements

Matching LiDAR and field measurements is important for comparison due to the variety in observation angles, projected areas and LAI definitions.

Matching the observation angle is necessary when comparing the gap probability, as the gap probability changes with the zenith angle even in a homogenous scene due to the change in path length. The ALS data generally have small observation angles, while some field instruments, such as LAI-2000, Fisheye camera, and TRAC, have larger observation zenith angles or wider fields of view. In this study, only upward photography was used for gap

probability validation after being cropped to a field of view similar to that of ALS. Both TRAC and upward photography were used for correcting clumping effect, and the results show that the final LAI validation with upward photography (RMSE = 0.41) is slightly better than that with TRAC (RMSE = 0.45). It is not a question of which instrument is better, because these two sets of data generally agree with each other well (Fig. 5.11), but more whether the viewing direction and field of view of the ALS and upward photography match better. The use of the near-vertical gap probability was also highlighted in several previous studies, and their results showed that using a smaller zenith angle close to the ALS data produced better results (Korhonen et al. 2011; Solberg et al. 2009).

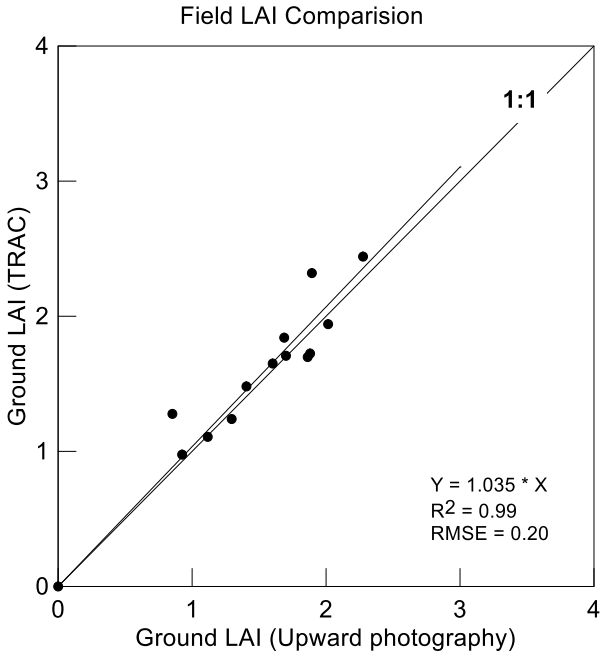


Fig. 5.11 Comparison of LAI using two field-based methods.

The LAI was used for the final validation because the LAI is defined vertically and thus has fewer problems in matching the observation zenith angles, as the change in path length caused by the observation angle has been considered in the LAI calculation with a cosine correction. Then, the gap probability at different angles was converted into the LAI for different representative areas.

Matching the LAI definition was also considered in this comparison. The same basic

theory, same viewing angle, and same classification were adopted in processing the ALS and photography data to reduce the uncertainties in comparison. They are comparable and enough for clumping validation because both the results of the ALS and upward photography data are clumping corrected area index without considering woody component, G function and needle-to-shoot area ratio. Because the leafy component and woody component are not distinguishable in both the ALS and upward photography data, the results of both the ALS and upward photography consist of the contribution of all plant components and thus represent the PAI for both. In addition, their G functions are also the same, as the ALS and upward photography have similar viewing angles. Since Beer-Lambert law-based method was used for both the ALS and upward photography, the G function has the same contribution and does not influence the comparison.

## 5.6 Conclusion

We present a grid cell method based on path length distribution model to calculate the clumping corrected LAI using the ALS data independently without additional measurements. Both the between-crowns and within-crowns clumping are corrected. The between-crowns clumping is corrected by separated the within- and between-crowns areas; and the within-crown clumping is corrected by migrating path length distribution to consider 3D foliage profile. The main advantage of using the path length distribution is that it is a physical model utilizing the advantage of 3D information while avoiding the disadvantage of identifying small gaps with large-footprint ALS data.

The LiDAR gap probability and path length distribution are the main inputs and main factors influencing the LAI estimation accuracy. The LPM and CHM were used as proxies of the gap probability and path length distribution, respectively. The LPM that using both first and last returns, provide a more reasonable estimation of gap probability. The CHM roughly characterizes the change in path lengths, while might slightly underestimate their magnitudes.

Limited field data show that the results are promising and a multi-level clumping analysis is consistent with the landscape flown. With the 0.4 m-footprint ALS data in this work, the results show that the path length distribution model is capable of characterizing the clumping corrected LAI robustly and rapidly in a large area. The ALS LAIs of different resolutions are consistent, with a difference of less than 5% from 5 m to 250 m resolutions. The path length distribution model itself does not have many parameters to adjust and is thus convenient and comparable for application. Due to its consistency with the resolution and its simple configuration, the method provides an opportunity to map the clumping corrected LAI operationally and to strengthen the ability of airborne LiDAR to validate the remote sensing products and to monitor vegetation changes. This grid cell method based on path length distribution worth further testing and application using more recent laser technology.

# Chapter 6 Summary and Perspective

In recent decades, the accuracy and efficiency requirements of leaf area index inversion have also been continuously improved along with the rapid development of global change, ecological assessment, precision agriculture and other fields. The optical indirect inversion method based on Beer-Lambert law is the main means of leaf area index ground measurement and airborne LiDAR inversion. Among them, the clumping effect, that is, the phenomenon that the leaves are not randomly distributed in space, is the main factor that restricts the accuracy of Beer-Lambert law to invert the leaf area index. Existing algorithms largely correct the clumping effect by consider the gap size distribution; however, the within-crown clumping caused by the inconsistent path length of the light penetrating canopy has not been well modeled. This limitation is gradually revealed as the measurement accuracy requirements are improved.

Active laser scanning technology is an emerging method developed in recent decades, while its 3D information has not been fully explored. At ground scale, estimating leaf area of isolated trees is important for urban research and traditional theory for contiguous stand need adaptation for TLS. At airborne scale, ALS can map regional LAI rapidly while its laser pulse size is too large to accurately obtain the gap distribution information for applying traditional clumping effect algorithm. Correcting clumping effect is still an unsolved problem in the airborne LiDAR retrieval.

In view of the above problems, this thesis focuses on the clumping effect and introduces

the path length distribution function to characterize the inconsistent path length within crown. A LAI inversion model based on the path length distribution is proposed. At ground scale, path length distribution model is implemented for individual tree leaf area measurement using TLS data by replacing the traditional cosine path length correction for continuous canopy with real path length distribution. At airborne scale, path length distribution model is implemented for correcting clumping effect using canopy height model acquired from ALS data. Consistent forest leaf area index retrieval using ground and airborne data is realized using path length distribution.

## 6.1 Major Findings and Discussions

Compared with the existing research, the research features and innovations of this thesis are as follows:

(1) A path length distribution model was proposed for considering the within-crown clumping and estimating leaf area index. The concept of path length distribution function is introduced, and the leaf area index inversion model based on path length distribution is established. One of the advantages of path length distribution theory is that it can characterize and handle crown shape-induced non-randomness within canopies. Such non-randomness, which may cause underestimation of up to 25%, has not been well addressed by existing algorithms. Both simulation and field measurements using traditional optical instruments show that the path length-based method can effectively characterize the LAI values of heterogeneous canopies. Deviation is less than 10% for all the validations. Through different forms of input, the model can be applied to existing ground and airborne instruments and platforms to effectively improve the accuracy of leaf area index measurement.

(2) A method for accurate leaf area estimation of isolated trees was proposed by replacing the traditional cosine path length correction for continuous canopy with real path length distribution. The real path length distribution was calculated through laser pulse-envelope intersections based on the reconstructed tree crown envelope from TLS point cloud. As a result,

the foliage area volume density (FAVD) was separated from path length distribution model for leaf area calculation. The new model is not limited by surrounding buildings or other objects in urban areas and eliminates the limitation of observation zenith angle. TLS-derived leaf area using path length distribution agrees well with the allometric measurement with an overestimation from 5m$^2$ to 18m$^2$ (3% to 10%). The results from different stations are globally consistent and is not sensitive to the scanning resolution. The use of weighted mean of different stations by sample numbers further improves the universality and efficiency of the proposed method. Integrating automatic segmentation algorithms into the calculation will be appealing for faster leaf area extraction of multiple independent trees with several scanning stations in urban areas.

(3) Independent clumping effect correction using ALS data was achieved with the use of path length distribution. The traditional clumping effect correction algorithm is difficult to be applied for airborne LiDAR data. The main limitation is that the airborne laser scanner has large footprint and low point cloud density, making it difficult to obtain the accurate gap distribution information required by the traditional ground aggregation index algorithm. In this thesis, the path length distribution model is introduced into the airborne LiDAR inversion, and the path length distribution is directly obtained by using the 3D point cloud to correct the clumping effect and estimate leaf area index. With the 0.4 m-footprint ALS data in this work, the results show that the path length distribution model is capable of characterizing the clumping corrected LAI robustly and rapidly in a large area. The ALS LAIs of different resolutions are consistent, with a difference of less than 5% from 5 m to 250 m resolutions. It avoids the limitation that the airborne LiDAR cannot obtain the accurate gap distribution and breaks through the technology of the independent correction of the clumping effect using ALS data, which greatly improves the accuracy and practicability of fast leaf area index mapping using airborne LiDAR. This grid cell method based on path length distribution worth further testing and application using more recent laser technology.

## 6.2 Perspectives

The path length distribution model proposed in this thesis has been successfully applied in leaf area estimation of isolated tree using TLS data and clumping effect correction using ALS data. The core for applying this model is the acquisition of the path length distribution. The acquisition of the path length distribution is not limited to the method proposed in this thesis, and there is still a broad space for expansion and improvement.

(1) Acquiring path length distribution with accurate envelope reconstruction using a matrix of voxels

In this study, the leaves are generally uniformly distributed within the envelope and the discrepancy of leaf distribution for more complex trees is not considered, which might cause underestimation for trees with complex structures. Further researches are needed to analyze the influence of envelope in other seasons. An accurate envelope reconstruction that uses a matrix of voxels will be useful for describing complex tree structures. Existing data shows that the time-of-flight laser scanner generally performs more stable in leaf area estimation, but the phase-shift laser scanner is lighter and faster. Comparing the time-of-flight with phase-shift laser scanner in one measurement will be interesting to analyze their differences quantitatively.

(2) Correcting clumping effect correction and estimating leaf area index based on full-waveform airborne laser scanner

Full-wavelength laser scanner provides more information than traditional discrete-return laser scanner, especially the pulse width information obtained when the laser pulse passes through the canopy. This kind of information has great potential application value for acquiring path length. Discrete-return data has certain limitations in obtaining the lower profile of the canopy. Although the inversion of the leaf area index can still be achieved by the relative path length, a more accurate absolute path length distribution can be obtained if the full waveform information can be obtained. It will contribute to the inversion of the leaf area density and

further improve the accuracy of the ALS estimation of leaf area index.

(3) Using satellite-borne LiDAR to correct clumping effects and estimate leaf area index

Spaceborne laser scanner can also acquire 3D information. Although its resolution is much lower than that of airborne laser scanner, their mechanisms are similar. It is also possible to obtain path length distribution information to correct the clumping effect. If the correction of the clumping effect of the spaceborne LiDAR data can be realized, the accuracy of the inversion of the leaf area index of the spaceborne LiDAR will be greatly improved, and a new global leaf area index data source different from the traditional one will be provided. The application of path distribution model in spaceborne laser scanner still has great challenges. Different from a small laser footprint laser scanner with a laser pulse corresponding to a path length, the spaceborne laser scanner footprint is in the tens of meters, covering a large area including the canopy and the ground, and the single echo contains different spaces. For information with different heights, it is necessary to explore the full waveform information and study the method of extracting the path length distribution from the full waveform information

# References

Abuelgasim, A.A., Fernandes, R.A., & Leblanc, S.G. (2006). Evaluation of national and global LAI products derived from optical remote sensing instruments over Canada. *IEEE TRANSACTIONS ON GEOSCIENCE AND REMOTE SENSING, 44*, 1872-1884

Alonzo, M., Bookhagen, B., McFadden, J.P., Sun, A., & Roberts, D.A. (2015). Mapping urban forest leaf area index with airborne LiDAR using penetration metrics and allometry. *REMOTE SENSING OF ENVIRONMENT, 162*, 141-153

Asner, G.P., Scurlock, J.M.O., & A. Hicke, J. (2003). Global synthesis of leaf area index observations: implications for ecological and remote sensing studies. *GLOBAL ECOLOGY AND BIOGEOGRAPHY, 12*, 191-205

Axelsson, P. (2000). DEM generation from laser scanner data using adaptive TIN models. *International Archives of Photogrammetry and Remote Sensing, 33*, 110-117

Bailey, B.N., & Mahaffee, W.F. (2017). Rapid measurement of the three-dimensional distribution of leaf orientation and the leaf angle probability density function using terrestrial LiDAR scanning. *REMOTE SENSING OF ENVIRONMENT, 194*, 63-76

Barclay, H.J., Trofymow, J.A., & Leach, R.I. (2000). Assessing bias from boles in calculating leaf area index in immature Douglas-fir with the LI-COR canopy analyzer. *AGRICULTURAL AND FOREST METEOROLOGY, 100*, 255-260

Baret, F., de Solan, B., Lopez-Lozano, R., Ma, K., & Weiss, M. (2010). GAI estimates of row crops from downward looking digital photos taken perpendicular to rows at 57.5 degrees zenith angle: Theoretical considerations based on 3D architecture models and application to wheat crops. *AGRICULTURAL AND FOREST METEOROLOGY, 150*, 1393-1401

Baret, F., Weiss, M., Lacaze, R., Camacho, F., Makhmara, H., Pacholcyzk, P., & Smets, B. (2013). GEOV1: LAI and FAPAR essential climate variables and FCOVER global time series capitalizing over existing products. Part1: Principles of development and production. *REMOTE SENSING OF ENVIRONMENT, 137*, 299-309

Beer (1852). Bestimmung der Absorption des rothen Lichts in farbigen Flüssigkeiten. *ANNALEN DER PHYSIK, 162*, 78-88

Beland, M., Baldocchi, D.D., Widlowski, J.L., Fournier, R.A., & Verstraete, M.M. (2014). On seeing the wood from the leaves and the role of voxel size in determining leaf area

distribution of forests with terrestrial LiDAR. *AGRICULTURAL AND FOREST METEOROLOGY, 184*, 82-97

Beland, M., Widlowski, J.L., Fournier, R.A., Cote, J.F., & Verstraete, M.M. (2011). Estimating leaf area distribution in savanna trees from terrestrial LiDAR measurements. *AGRICULTURAL AND FOREST METEOROLOGY, 151*, 1252-1266

Benjamin, M.T., & Winer, A.M. (1998). Estimating the ozone-forming potential of urban trees and shrubs. *ATMOSPHERIC ENVIRONMENT, 32*, 53-68

Black, T.A., Chen, J.M., Lee, X.H., & Sagar, R.M. (1991). Characteristics of Shortwave and Longwave Irradiances under a Douglas-Fir Forest Stand. *Canadian Journal of Forest Research-Revue Canadienne De Recherche Forestiere, 21*, 1020-1028

Boudon, F., Preuksakarn, C., Ferraro, P., Diener, J., Nacry, P., Nikinmaa, E., & Godin, C. (2014). Quantitative assessment of automatic reconstructions of branching systems obtained from laser scanning. *ANNALS OF BOTANY, 114*, 853-862

Bournez, E., Landes, T., Saudreau, M., Kastendeuch, P., & Najjar, G. (2017). From TLS point clouds to 3D models of trees: a comparison of existing algorithms for 3D tree reconstruction. *ISPRS-International Archives of the Photogrammetry, Remote Sensing and Spatial Information Sciences, 42*, 2

Bouvier, M., Durrieu, S., Fournier, R.A., & Renaud, J.P. (2015). Generalizing predictive models of forest inventory attributes using an area-based approach with airborne LiDAR data. *REMOTE SENSING OF ENVIRONMENT, 156*, 322-334

Breda, N.J.J. (2003). Ground-based measurements of leaf area index: a review of methods, instruments and current controversies. *JOURNAL OF EXPERIMENTAL BOTANY, 54*, 2403-2417

Calders, K., Schenkels, T., Bartholomeus, H., Armston, J., Verbesselt, J., & Herold, M. (2015). Monitoring spring phenology with high temporal resolution terrestrial LiDAR measurements. *AGRICULTURAL AND FOREST METEOROLOGY, 203*, 158-168

Campbell, G.S. (1990). Derivation of an angle density function for canopies with ellipsoidal leaf angle distributions. *AGRICULTURAL AND FOREST METEOROLOGY, 49*, 173-176

Cao, B., Du, Y.M., Li, J., Li, H., Li, L., Zhang, Y., Zou, J., & Liu, Q.H. (2015). Comparison of Five Slope Correction Methods for Leaf Area Index Estimation From Hemispherical Photography. *IEEE GEOSCIENCE AND REMOTE SENSING LETTERS, 12*, 1958-1962

Chason, J.W., Baldocchi, D.D., & Huston, M.A. (1991). A comparison of direct and indirect methods for estimating forest canopy leaf area. *AGRICULTURAL AND FOREST METEOROLOGY, 57*, 107-128

Chen, C.M. (2006). CiteSpace II: Detecting and visualizing emerging trends and transient patterns in scientific literature. *JOURNAL OF THE AMERICAN SOCIETY FOR INFORMATION SCIENCE AND TECHNOLOGY, 57*, 359-377

Chen, J.M. (1996). Optically-based methods for measuring seasonal variation of leaf area index in boreal conifer stands. *AGRICULTURAL AND FOREST METEOROLOGY, 80*, 135-163

Chen, J.M. (2013). Remote Sensing of Leaf Area Index of Vegetation Covers. Guangxing Wang, & Q. Weng (Eds.), *Remote Sensing of Natural Resources* (pp. 375-397). Boca Raton, FL: CRC Press, Taylor and Francis Group

Chen, J.M. (2018). Remote Sensing of Leaf Area Index and Clumping Index. S. Liang (Ed.), *Comprehensive Remote Sensing* (pp. 53-77). Oxford: Elsevier

Chen, J.M., & Black, T.A. (1991). Measuring Leaf-Area Index of Plant Canopies with Branch Architecture. *AGRICULTURAL AND FOREST METEOROLOGY, 57*, 1-12

Chen, J.M., & Black, T.A. (1992a). Defining leaf area index for non-flat leaves. *Plant, Cell & Environment, 15*, 421-429

Chen, J.M., & Black, T.A. (1992b). Foliage area and architecture of plant canopies from sunfleck size distributions. *AGRICULTURAL AND FOREST METEOROLOGY, 60*, 249-266

Chen, J.M., Black, T.A., & Adams, R.S. (1991). Evaluation of hemispherical photography for determining plant area index and geometry of a forest stand. *AGRICULTURAL AND FOREST METEOROLOGY, 56*, 129-143

Chen, J.M., & Cihlar, J. (1995a). Plant canopy gap-size analysis theory for improving optical measurements of leaf-area index. *APPLIED OPTICS, 34*, 6211-6222

Chen, J.M., & Cihlar, J. (1995b). Quantifying the effect of canopy architecture on optical measurements of leaf area index using two gap size analysis methods. *IEEE TRANSACTIONS ON GEOSCIENCE AND REMOTE SENSING, 33*, 777-787

Chen, J.M., & Cihlar, J. (1996). Retrieving leaf area index of boreal conifer forests using landsat TM images. *REMOTE SENSING OF ENVIRONMENT, 55*, 153-162

Chen, J.M., & Leblanc, S.G. (1997). A four-scale bidirectional reflectance model based on canopy architecture. *IEEE TRANSACTIONS ON GEOSCIENCE AND REMOTE SENSING, 35*, 1316-1337

Chen, J.M., Rich, P.M., Gower, S.T., Norman, J.M., & Plummer, S. (1997). Leaf area index of boreal forests: Theory, techniques, and measurements. *J. Geophys. Res., 102*, 29429-29443

Chianucci, F., & Cutini, A. (2012). Digital hemispherical photography for estimating forest canopy properties: current controversies and opportunities. *Iforest-Biogeosciences and Forestry, 5*, 290-295

Chianucci, F., & Cutini, A. (2013). Estimation of canopy properties in deciduous forests with digital hemispherical and cover photography. *AGRICULTURAL AND FOREST METEOROLOGY, 168*, 130-139

Chianucci, F., Cutini, A., Corona, P., & Puletti, N. (2014). Estimation of leaf area index in understory deciduous trees using digital photography. *AGRICULTURAL AND FOREST METEOROLOGY, 198*, 259-264

Chianucci, F., Puletti, N., Giacomello, E., Cutini, A., & Corona, P. (2015). Estimation of leaf area index in isolated trees with digital photography and its application to urban forestry. *URBAN FORESTRY & URBAN GREENING, 14*, 377-382

Clark, D.B., Olivas, P.C., Oberbauer, S.F., Clark, D.A., & Ryan, M.G. (2008). First direct landscape-scale measurement of tropical rain forest Leaf Area Index, a key driver of global primary productivity. *ECOLOGY LETTERS, 11*, 163-172

Colaizzi, P.D., Evett, S.R., Brauer, D.K., Howell, T.A., Tolk, J.A., & Copeland, K.S. (2017). Allometric Method to Estimate Leaf Area Index for Row Crops. *AGRONOMY JOURNAL, 109*, 883-894

Coops, N.C., Hilker, T., Wulder, M.A., St-Onge, B., Newnham, G., Siggins, A., & Trofymow, J.A. (2007). Estimating canopy structure of Douglas-fir forest stands from discrete-return LiDAR. *TREES-STRUCTURE AND FUNCTION, 21*, 295-310

Cutini, A., Matteucci, G., & Mugnozza, G.S. (1998). Estimation of leaf area index with the Li-Cor LAI 2000 in deciduous forests. *FOREST ECOLOGY AND MANAGEMENT, 105*, 55-65

Daughtry, C.S.T. (1990). Direct measurements of canopy structure. *Remote Sensing Reviews, 5*, 45 - 60

De Wit, C.T. (1965). *Photosynthesis of leaf canopies*. Wageningen: Centre for Agricultural Publications and Documentation

Deblonde, G., Penner, M., & Royer, A. (1994). Measuring Leaf-Area Index with the Li-Cor Lai-2000 in Pine Stands. *ECOLOGY, 75*, 1507-1511

Demarez, V., Duthoit, S., Baret, F., Weiss, M., & Dedieu, G. (2008). Estimation of leaf area and clumping indexes of crops with hemispherical photographs. *AGRICULTURAL AND FOREST METEOROLOGY, 148*, 644-655

Dou, B.C., Wen, J.G., Li, X.H., Liu, Q., Peng, J.J., Xiao, Q., Zhang, Z.G., Tang, Y., Wu, X.D., Lin, X.W., You, D.Q., Li, H., Li, L., Zeng, Y.L., Cai, E.L., & Zhang, J.L. (2016). Wireless Sensor Network of Typical Land Surface Parameters and Its Preliminary Applications for Coarse-Resolution Remote Sensing Pixel. *INTERNATIONAL JOURNAL OF DISTRIBUTED SENSOR NETWORKS*

Duursma, R.A., Marshall, J.D., & Robinson, A.P. (2003). Leaf area index inferred from solar beam transmission in mixed conifer forests on complex terrain. *AGRICULTURAL AND FOREST METEOROLOGY, 118*, 221-236

Edelsbrunner, H., & Mücke, E.P. (1994). Three-dimensional alpha shapes. *ACM Transactions on Graphics (TOG), 13*, 43-72

España, M.L., Baret, F., & Weiss, M. (2008). Slope correction for LAI estimation from gap fraction measurements. *AGRICULTURAL AND FOREST METEOROLOGY, 148*, 1553-1562

Fan, W.J., Liu, Y., Xu, X.R., Chen, G.X., & Zhang, B.T. (2014). A New FAPAR Analytical Model Based on the Law of Energy Conservation: A Case Study in China. *IEEE JOURNAL OF SELECTED TOPICS IN APPLIED EARTH OBSERVATIONS AND REMOTE SENSING, 7*, 3945-3955

Fang, H.L., Wei, S.S., Jiang, C.Y., & Scipal, K. (2012). Theoretical uncertainty analysis of global MODIS, CYCLOPES, and GLOBCARBON LAI products using a triple collocation method. *REMOTE SENSING OF ENVIRONMENT, 124*, 610-621

Fassnacht, K.S., Gower, S.T., Norman, J.M., & McMurtric, R.E. (1994). A comparison of optical and direct methods for estimating foliage surface area index in forests. *AGRICULTURAL AND FOREST METEOROLOGY, 71*, 183-207

Frazer, G., Canham, C., & Lertzman, K. (1999). *Gap Light Analyzer (GLA): Imaging software to extract canopy structure and gap light transmission indices from true-colour fisheye photographs, users manual and program documentation*. Copyright © 1999: Simon Fraser University, Burnaby, British Columbia, and the Institute of Ecosystem Studies, Millbrook, New York

Fu, Z., Wang, J., Song, J.L., Zhou, H.M., Pang, Y., & Chen, B.S. (2011). Estimation of forest canopy leaf area index using MODIS, MISR, and LiDAR observations. *JOURNAL OF APPLIED REMOTE SENSING, 5*

Garcia, M., Gajardo, J., Riano, D., Zhao, K.G., Martin, P., & Ustin, S. (2015). Canopy clumping appraisal using terrestrial and airborne laser scanning. *REMOTE SENSING OF ENVIRONMENT, 161*, 78-88

Garrigues, S., Shabanov, N.V., Swanson, K., Morisette, J.T., Baret, F., & Myneni, R.B. (2008). Intercomparison and sensitivity analysis of Leaf Area Index retrievals from LAI-2000, AccuPAR, and digital hemispherical photography over croplands. *AGRICULTURAL AND FOREST METEOROLOGY, 148*, 1193-1209

Garrity, S. (2014). LAI: Theory and Practice v. I.0 Copyright©2014. Decagon Devices, Inc. U.S.A: Decagon Devices

GCOS (2011). Systematic Observation Requirements for Satellite-based Products for Climate Supplemental details to the satellite-based component of the Implementation Plan for the Global Observing System for Climate in Support of the UNFCCC - 2011 Update. *Supplemental details to the satellite-based component of the "Implementation Plan for the Global Observing System for Climate in Support of the UNFCCC (2010 Update)"* (p. 138). Switzerland: World Meteorological Organization

Goel, N.S., & Strebel, D.E. (1984). Simple Beta Distribution Representation of Leaf Orientation in Vegetation Canopies. *AGRONOMY JOURNAL, 76*, 800-802

Gonsamo, A., & Pellikka, P. (2008). Methodology comparison for slope correction in canopy leaf area index estimation using hemispherical photography. *FOREST ECOLOGY AND MANAGEMENT, 256*, 749-759

Gonsamo, A., & Pellikka, P. (2009). The computation of foliage clumping index using hemispherical photography. *AGRICULTURAL AND FOREST METEOROLOGY, 149*, 1781-1787

Gonsamo, A., Walter, J.M.N., & Pellikka, P. (2011). CIMES: A package of programs for determining canopy geometry and solar radiation regimes through hemispherical photographs. *COMPUTERS AND ELECTRONICS IN AGRICULTURE, 79*, 207-215

Gower, S.T., Kucharik, C.J., & Norman, J.M. (1999). Direct and Indirect Estimation of Leaf Area Index, fAPAR, and Net Primary Production of Terrestrial Ecosystems. *REMOTE SENSING OF ENVIRONMENT, 70*, 29-51

Gower, S.T., & Norman, J.M. (1991). Rapid Estimation of Leaf-Area Index in Conifer and Broad-Leaf Plantations. *ECOLOGY, 72*, 1896-1900

Grau, E., Durrieu, S., Fournier, R., Gastellu-Etchegorry, J.P., & Yin, T.G. (2017). Estimation of 3D vegetation density with Terrestrial Laser Scanning data using voxels. A sensitivity analysis of influencing parameters. *REMOTE SENSING OF ENVIRONMENT, 191*, 373-388

Harding, D.J., & Carabajal, C.C. (2005). ICESat waveform measurements of within-footprint topographic relief and vegetation vertical structure. *GEOPHYSICAL RESEARCH LETTERS, 32*

Heiskanen, J., Korhonen, L., Hietanen, J., & Pellikka, P.K.E. (2015). Use of airborne LiDAR for estimating canopy gap fraction and leaf area index of tropical montane forests. *INTERNATIONAL JOURNAL OF REMOTE SENSING, 36*, 2569-2583

Hopkinson, C., Lovell, J., Chasmer, L., Jupp, D., Kljun, N., & van Gorsel, E. (2013). Integrating terrestrial and airborne LiDAR to calibrate a 3D canopy model of effective leaf area index. *REMOTE SENSING OF ENVIRONMENT, 136*, 301-314

Hosoi, F., & Omasa, K. (2006). Voxel-Based 3-D Modeling of Individual Trees for Estimating Leaf Area Density Using High-Resolution Portable Scanning LiDAR. *IEEE TRANSACTIONS ON GEOSCIENCE AND REMOTE SENSING, 44*, 3610-3618

Hosoi, F., & Omasa, K. (2007). Factors contributing to accuracy in the estimation of the woody canopy leaf area density profile using 3D portable LiDAR imaging. *JOURNAL OF EXPERIMENTAL BOTANY, 58*, 3463-3473

Houghton, J. (2002). *The physics of atmospheres*. Cambridge University Press

Hu, R., Luo, J., Yan, G., Zou, J., & Mu, X. (2016a). Indirect Measurement of Forest Leaf Area Index Using Path Length Distribution Model and Multispectral Canopy Imager. *IEEE*

*JOURNAL OF SELECTED TOPICS IN APPLIED EARTH OBSERVATIONS AND REMOTE SENSING, 9*, 2532-2539

Hu, R., Luo, J., Yan, G., Zou, J., & Mu, X. (2016b). Indirect Measurement of Forest Leaf Area Index Using Path Length Distribution Model and Multispectral Canopy Imager. *IEEE JOURNAL OF SELECTED TOPICS IN APPLIED EARTH OBSERVATIONS AND REMOTE SENSING, PP*, 1-8

Hu, R., Yan, G., Mu, X., & Luo, J. (2014). Indirect measurement of leaf area index on the basis of path length distribution. *REMOTE SENSING OF ENVIRONMENT, 155*, 239-247

Hu, R., Yan, G., Nerry, F., Liu, Y., Jiang, Y., Wang, S., Chen, Y., Mu, X., Zhang, W., & Xie, D. (2018). Using Airborne Laser Scanner and Path Length Distribution Model to Quantify Clumping Effect and Estimate Leaf Area Index. *IEEE TRANSACTIONS ON GEOSCIENCE AND REMOTE SENSING, 56*, 3196 - 3209

Hutchison, B.A., Matt, D.R., Mcmillen, R.T., Gross, L.J., Tajchman, S.J., & Norman, J.M. (1986). The Architecture of a Deciduous Forest Canopy in Eastern Tennessee, USA. *JOURNAL OF ECOLOGY, 74*, 635-646

Hwang, Y., Ryu, Y., Kimm, H., Jiang, C., Lang, M., Macfarlane, C., & Sonnentag, O. (2016). Correction for light scattering combined with sub-pixel classification improves estimation of gap fraction from digital cover photography. *AGRICULTURAL AND FOREST METEOROLOGY, 222*, 32-44

Isenburg, M. (2016). LAStools - efficient LiDAR processing software.

Jennings, S.B., Brown, N.D., & Sheil, D. (1999). Assessing forest canopies and understorey illumination: canopy closure, canopy cover and other measures. *FORESTRY, 72*, 59-73

Jensen, J.L.R., Humes, K.S., Vierling, L.A., & Hudak, A.T. (2008). Discrete return LiDAR-based prediction of leaf area index in two conifer forests. *REMOTE SENSING OF ENVIRONMENT, 112*, 3947-3957

Jonckheere, I., Fleck, S., Nackaerts, K., Muys, B., Coppin, P., Weiss, M., & Baret, F. (2004). Review of methods for in situ leaf area index determination: Part I. Theories, sensors and hemispherical photography. *AGRICULTURAL AND FOREST METEOROLOGY, 121*, 19-35

Jupp, D.L.B., Culvenor, D.S., Lovell, J.L., Newnham, G.J., Strahler, A.H., & Woodcock, C.E. (2009). Estimating forest LAI profiles and structural parameters using a ground-based laser called 'Echidna (R)'. *TREE PHYSIOLOGY, 29*, 171-181

Khosravipour, A., Skidmore, A.K., Isenburg, M., Wang, T.J., & Hussin, Y.A. (2014). Generating Pit-free Canopy Height Models from Airborne LiDAR. *PHOTOGRAMMETRIC ENGINEERING AND REMOTE SENSING, 80*, 863-872

Kobayashi, H., Ryu, Y., Baldocchi, D.D., Welles, J.M., & Norman, J.M. (2013). On the correct estimation of gap fraction: How to remove scattered radiation in gap fraction measurements? *AGRICULTURAL AND FOREST METEOROLOGY, 174*, 170-183

Koch, B., Heyder, U., & Weinacker, H. (2006). Detection of individual tree crowns in airborne LiDAR data. *PHOTOGRAMMETRIC ENGINEERING AND REMOTE SENSING, 72*, 357-363

Korhonen, L., Korpela, I., Heiskanen, J., & Maltamo, M. (2011). Airborne discrete-return LIDAR data in the estimation of vertical canopy cover, angular canopy closure and leaf area index. *REMOTE SENSING OF ENVIRONMENT, 115*, 1065-1080

Kucharik, C.J., Norman, J.M., & Gower, S.T. (1998a). Measurements of branch area and adjusting leaf area index indirect measurements. *AGRICULTURAL AND FOREST METEOROLOGY, 91*, 69-88

Kucharik, C.J., Norman, J.M., & Gower, S.T. (1998b). Measurements of leaf orientation, light distribution and sunlit leaf area in a boreal aspen forest. *AGRICULTURAL AND FOREST METEOROLOGY, 91*, 127-148

Kucharik, C.J., Norman, J.M., & Gower, S.T. (1999). Characterization of radiation regimes in nonrandom forest canopies: theory, measurements, and a simplified modeling approach. *TREE PHYSIOLOGY, 19*, 695-706

Kucharik, C.J., Norman, J.M., Murdock, L.M., & Gower, S.T. (1997). Characterizing canopy nonrandomness with a multiband vegetation imager (MVI). *J. Geophys. Res., 102*, 29455-29473

Kuusk, A. (1995). A fast, invertible canopy reflectance model. *REMOTE SENSING OF ENVIRONMENT, 51*, 342-350

Lang, A.R.G. (1973). Leaf orientation of a cotton plant. *AGRICULTURAL METEOROLOGY, 11*, 37-51

Lang, A.R.G. (1991). Application of Some of Cauchys Theorems to Estimation of Surface-Areas of Leaves, Needles and Branches of Plants, and Light Transmittance. *AGRICULTURAL AND FOREST METEOROLOGY, 55*, 191-212

Lang, A.R.G., McMurtrie, R.E., & Benson, M.L. (1991). Validity of surface area indices of Pinus radiata estimated from transmittance of the sun's beam. *AGRICULTURAL AND FOREST METEOROLOGY, 57*, 157-170

Lang, A.R.G., & Xiang, Y. (1986). Estimation of leaf area index from transmission of direct sunlight in discontinuous canopies. *AGRICULTURAL AND FOREST METEOROLOGY, 37*, 229-243

Lang, A.R.G., Xiang, Y., & Norman, J.M. (1985). Crop structure and the penetration of direct sunlight. *AGRICULTURAL AND FOREST METEOROLOGY, 35*, 83-101

Leblanc, S., Chen, J., & Kwong, M. (2005a). Tracing Radiation and Architecture of Canopies MANUAL 2.1.4. (pp. 1-27): Natural Resources Canada

Leblanc, S.G. (2002). Correction to the plant canopy gap-size analysis theory used by the Tracing Radiation and Architecture of Canopies instrument. *APPLIED OPTICS, 41*, 7667-7670

Leblanc, S.G., & Chen, J.M. (2001). A practical scheme for correcting multiple scattering effects on optical LAI measurements. *AGRICULTURAL AND FOREST METEOROLOGY, 110*, 125-139

Leblanc, S.G., Chen, J.M., Fernandes, R., Deering, D.W., & Conley, A. (2005b). Methodology comparison for canopy structure parameters extraction from digital hemispherical photography in boreal forests. *AGRICULTURAL AND FOREST METEOROLOGY, 129*, 187-207

Leblanc, S.G., & Fournier, R.A. (2014). Hemispherical photography simulations with an architectural model to assess retrieval of leaf area index. *AGRICULTURAL AND FOREST METEOROLOGY, 194*, 64-76

Lefsky, M.A., Cohen, W.B., Acker, S.A., Parker, G.G., Spies, T.A., & Harding, D. (1999). LiDAR remote sensing of the canopy structure and biophysical properties of Douglas-fir western hemlock forests. *REMOTE SENSING OF ENVIRONMENT, 70*, 339-361

Lefsky, M.A., Cohen, W.B., Parker, G.G., & Harding, D.J. (2002). LiDAR remote sensing for ecosystem studies. *BIOSCIENCE, 52*, 19-30

Li-COR (2011). LAI-2200 Plant Canopy Analyzer Instruction Manual.

Liang, S.L., Zhao, X., Liu, S.H., Yuan, W.P., Cheng, X., Xiao, Z.Q., Zhang, X.T., Liu, Q., Cheng, J., Tang, H.R., Qu, Y.H., Bo, Y.C., Qu, Y., Ren, H.Z., Yu, K., & Townshend, J. (2013). A long-term Global LAnd Surface Satellite (GLASS) data-set for environmental studies. *International Journal of Digital Earth, 6*, 5-33

Lim, K., Treitz, P., Baldwin, K., Morrison, I., & Green, J. (2003a). LiDAR remote sensing of biophysical properties of tolerant northern hardwood forests. *CANADIAN JOURNAL OF REMOTE SENSING, 29*, 658-678

Lim, K., Treitz, P., Wulder, M., St-Onge, B., & Flood, M. (2003b). LiDAR remote sensing of forest structure. *PROGRESS IN PHYSICAL GEOGRAPHY, 27*, 88-106

Lin, Y., & West, G. (2016). Retrieval of effective leaf area index (LAIe) and leaf area density (LAD) profile at individual tree level using high density multi-return airborne LiDAR. *INTERNATIONAL JOURNAL OF APPLIED EARTH OBSERVATION AND GEOINFORMATION, 50*, 150-158

Liu, J., Pattey, E., & Admiral, S. (2013). Assessment of in situ crop LAI measurement using unidirectional view digital photography. *AGRICULTURAL AND FOREST METEOROLOGY, 169*, 25-34

Liu, Y., Hu, R., Mu, X., & Yan, G. (2011). A method for leaf gap fraction estimation based on multispectral digital images from Multispectral Canopy Imager. *2011 IEEE International Geoscience and Remote Sensing Symposium* (pp. 3042-3045): IEEE

Lovell, J.L., Jupp, D.L.B., Culvenor, D.S., & Coops, N.C. (2003). Using airborne and ground-based ranging LiDAR to measure canopy structure in Australian forests. *CANADIAN JOURNAL OF REMOTE SENSING, 29*, 607-622

Luo, S.Z., Wang, C., Li, G.C., & Xi, X.H. (2013). Retrieving leaf area index using ICESat/GLAS full-waveform data. *Remote Sensing Letters, 4*, 745-753

Luo, S.Z., Wang, C., Pan, F.F., Xi, X.H., Li, G.C., Nie, S., & Xia, S.B. (2015). Estimation of wetland vegetation height and leaf area index using airborne laser scanning data. *ECOLOGICAL INDICATORS, 48*, 550-559

Ma, L., Zheng, G., Eitel, J.U.H., Magney, T.S., & Moskal, L.M. (2017). Retrieving forest canopy extinction coefficient from terrestrial and airborne LiDAR. *AGRICULTURAL AND FOREST METEOROLOGY, 236*, 1-21

Macfarlane, C. (2011). Classification method of mixed pixels does not affect canopy metrics from digital images of forest overstorey. *AGRICULTURAL AND FOREST METEOROLOGY, 151*, 833-840

Macfarlane, C., Grigg, A., & Evangelista, C. (2007a). Estimating forest leaf area using cover and fullframe fisheye photography: Thinking inside the circle. *AGRICULTURAL AND FOREST METEOROLOGY, 146*, 1-12

Macfarlane, C., Hoffman, M., Eamus, D., Kerp, N., Higginson, S., McMurtrie, R., & Adams, M. (2007b). Estimation of leaf area index in eucalypt forest using digital photography. *AGRICULTURAL AND FOREST METEOROLOGY, 143*, 176-188

Macfarlane, C., Ryu, Y., Ogden, G.N., & Sonnentag, O. (2014). Digital canopy photography: Exposed and in the raw. *AGRICULTURAL AND FOREST METEOROLOGY, 197*, 244-253

McNeil, B.E., Pisek, J., Lepisk, H., & Flamenco, E.A. (2016). Measuring leaf angle distribution in broadleaf canopies using UAVs. *AGRICULTURAL AND FOREST METEOROLOGY, 218*, 204-208

Milenković, M., Wagner, W., Quast, R., Hollaus, M., Ressl, C., & Pfeifer, N. (2017). Total canopy transmittance estimated from small-footprint, full-waveform airborne LiDAR. *ISPRS JOURNAL OF PHOTOGRAMMETRY AND REMOTE SENSING, 128*, 61-72

Miller, J. (1967). A formula for average foliage density. *AUSTRALIAN JOURNAL OF BOTANY, 15*, 141-144

Monsi, M., & Saeki, T. (1953). Über den Lichtfaktor in den Pflanzengesellschaften und seine Bedeutung für die Stoffproduktion. *JAPANESE JOURNAL OF BOTANY, 14*, 22-52

Monsi, M., & Saeki, T. (2005). On the factor light in plant communities and its importance for matter production. *ANNALS OF BOTANY, 95*, 549-567

Monteith, J.L. (1965). Light Distribution and Photosynthesis in Field Crops. *ANNALS OF BOTANY, 29*, 17-37

Montes, F., Pita, P., Rubio, A., & Canellas, I. (2007). Leaf area index estimation in mountain even-aged Pinus silvestris L. stands from hemispherical photographs. *AGRICULTURAL AND FOREST METEOROLOGY, 145*, 215-228

Moorthy, I., Miller, J.R., Hu, B.X., Chen, J., & Li, Q.M. (2008). Retrieving crown leaf area index from an individual tree using ground-based LiDAR data. *CANADIAN JOURNAL OF REMOTE SENSING, 34*, 320-332

Morsdorf, F., Kotz, B., Meier, E., Itten, K.I., & Allgower, B. (2006). Estimation of LAI and fractional cover from small footprint airborne laser scanning data based on gap fraction. *REMOTE SENSING OF ENVIRONMENT, 104*, 50-61

Mu, X., Hu, R., Zeng, Y., McVicar, T.R., Ren, H., Song, W., Wang, Y., Casa, R., Qi, J., Xie, D., & Yan, G. (2017). Estimating structural parameters of agricultural crops from ground-based multi-angular digital images with a fractional model of sun and shade components. *AGRICULTURAL AND FOREST METEOROLOGY, 246*, 162-177

Mu, X.H., Hu, M.G., Song, W.J., Ruan, G.Y., Ge, Y., Wang, J.F., Huang, S., & Yan, G.J. (2015). Evaluation of Sampling Methods for Validation of Remotely Sensed Fractional Vegetation Cover. *Remote Sensing, 7*, 16164-16182

Myneni, R.B., Hoffman, S., Knyazikhin, Y., Privette, J.L., Glassy, J., Tian, Y., Wang, Y., Song, X., Zhang, Y., Smith, G.R., Lotsch, A., Friedl, M., Morisette, J.T., Votava, P., Nemani, R.R., & Running, S.W. (2002). Global products of vegetation leaf area and fraction absorbed PAR from year one of MODIS data. *REMOTE SENSING OF ENVIRONMENT, 83*, 214-231

Myneni, R.B., Nemani, R.R., & Running, S.W. (1997). Estimation of global leaf area index and absorbed par using radiative transfer models. *IEEE TRANSACTIONS ON GEOSCIENCE AND REMOTE SENSING, 35*, 1380-1393

Myneni, R.B., Ross, J., & Asrar, G. (1989). A review on the theory of photon transport in leaf canopies. *AGRICULTURAL AND FOREST METEOROLOGY, 45*, 1-153

Nagler, P.L., Glenn, E.P., Thompson, T.L., & Huete, A. (2004). Leaf area index and normalized difference vegetation index as predictors of canopy characteristics and light interception by riparian species on the Lower Colorado River. *AGRICULTURAL AND FOREST METEOROLOGY, 125*, 1-17

Najjar, G., Colin, J., Kastendeuch, P., Ngao, J., Saudreau, M., Landes, T., Ameglio, T., Luhahe, R., Guillemin, S., & Schreiner, G. (2015). A three years long fieldwork experiment to monitor the role of vegetation on the urban climate of the city of Strasbourg, France. *International conférence on urban climate, 12th symposium, Toulouse, France 20-24 july*

Neumann, H.H., Den Hartog, G., & Shaw, R.H. (1989). Leaf area measurements based on hemispheric photographs and leaf-litter collection in a deciduous forest during autumn leaf-fall. *AGRICULTURAL AND FOREST METEOROLOGY, 45*, 325-345

Newnham, G., Armston, J., Muir, J., Goodwin, N., Tindall, D., Culvenor, D., Püschel, P., Nyström, M., & Johansen, K. (2012). Evaluation of terrestrial laser scanners for measuring vegetation structure. *CSIRO Sustainable Agriculture Flagship*

Ni-Meister, W., Jupp, D.L.B., & Dubayah, R. (2001). Modeling LiDAR waveforms in heterogeneous and discrete canopies. *IEEE TRANSACTIONS ON GEOSCIENCE AND REMOTE SENSING, 39*, 1943-1958

Nilson, T. (1971). A theoretical analysis of the frequency of gaps in plant stands. *AGRICULTURAL METEOROLOGY, 8*, 25-38

Nilson, T. (1999). Inversion of gap frequency data in forest stands. *AGRICULTURAL AND FOREST METEOROLOGY, 98–99*, 437-448

Nowak, D.J., Crane, D.E., Stevens, J.C., Hoehn, R.E., Walton, J.T., & Bond, J. (2008). A ground-based method of assessing urban forest structure and ecosystem services

Pearse, G.D., Watt, M.S., & Morgenroth, J. (2016). Comparison of optical LAI measurements under diffuse and clear skies after correcting for scattered radiation. *AGRICULTURAL AND FOREST METEOROLOGY, 221*, 61-70

Peper, P.J., & McPherson, E.G. (1998). Comparison of five methods for estimating leaf area index of open-grown deciduous trees. *Journal of Arboriculture, 24*, 98-111

Peper, P.J., & McPherson, E.G. (2003). Evaluation of four methods for estimating leaf area of isolated trees. *URBAN FORESTRY & URBAN GREENING, 2*, 19-29

Pinty, B., Gobron, N., Widlowski, J.-L., Gerstl, S.A.W., Verstraete, M.M., Antunes, M., Bacour, C., Gascon, F., Gastellu, J.-P., Goel, N., Jacquemoud, S., North, P., Qin, W., & Thompson, R. (2001). Radiation transfer model intercomparison (RAMI) exercise. *Journal of Geophysical Research: Atmospheres, 106*, 11937-11956

Pisek, J., Lang, M., Nilson, T., Korhonen, L., & Karu, H. (2011a). Comparison of methods for measuring gap size distribution and canopy nonrandomness at Järvselja RAMI (RAdiation transfer Model Intercomparison) test sites. *AGRICULTURAL AND FOREST METEOROLOGY, 151*, 365-377

Pisek, J., Ryu, Y., & Alikas, K. (2011b). Estimating leaf inclination and G-function from leveled digital camera photography in broadleaf canopies. *TREES-STRUCTURE AND FUNCTION, 25*, 919-924

Pisek, J., Ryu, Y., Sprintsin, M., He, L.M., Oliphant, A.J., Korhonen, L., Kuusk, J., Kuusk, A., Bergstrom, R., Verrelst, J., & Alikas, K. (2013a). Retrieving vegetation clumping index from Multi-angle Imaging SpectroRadiometer (MISR) data at 275 m resolution. *REMOTE SENSING OF ENVIRONMENT, 138*, 126-133

Pisek, J., Sonnentag, O., Richardson, A.D., & Mottus, M. (2013b). Is the spherical leaf inclination angle distribution a valid assumption for temperate and boreal broadleaf tree species? *AGRICULTURAL AND FOREST METEOROLOGY, 169*, 186-194

Plummer, S., Arino, O., Simon, M., & Steffen, W. (2006). Establishing A Earth Observation Product Service For The Terrestrial Carbon Community: The Globcarbon Initiative. *Mitigation and Adaptation Strategies for Global Change, 11*, 97-111

Qi, J., Xie, D., Guo, D., & Yan, G. (2017). A Large-Scale Emulation System for Realistic Three-Dimensional (3-D) Forest Simulation. *IEEE JOURNAL OF SELECTED TOPICS IN APPLIED EARTH OBSERVATIONS AND REMOTE SENSING, 10*, 4834-4843

Qu, Y.H., Han, W.C., Fu, L.Z., Li, C.R., Song, J.L., Zhou, H.M., Bo, Y.C., & Wang, J.D. (2014). LAINet - A wireless sensor network for coniferous forest leaf area index measurement: Design, algorithm and validation. *COMPUTERS AND ELECTRONICS IN AGRICULTURE, 108*, 200-208

Radtke, P.J., & Bolstad, P.V. (2001). Laser point-quadrat sampling for estimating foliage-height profiles in broad-leaved forests. *Canadian Journal of Forest Research-Revue Canadienne De Recherche Forestiere, 31*, 410-418

Ren, H., Liu, R., Yan, G., Mu, X., Li, Z.-L., Nerry, F., & Liu, Q. (2014). Angular Normalization of Land Surface Temperature and Emissivity Using Multiangular Middle and Thermal Infrared Data. *IEEE TRANSACTIONS ON GEOSCIENCE AND REMOTE SENSING, 52*, 4913-4931

Ren, H., Yan, G., Liu, R., Nerry, F., Li, Z.-L., & Hu, R. (2013). Impact of sensor footprint on measurement of directional brightness temperature of row crop canopies. *REMOTE SENSING OF ENVIRONMENT, 134*, 135-151

Riano, D., Valladares, F., Condes, S., & Chuvieco, E. (2004). Estimation of leaf area index and covered ground from airborne laser scanner (LiDAR) in two contrasting forests. *AGRICULTURAL AND FOREST METEOROLOGY, 124*, 269-275

Rich, P.M. (1990). Characterizing plant canopies with hemispherical photographs. *Remote Sensing Reviews, 5*, 13-29

Richardson, J.J., Moskal, L.M., & Kim, S.-H. (2009). Modeling approaches to estimate effective leaf area index from aerial discrete-return LIDAR. *AGRICULTURAL AND FOREST METEOROLOGY, 149*, 1152-1160

Roberts, S.D., Dean, T.J., & Evans, D.L. (2003). Family influences on leaf area estimates derived from crown and tree dimensions in Pinus taeda. *FOREST ECOLOGY AND MANAGEMENT, 172*, 261-270

Roberts, S.D., Dean, T.J., Evans, D.L., McCombs, J.W., Harrington, R.L., & Glass, P.A. (2005). Estimating individual tree leaf area in loblolly pine plantations using LiDAR-derived measurements of height and crown dimensions. *FOREST ECOLOGY AND MANAGEMENT, 213*, 54-70

Ross, J. (1981). *Radiation Regime and Architecture of Plant Stands*. The Hague: Dr. W. Junk Publishers

Ryu, Y., Nilson, T., Kobayashi, H., Sonnentag, O., Law, B.E., & Baldocchi, D.D. (2010a). On the correct estimation of effective leaf area index: Does it reveal information on clumping effects? *AGRICULTURAL AND FOREST METEOROLOGY, 150*, 463-472

Ryu, Y., Sonnentag, O., Nilson, T., Vargas, R., Kobayashi, H., Wenk, R., & Baldocchi, D.D. (2010b). How to quantify tree leaf area index in an open savanna ecosystem: A multi-instrument and multi-model approach. *AGRICULTURAL AND FOREST METEOROLOGY, 150*, 63-76

Ryu, Y., Verfaillie, J., Macfarlane, C., Kobayashi, H., Sonnentag, O., Vargas, R., Ma, S., & Baldocchi, D.D. (2012). Continuous observation of tree leaf area index at ecosystem scale using upward-pointing digital cameras. *REMOTE SENSING OF ENVIRONMENT, 126*, 116-125

Schleppi, P., Conedera, M., Sedivy, I., & Thimonier, A. (2007). Correcting non-linearity and slope effects in the estimation of the leaf area index of forests from hemispherical photographs. *AGRICULTURAL AND FOREST METEOROLOGY, 144*, 236-242

Schneider, F.D., Letterer, R., Morsdorf, F., Gastellu-Etchegorry, J.P., Lauret, N., Pfeifer, N., & Schaepman, M.E. (2014). Simulating imaging spectrometer data: 3D forest modeling

based on LiDAR and in situ data. *REMOTE SENSING OF ENVIRONMENT, 152*, 235-250

Schutz, B.E., Zwally, H.J., Shuman, C.A., Hancock, D., & DiMarzio, J.P. (2005). Overview of the ICESat Mission. *GEOPHYSICAL RESEARCH LETTERS, 32*

Seidel, D., Fleck, S., & Leuschner, C. (2012). Analyzing forest canopies with ground-based laser scanning: A comparison with hemispherical photography. *AGRICULTURAL AND FOREST METEOROLOGY, 154*, 1-8

Simioni, G., Gignoux, J., Le Roux, X., Appe, R., & Benest, D. (2004). Spatial and temporal variations in leaf area index, specific leaf area and leaf nitrogen of two co-occurring savanna tree species. *TREE PHYSIOLOGY, 24*, 205-216

Simpson, J.R. (1998). Urban forest impacts on regional cooling and heating energy use: Sacramento County case study. *Journal of Arboriculture, 24*, 201-209

Smith, N.J. (1993). Estimating leaf area index and light extinction coefficients in stands of Douglas-fir (Pseudotsuga menziesii). *CANADIAN JOURNAL OF FOREST RESEARCH, 23*, 317-321

Solberg, S., Brunner, A., Hanssen, K.H., Lange, H., Naesset, E., Rautiainen, M., & Stenberg, P. (2009). Mapping LAI in a Norway spruce forest using airborne laser scanning. *REMOTE SENSING OF ENVIRONMENT, 113*, 2317-2327

Solberg, S., Naesset, E., Hanssen, K.H., & Christiansen, E. (2006). Mapping defoliation during a severe insect attack on Scots pine using airborne laser scanning. *REMOTE SENSING OF ENVIRONMENT, 102*, 364-376

Song, W.J., Mu, X.H., Yan, G.J., & Huang, S. (2015). Extracting the Green Fractional Vegetation Cover from Digital Images Using a Shadow-Resistant Algorithm (SHAR-LABFVC). *Remote Sensing, 7*, 10425-10443

Sonohat, G., Sinoquet, H., Kulandaivelu, V., Combes, D., & Lescourret, F. (2006). Three-dimensional reconstruction of partially 3D-digitized peach tree canopies. *TREE PHYSIOLOGY, 26*, 337-351

Stark, S.C., Leitold, V., Wu, J.L., Hunter, M.O., de Castilho, C.V., Costa, F.R.C., McMahon, S.M., Parker, G.G., Shimabukuro, M.T., Lefsky, M.A., Keller, M., Alves, L.F., Schietti, J., Shimabukuro, Y.E., Brandão, D.O., Woodcock, T.K., Higuchi, N., de Camargo, P.B., de Oliveira, R.C., & Saleska, S.R. (2012). Amazon forest carbon dynamics predicted by profiles of canopy leaf area and light environment. *ECOLOGY LETTERS, 15*, 1406-1414

Stenberg, P. (1996a). Correcting LAI-2000 estimates for the clumping of needles in shoots of conifers. *AGRICULTURAL AND FOREST METEOROLOGY, 79*, 1-8

Stenberg, P. (1996b). Simulations of the effects of shoot structure and orientation on vertical gradients in intercepted light by conifer canopies. *TREE PHYSIOLOGY, 16*, 99-108

Strahler, A.H., Jupp, D.L.B., Woodcock, C.E., Schaaf, C.B., Yao, T., Zhao, F., Yang, X.Y., Lovell, J., Culvenor, D., Newnham, G., Ni-Miester, W., & Boykin-Morris, W. (2008). Retrieval of forest structural parameters using a ground-based LiDAR instrument (Echidna (R)). *CANADIAN JOURNAL OF REMOTE SENSING, 34*, S426-S440

Tang, H., Brolly, M., Zhao, F., Strahler, A.H., Schaaf, C.L., Ganguly, S., Zhang, G., & Dubayah, R. (2014a). Deriving and validating Leaf Area Index (LAI) at multiple spatial scales through LiDAR remote sensing: A case study in Sierra National Forest, CA. *REMOTE SENSING OF ENVIRONMENT, 143*, 131-141

Tang, H., Dubayah, R., Brolly, M., Ganguly, S., & Zhang, G. (2014b). Large-scale retrieval of leaf area index and vertical foliage profile from the spaceborne waveform LiDAR (GLAS/ICESat). *REMOTE SENSING OF ENVIRONMENT, 154*, 8-18

Tang, H., Dubayah, R., Swatantran, A., Hofton, M., Sheldon, S., Clark, D.B., & Blair, B. (2012). Retrieval of vertical LAI profiles over tropical rain forests using waveform LiDAR at La Selva, Costa Rica. *REMOTE SENSING OF ENVIRONMENT, 124*, 242-250

Thanisawanyangkura, S., Sinoquet, H., Rivet, P., Cretenet, M., & Jallas, E. (1997). Leaf orientation and sunlit leaf area distribution in cotton. *AGRICULTURAL AND FOREST METEOROLOGY, 86*, 1-15

Thomas, S.C., & Winner, W.E. (2000). A rotated ellipsoidal angle density function improves estimation of foliage inclination distributions in forest canopies. *AGRICULTURAL AND FOREST METEOROLOGY, 100*, 19-24

Thomas, V., Noland, T., Treitz, P., & McCaughey, J.H. (2011). Leaf area and clumping indices for a boreal mixed-wood forest: LiDAR, hyperspectral, and Landsat models. *INTERNATIONAL JOURNAL OF REMOTE SENSING, 32*, 8271-8297

Tian, X., Li, Z.Y., Chen, E.X., Liu, Q.H., Yan, G.J., Wang, J.D., Niu, Z., Zhao, S.J., Li, X., Pang, Y., Su, Z.B., van der Tol, C., Liu, Q.W., Wu, C.Y., Xiao, Q., Yang, L., Mu, X.H., Bo, Y.C., Qu, Y.H., Zhou, H.M., Gao, S.H., Chai, L.N., Huang, H.G., Fan, W.J., Li, S.H., Bai, J.H., Jiang, L.M., & Zhou, J. (2015a). The Complicate Observations and Multi-Parameter Land Information Constructions on Allied Telemetry Experiment (COMPLICATE). *Plos One, 10*

Tian, X., Li, Z.Y., van der Tol, C., Su, Z., Li, X., He, Q.S., Bao, Y.F., Chen, E.X., & Li, L.H. (2011). Estimating zero-plane displacement height and aerodynamic roughness length using synthesis of LiDAR and SPOT-5 data. *REMOTE SENSING OF ENVIRONMENT, 115*, 2330-2341

Tian, Y., Zheng, Y., Zheng, C.M., Xiao, H.L., Fan, W.J., Zou, S.B., Wu, B., Yao, Y.Y., Zhang, A.J., & Liu, J. (2015b). Exploring scale-dependent ecohydrological responses in a large endorheic river basin through integrated surface water-groundwater modeling. *WATER RESOURCES RESEARCH, 51*, 4065-4085

Van der Zande, D., Hoet, W., Jonckheere, L., van Aardt, J., & Coppin, P. (2006). Influence of measurement set-up of ground-based LiDAR for derivation of tree structure. *AGRICULTURAL AND FOREST METEOROLOGY, 141*, 147-160

Vincent, G., Sabatier, D., Blanc, L., Chave, J., Weissenbacher, E., Pelissier, R., Fonty, E., Molino, J.F., & Couteron, P. (2012). Accuracy of small footprint airborne LiDAR in its predictions of tropical moist forest stand structure. *REMOTE SENSING OF ENVIRONMENT, 125*, 23-33

Walter, J.M.N., & Torquebiau, E.F. (2000). The computation of forest leaf area index on slope using fish-eye sensors. *COMPTES RENDUS DE L ACADEMIE DES SCIENCES SERIE III-SCIENCES DE LA VIE-LIFE SCIENCES, 323*, 801-813

Wang, C., Menenti, M., Stoll, M.P., Feola, A., Belluco, E., & Marani, M. (2009). Separation of Ground and Low Vegetation Signatures in LiDAR Measurements of Salt-Marsh Environments. *IEEE TRANSACTIONS ON GEOSCIENCE AND REMOTE SENSING, 47*, 2014-2023

Wang, W.M., Li, Z.L., & Su, H.B. (2007). Comparison of leaf angle distribution functions: Effects on extinction coefficient and fraction of sunlit foliage. *AGRICULTURAL AND FOREST METEOROLOGY, 143*, 106-122

Watson, D.J. (1947). Comparative Physiological Studies on the Growth of Field Crops: I. Variation in Net Assimilation Rate and Leaf Area between Species and Varieties, and within and between Years. *ANNALS OF BOTANY, 11*, 41-76

Watson, D.J. (1958). The Dependence of Net Assimilation Rate on Leaf-area Index. *ANNALS OF BOTANY, 22*, 37-54

Webb, N., Nichol, C., Wood, J., & Potter, E. (2016). User manual for the SunScan Canopy Analysis System, type SS1, Version: 3.3. (p. 82). Cambridge, UK: Delta-T Devices Ltd

Weiss, M., & Baret, F. (2016). CAN_EYE V6.4.6 USER MANUAL. In: EMMAH (Mediterranean Environment and Agro-Hydro System Modelisation) Laboratory. French National Institute of Agricultural Research (INRA)

Weiss, M., Baret, F., Smith, G.J., Jonckheere, I., & Coppin, P. (2004). Review of methods for in situ leaf area index (LAI) determination: Part II. Estimation of LAI, errors and sampling. *AGRICULTURAL AND FOREST METEOROLOGY, 121*, 37-53

Welles, J.M. (1990). Some indirect methods of estimating canopy structure. *Remote Sensing Reviews, 5*, 31-43

Welles, J.M., & Cohen, S. (1996). Canopy structure measurement by gap fraction analysis using commercial instrumentation. *JOURNAL OF EXPERIMENTAL BOTANY, 47*, 1335-1342

Welles, J.M., & Norman, J.M. (1991). Instrument for Indirect Measurement of Canopy Architecture. *AGRONOMY JOURNAL, 83*, 818-825

Whitford, K.R., Colquhoun, I.J., Lang, A.R.G., & Harper, B.M. (1995). Measuring Leaf-Area Index in a Sparse Eucalypt Forest - a Comparison of Estimates from Direct Measurement, Hemispherical Photography, Sunlight Transmittance and Allometric Regression. *AGRICULTURAL AND FOREST METEOROLOGY, 74*, 237-249

Widlowski, J.L., Pinty, B., Clerici, M., Dai, Y., De Kauwe, M., de Ridder, K., Kallel, A., Kobayashi, H., Lavergne, T., Ni-Meister, W., Olchev, A., Quaife, T., Wang, S., Yang, W., Yang, Y., & Yuan, H. (2011). RAMI4PILPS: An intercomparison of formulations for the partitioning of solar radiation in land surface models. *Journal of Geophysical Research: Biogeosciences, 116*, G02019

Widlowski, J.L., Pinty, B., Lopatka, M., Atzberger, C., Buzica, D., Chelle, M., Disney, M., Gastellu-Etchegorry, J.P., Gerboles, M., Gobron, N., Grau, E., Huang, H., Kallel, A., Kobayashi, H., Lewis, P.E., Qin, W., Schlerf, M., Stuckens, J., & Xie, D. (2013). The fourth radiation transfer model intercomparison (RAMI-IV): Proficiency testing of canopy reflectance models with ISO-13528. *Journal of Geophysical Research: Atmospheres, 118*, 6869-6890

Widlowski, J.L., Taberner, M., Pinty, B., Bruniquel-Pinel, V., Disney, M., Fernandes, R., Gastellu-Etchegorry, J.P., Gobron, N., Kuusk, A., Lavergne, T., Leblanc, S., Lewis, P.E., Martin, E., Mõttus, M., North, P.R.J., Qin, W., Robustelli, M., Rochdi, N., Ruiloba, R., Soler, C., Thompson, R., Verhoef, W., Verstraete, M.M., & Xie, D. (2007). Third Radiation Transfer Model Intercomparison (RAMI) exercise: Documenting progress in canopy reflectance models. *Journal of Geophysical Research: Atmospheres, 112*, D09111

Wilson, J.W. (1960). Inclined Point Quadrats. *NEW PHYTOLOGIST, 59*, 1-8

Woodgate, W., Armston, J.D., Disney, M., Suarez, L., Jones, S.D., Hill, M.J., Wilkes, P., & Soto-Berelov, M. (2017). Validating canopy clumping retrieval methods using hemispherical photography in a simulated Eucalypt forest. *AGRICULTURAL AND FOREST METEOROLOGY, 247*, 181-193

Woodgate, W., Disney, M., Armston, J.D., Jones, S.D., Suarez, L., Hill, M.J., Wilkes, P., Soto-Berelov, M., Haywood, A., & Mellor, A. (2015). An improved theoretical model of canopy gap probability for Leaf Area Index estimation in woody ecosystems. *FOREST ECOLOGY AND MANAGEMENT, 358*, 303-320

Xie, D.H., Wang, Y., Hu, R.H., Chen, Y.M., Yan, G.J., Zhang, W.M., & Wang, P.J. (2017). Modified gap fraction model of individual trees for estimating leaf area using terrestrial laser scanner. *JOURNAL OF APPLIED REMOTE SENSING, 11*

Yan, G., Hu, R., Luo, J., Mu, X., Xie, D., & Zhang, W. (2016a). Review of indirect methods for leaf area index measurement. *Journal of Remote Sensing, 20*, 958-978

Yan, G., Hu, R., Wang, Y., Ren, H., Song, W., Qi, J., & Chen, L. (2016b). Scale Effect in Indirect Measurement of Leaf Area Index. *IEEE TRANSACTIONS ON GEOSCIENCE AND REMOTE SENSING, 54*, 3475-3484

Yan, G., Zhang, W., Zhu, L., & Zou, J. (2008). Multispectral canopy imager. C.N.

Yan, G.J., Ren, H.Z., Hu, R.H., Yan, K., & Zhang, W.M. (2012). A PORTABLE MULTI-ANGLE OBSERVATION SYSTEM. *2012 IEEE International Geoscience and Remote Sensing Symposium* (pp. 6916-6919). New York: IEEE

Yan, K., Park, T., Yan, G., Liu, Z., Yang, B., Chen, C., Nemani, R., Knyazikhin, Y., & Myneni, R. (2016c). Evaluation of MODIS LAI/FPAR Product Collection 6. Part 2: Validation and Intercomparison. *Remote Sensing, 8*, 460

Yan, K., Park, T., Yan, G.J., Liu, Z., Yang, B., Chen, C., Nemani, R.R., Knyazikhin, Y., & Myneni, R.B. (2016d). Evaluation of MODIS LAI/FPAR Product Collection 6. Part 2: Validation and Intercomparison. *Remote Sensing, 8*

Yao, T., Yang, X.Y., Zhao, F., Wang, Z.S., Zhang, Q.L., Jupp, D., Lovell, J., Culvenor, D., Newnham, G., Ni-Meister, W., Schaaf, C., Woodcock, C., Wang, J.D., Li, X.W., & Strahler, A. (2011). Measuring forest structure and biomass in New England forest stands using Echidna ground-based LiDAR. *REMOTE SENSING OF ENVIRONMENT, 115*, 2965-2974

Yin, G.F., Li, A.N., Jin, H.A., Zhao, W., Bian, J.H., Qu, Y.H., Zeng, Y.L., & Xu, B.D. (2017). Derivation of temporally continuous LAI reference maps through combining the LAINet observation system with CACAO. *AGRICULTURAL AND FOREST METEOROLOGY, 233*, 209-221

Zeng, Y., Li, J., Liu, Q., Hu, R., Mu, X., Fan, W., Xu, B., Yin, G., & Wu, S. (2015). Extracting Leaf Area Index by Sunlit Foliage Component from Downward-Looking Digital Photography under Clear-Sky Conditions. *Remote Sensing, 7*, 13410

Zeng, Y.L., Li, J., Liu, Q.H., Li, L.H., Xu, B.D., Yin, G.F., & Peng, J.J. (2014). A Sampling Strategy for Remotely Sensed LAI Product Validation Over Heterogeneous Land Surfaces. *IEEE JOURNAL OF SELECTED TOPICS IN APPLIED EARTH OBSERVATIONS AND REMOTE SENSING, 7*, 3128-3142

Zhang, W., Chen, Y., Wang, H., Chen, M., Wang, X., & Yan, G. (2016a). Efficient registration of terrestrial LiDAR scans using a coarse-to-fine strategy for forestry applications. *AGRICULTURAL AND FOREST METEOROLOGY, 225*, 8-23

Zhang, W.M., Qi, J.B., Wan, P., Wang, H.T., Xie, D.H., Wang, X.Y., & Yan, G.J. (2016b). An Easy-to-Use Airborne LiDAR Data Filtering Method Based on Cloth Simulation. *Remote Sensing, 8*

Zhang, Y.Q., Chen, J.M., & Miller, J.R. (2005). Determining digital hemispherical photograph exposure for leaf area index estimation. *AGRICULTURAL AND FOREST METEOROLOGY, 133*, 166-181

Zhao, F., Yang, X., Schull, M.A., Román-Colón, M.O., Yao, T., Wang, Z., Zhang, Q., Jupp, D.L.B., Lovell, J.L., Culvenor, D.S., Newnham, G.J., Richardson, A.D., Ni-Meister, W., Schaaf, C.L., Woodcock, C.E., & Strahler, A.H. (2011). Measuring effective leaf area index, foliage profile, and stand height in New England forest stands using a full-waveform ground-based LiDAR. *REMOTE SENSING OF ENVIRONMENT, 115*, 2954-2964

Zhao, K.G., Garcia, M., Liu, S., Guo, Q.H., Chen, G., Zhang, X.S., Zhou, Y.Y., & Meng, X.L. (2015). Terrestrial LiDAR remote sensing of forests: Maximum likelihood estimates of canopy profile, leaf area index, and leaf angle distribution. *AGRICULTURAL AND FOREST METEOROLOGY, 209*, 100-113

Zhao, K.G., & Popescu, S. (2009). LiDAR-based mapping of leaf area index and its use for validating GLOBCARBON satellite LAI product in a temperate forest of the southern USA. *REMOTE SENSING OF ENVIRONMENT, 113*, 1628-1645

Zheng, G., & Moskal, L.M. (2009). Retrieving Leaf Area Index (LAI) Using Remote Sensing: Theories, Methods and Sensors. *SENSORS, 9*, 2719-2745

Zou, J., Yan, G., Zhu, L., & Zhang, W. (2009). Woody-to-total area ratio determination with a multispectral canopy imager. *TREE PHYSIOLOGY, 29*, 1069-1080

Zou, J., Yan, G.J., & Chen, L. (2015). Estimation of Canopy and Woody Components Clumping Indices at Three Mature Picea crassifolia Forest Stands. *IEEE JOURNAL OF SELECTED TOPICS IN APPLIED EARTH OBSERVATIONS AND REMOTE SENSING, 8*, 1413-1422

Zwally, H.J., Schutz, B., Abdalati, W., Abshire, J., Bentley, C., Brenner, A., Bufton, J., Dezio, J., Hancock, D., Harding, D., Herring, T., Minster, B., Quinn, K., Palm, S., Spinhirne, J., & Thomas, R. (2002). ICESat's laser measurements of polar ice, atmosphere, ocean, and land. *JOURNAL OF GEODYNAMICS, 34*, 405-445

# List of Publications

**Hu, R.**, Bournez, E., Cheng, S., Jiang, H., Nerry, F., Landes, T., Saudreau, M., Kastendeuch, P., Najjar, G., Colin, J., & Yan, G. (2018). Estimating the leaf area of an individual tree in urban areas using terrestrial laser scanner and path length distribution model. *ISPRS JOURNAL OF PHOTOGRAMMETRY AND REMOTE SENSING, 144*, 357-368

**Hu, R.**, Yan, G., Nerry, F., Liu, Y., Jiang, Y., Wang, S., Chen, Y., Mu, X., Zhang, W., & Xie, D. (2018). Using Airborne Laser Scanner and Path Length Distribution Model to Quantify Clumping Effect and Estimate Leaf Area Index. *IEEE TRANSACTIONS ON GEOSCIENCE AND REMOTE SENSING*, 56, 3196-3209

Mu, X., **Hu, R.**, Zeng, Y., McVicar, T.R., Ren, H., Song, W., Wang, Y., Casa, R., Qi, J., Xie, D., & Yan, G. (2017). Estimating structural parameters of agricultural crops from ground-based multi-angular digital images with a fractional model of sun and shade components. *AGRICULTURAL AND FOREST METEOROLOGY, 246*, 162-177

**Hu, R**., Luo, J., Yan, G., Zou, J., & Mu, X. (2016). Indirect Measurement of Forest Leaf Area Index Using Path Length Distribution Model and Multispectral Canopy Imager. *IEEE JOURNAL OF SELECTED TOPICS IN APPLIED EARTH OBSERVATIONS AND REMOTE SENSING, 9*, 2532-2539

Yan, G., **Hu, R.**, Wang, Y., Ren, H., Song, W., Qi, J., & Chen, L. (2016). Scale Effect in Indirect Measurement of Leaf Area Index. *IEEE TRANSACTIONS ON GEOSCIENCE AND REMOTE SENSING, 54*, 3475-3484

Wang, Y., Xie, D., Liu, S., **Hu, R.**, Li, Y., & Yan, G. (2016). Scaling of FAPAR from the Field to the Satellite. *REMOTE SENSING, 8*, 310

Zeng, Y., Li, J., Liu, Q., **Hu, R.**, Mu, X., Fan, W., Xu, B., Yin, G., & Wu, S. (2015). Extracting Leaf Area Index by Sunlit Foliage Component from Downward-Looking Digital Photography under Clear-Sky Conditions. *REMOTE SENSING, 7*, 13410

**Hu, R**., Yan, G., Mu, X., & Luo, J. (2014). Indirect measurement of leaf area index on the basis of path length distribution. *REMOTE SENSING OF ENVIRONMENT, 155*, 239-247

Ren, H., Yan, G., Liu, R., **Hu, R.**, Wang, T., & Mu, X. (2013). Spectral Recalibration for In-Flight Broadband Sensor Using Man-Made Ground Targets. *IEEE TRANSACTIONS ON GEOSCIENCE AND REMOTE SENSING, 51*, 4316-4329

Ren, H., Yan, G., Liu, R., Nerry, F., Li, Z.-L., & **Hu, R.** (2013). Impact of sensor footprint on measurement of directional brightness temperature of row crop canopies. *REMOTE SENSING OF ENVIRONMENT, 134*, 135-151